TEMPORAL TRENDS IN THE CO_2 CONTENT OF HAWAIIAN COASTAL WATERS AND CLIMATIC DRIVERS: AN EIGHT YEAR TIME-SERIES PERSPECTIVE

A THESIS SUBMITTED TO THE GRADUATE DIVISION OF THE UNIVERSITY OF HAWAIʻI AT MĀNOA

IN PARTIAL FULFILLMENT OF THE REQUIREMENT FOR THE DEGREE OF

MASTER OF SCIENCE

IN

OCEANOGRAPHY

MAY 2017

By

Gerianne J. Terlouw

Thesis Committee:

Eric H. De Carlo, Chairperson

Yuan-Hui Li

Fred T. Mackenzie

ACKNOWLEDGEMENTS

I would like to thank my advisor Eric De Carlo and my committee members Yuan-Hui (Telu) Li and Fred Mackenzie for their guidance, patience, and immense knowledge. Special thanks current and past members of the De Carlo lab, Ryan Tabata, Sara Coffey, Pat Drupp, Bobby Thompson, Noah Howins, Anthony Barro, and Eric Wadnal, Sami Chen, and Joelle Kubeneck, you all made the lab and field work so much more fun. Thanks to Jason Jones and Garett Johnson at the Hawaii Institute for Marine Biology for your assistance with dive and boat operations. Thanks to the department of oceanography staff, Kathy Kozuma, Van Tran, Catalpa Kong. Kristin Uyemura Momohara, and Pamela Petras. Finally, I would like to acknowledge the University of Hawaii Sea Grant Program and the NOAA PMEL carbon group for funding this research.

LIST OF TABLES

LIST OF FIGURES

TABLE OF CONTENTS

CHAPTER I: INTRODUCTION

Understanding how the biogeochemistry of coral reefs varies temporally and spatially is essential for predicting how these ecosystems will respond and adapt to anthropogenic emissions of CO_2 to the atmosphere and consequent climate change and ocean acidification (OA). Climate change affects marine ecosystems in many ways, but OA is one of the more widely discussed threats (Orr et al. 2005; Doney et al. 2009). The global ocean is primarily a sink for atmospheric CO_2: Through the process of air-sea gas exchange, approximately 25% of all CO_2 released from fossil fuel burning, cement production, and land-use changes is taken up by the oceans (Le Quéré et al. 2015). This flux of CO_2 into the ocean causes a shift in the equilibrium of the CO_2-carbonic acid system in seawater: seawater pCO_2 increases, resulting in a decrease in the pH, carbonate ion concentration (CO_3^{2-}), and saturation state (Ω) of seawater with respect to calcium carbonate minerals. This is potentially problematic for marine calcifiers like corals because the stability of their $CaCO_3$ skeletons is directly proportional to Ω (Kleypas et al. 1999; Hoegh-Guldberg et al. 2008; Silverman et al. 2009).

Detecting a climate change signal in seawater is challenging, because the natural "background" variability in the CO_2-carbonic acid system can be large, especially in productive coastal ecosystems like coral reefs. Biogeochemical processes such as photosynthesis and the respiration of organic matter, and calcification and the dissolution of carbonate minerals, as well as physical processes like temperature fluctuations, tides, currents, and waves, can all affect parameters of the CO_2-carbonic acid system on diurnal, seasonal, and inter-annual time scales (Kayanne et al. 1995; Bates et al. 2010; Drupp et al. 2013). Accurate measurements of CO_2-carbonic acid system parameters, as well as a thorough understanding of the natural variability in seawater on different time-scales are essential.

The iconic "Keeling curve", a time-series of atmospheric CO_2 concentrations acquired through continuous monitoring of air at the Mauna Loa observatory since 1958, provided the first significant

evidence of human-induced change in the composition of greenhouse gases in the atmosphere (Keeling et al., 1976; Thoning et al., 1989). This is an excellent example of the value of continuous monitoring, and how data gain an increasing importance over time. Continuous monitoring of the seawater CO_2-carbonic acid system is relatively new. Since 2004, NOAA's Pacific Marine Environmental Laboratory (PMEL) has developed a global network of CO_2 time-series observations using ship-based underway measurements as well as fixed moored autonomous pCO_2 systems ($MAPCO_2$) with sensors that measure pCO_2 in the surface water and overlying atmosphere (http://www.pmel.noaa.gov/co2/story/Buoys+and+Autonomous+Systems).

My research for this MS thesis focused on the analysis of time-series data from $MAPCO_2$ buoys at three coral reef sites around the island of Oahu, Hawaii. The goal of this study was to create a climatology for seawater pCO_2 and air-sea CO_2 fluxes on Hawaiian coral reefs. Such a climatology can serve as a baseline for current and evolving CO_2-carbonic acid system conditions in seawater to which we can then compare future changes.

The main objectives of this research project are to:

- Determine the quality and reliability (internal consistency) of the CO_2-carbonic acid system data collected by our research group;
- Identify the main biogeochemical and physical drivers of pCO_2 variability in seawater at each coral reef study site; and
- Examine if inter-annual variability in pCO_2 and air-sea CO_2 fluxes reflects intermediate term climate oscillations or longer term climate change.

The approach I am taking is to:

- Carry out measurements where the CO_2-carbonic acid system is over constrained. i.e. more than two parameters among pCO_2, pH, DIC (dissolved inorganic carbon), and TA (total titration alkalinity) are measured;
- Compare time-series of pCO_2 and air-sea CO_2 fluxes at different coral reef environments, as well as an open ocean site;
- Evaluate correlations between pCO_2 and other measured environmental parameters; and
- Correlate and compare pCO_2 data to indices of large-scale climate oscillations such as the El Niño Southern Oscillations (Niño 3.4), North Pacific Gyre Oscillation (NPGO), and Pacific Decadal Oscillation (PDO).

In chapter 2 of this thesis, the internal consistency of the CO_2-carbonic acid data — pH, pCO_2, TA and DIC— collected by our research group is examined. The chapter starts with an introduction to the CO_2-carbonic acid system in seawater, and a discussion of measurements, calculations, and uncertainties associated with the analytical data. Through three case studies, the measured and predicted values of chosen parameters are compared to discern which calculated parameters are statistically reliable. Chapter 3 is a synthesis of a nearly eight-year long time-series data set of seawater pCO_2 and air-sea CO_2 fluxes at three coral reef sites around Oahu, Hawaii. These data are compared to a similar time-series data set from the open ocean (WHOTS mooring [http://www.pmel.noaa.gov/co2/story/WHOTS]) in the North Pacific Subtropical gyre, co-located with the deep water station ALOHA (A Long-Term Oligotrophic Habitat Assessment), which is the field site of the Hawaii Ocean Time-series (HOT) program. Additionally, the relationship between inter-annual pCO_2 variability and climate variability are examined. Chapter 4 is the conclusion of this thesis and discusses the main findings and their implications for monitoring studies in coral reefs and measurements of the CO_2-carbonic acid system in coastal environments.

CHAPTER II: INTERNAL CONSISTENCY OF THE CO_2-CARBONIC ACID SYSTEM DATA

Measurements of the various parameters of the CO_2-carbonic acid system in seawater are used to describe and interpret biogeochemical processes such as primary production and respiration, calcification and dissolution, and air-sea CO_2 gas exchange. Four CO_2-carbonic acid system parameters can be measured analytically: pH, total alkalinity (TA), pCO_2, and dissolved inorganic carbon (DIC). All analytical data have uncertainties. For the CO_2-carbonic acid system in seawater, these uncertainties are often of the same order of magnitude as the changes that we are trying to measure and can therefore not be ignored. For example, the rate of oceanic uptake of anthropogenic CO_2 from the atmosphere is approximately 2 µatm yr^{-1}, and for state-of-the-art pCO_2 sensors the uncertainty in the measured value is also 2 µatm (Sutton et al. 2014). Other parameters, such as the aragonite saturation state ($\Omega_{arag.}$), are not measured and have to be calculated from any two of the four measurable CO_2-carbonic acid parameters using a program like CO2SYS (Lewis & Wallace 1998). If any pair of measureable parameters is known (i.e., two of pH, TA, pCO_2, or DIC), the rest of the CO_2-carbonic acid system is constrained through thermodynamic relationships and can thus be calculated. In theory, any pair of parameters should give identical calculated values for other carbonate system parameters. Unfortunately, due to uncertainties in analytical measurements and in the thermodynamic constants related to the CO_2-carbonic acid system, calculated values contain errors, the magnitude of which depends to a significant extent on the choice of the measured parameters (e.g. Dickson & Riley, 1978; Millero, 2007).

The goal of this chapter is to examine the internal consistency of the CO_2-carbonic acid system data collected by our research group. This means that the agreement between calculated and measured values of different carbonate system parameters will be examined to determine which pair of carbonate input parameters (pH, pCO_2, TA, and DIC) results in the most accurate estimate of the measured value.

Examination of CO_2-carbonic acid system data collected is then carried out through three case studies:

Case study 1: Four CO_2-carbonic acid parameters — pH, pCO_2, TA, and DIC — measured over a diurnal cycle

Case study 2: Use of TA and DIC data from bottle samples to verify autonomously collected pCO_2

Case study 3: Autonomous pCO_2 and pH: Three months of time-series data

Each case study focuses on a different part of a larger data set and is designed to answer a specific question related to the internal consistency of the data:

Question 1: Which pair of parameters is best suited for calculating the full CO_2-carbonic acid system?

Question 2: Can autonomous pCO_2 data be verified reliably by calculating pCO_2 from TA and DIC?

Question 3: Can we use our autonomous pH and pCO_2 — the only two parameters at present that can be measured autonomously with commercially available instruments —for reliable calculation of the CO_2-carbonic acid system?

2.1 The CO_2-carbonic acid system in seawater: Theory, analytical methods, and calculations

When atmospheric CO_2 dissolves in seawater, it hydrates, and carbonic acid (H_2CO_3) is formed. This is a weak acid that dissociates to form bicarbonate (HCO_3^-), carbonate (CO_3^{2-}), and hydrogen ions (H^+). The concentration of H_2CO_3 in seawater, however, is less than 0.3 % of the dissolved CO_2 (CO_2 [aq]). These acid-base species form the basis of the CO_2-carbonic acid system in seawater. A schematic

representation of the system in seawater is shown in Figure 2.1. Dissolved CO_2 (aq) in seawater is in equilibrium with atmospheric CO_2 (g), and they are related to each other by the solubility coefficient of CO_2, K'_0 (Eq. 2.1) (Weiss 1974). The various ionic species in seawater are related to each other by apparent equilibrium constants K'_1 (Eq. 2.2) and K'_2 (Eq. 2.3), which are functions of sea surface temperature (SST), pressure, and salinity (Park 1969). The pH is defined as the negative logarithm of the hydrogen ion concentration (Eq. 2.4) and dissolved inorganic carbon (DIC, also referred to as total CO_2 [TCO_2]) is the sum of all the dissolved CO_2-carbonic acid species (Eq. 2.5). The total alkalinity (TA) is the charge balance for all ions in seawater, and is defined as the number of moles of H^+ equivalent to the excess of proton acceptors (Eq. 2.6). The dominant proton acceptors in seawater are the conjugate bases of H_2CO_3: HCO_3^- and CO_3^{2-}. For an accurate and complete description of TA, however, boric acid ($B(OH)_3$), borate ($B(OH)_4^-$), hydroxide (OH^-) and the conjugate bases of phosphoric acid and nitrate (NO_3^-), as well as some generally minor concentrations of any other weak organic acids or bases present in seawater should be taken into account (Zeebe & Wolf-Gladrow 2001). The carbonate alkalinity (CA, Eq. 2.7) is defined as the number of moles of H^+ equivalent to the excess of CO_2-carbonic acid proton acceptors (HCO_3^- and CO_3^{2-}), and has to be calculated from TA (Eq. 2.6). If the concentration of $B(OH)_3$) and $B(OH)_4^-$, along with the dissociated phosphoric acid ions ($H_2PO_4^-$, $HPO_4^{2-} + PO_4^{3-}$), NO_3^-, and silicate ($SiO(OH)_3^-$), are known, CA can be calculated by subtracting these ions from TA (Eq. 2.8). The TA is a measurable quantity, but for carbonate system calculations, the CA is the important parameter.

The saturation state of seawater with respect to a calcium carbonate polymorph (Eq. 2.9) is a measure of the thermodynamic stability of the mineral, and is defined as the product of the CO_3^{2-} and calcium (Ca^{2+}) ion concentrations over the solubility product constant (K'_{sp}) of calcium carbonate in seawater at a given temperature, pressure, and salinity (Morse et al. 2007). A more detailed description of the CO_2-carbonic acid system in seawater has been prepared by Zeebe and Wolf-Gladrow (2001).

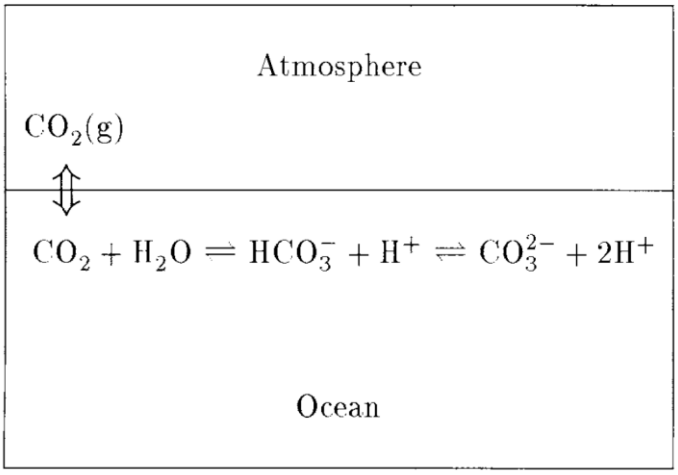

Figure 2.1 Schematic Illustration of the CO_2-carbonic acid system in the ocean (Zeebe & Wolf-Gladrow, 2001)

(2.1) $K_0 = [CO_2]\ (aq) / [CO_2]\ (g)$

(2.2) $K'_1 = [HCO_3^-]\ [H^+] / [CO_2^*]$

(2.3) $K'_2 = [CO_3^{2-}]\ [H^+] / [HCO_3^-]$

(2.4) $pH = -\log [H^+]$

(2.5) $DIC = [CO_2^*] + [HCO_3^-] + [CO_3^{2-}]$

Where CO_2^* is the sum of aqueous CO_2 species: $[CO_2]$ and $[H_2CO_3]$.

(2.6) $TA = [HCO_3^-] + 2\ [CO_3^{2-}] + [B(OH)_4^-] + [OH^-] + [HPO_4^-]\ 2[HPO_4^{2-}] + 3[PO_4^{3-}] + [SiO(OH)_3^-] - [H^+] + \text{organic bases}$

(2.7) $CA = [HCO_3^-] + 2\ [CO_3^{2-}]$

(2.8) $CA = TA - \left([B(OH)_4^-] + [OH^-] + [HPO_4^{2-}] + 2[HPO_4^{2-}] + 3[PO_4^{3-}] + [SiO(OH)^{3-}] - [H^+] + \text{organic bases}\right)$

(2.9) $\Omega_x = [CO_3^{2-}]\ [Ca^{2+}] / K'_{SPx}$

Of the six CO_2-carbonic acid system parameters, CO_2, HCO_3^-, CO_3^{2-}, H^+, TA, and DIC, four are routinely determined; DIC, TA, pH, and pCO_2 (or CO_2 fugacity fCO_2). The state-of-the-art of analytical techniques of these parameters is described in the Guide to Best Practices for Ocean CO_2 Measurements (Dickson et al. 2007). All CO_2-carbonic acid system parameters are related to each other by thermodynamic relationships (Eq. 2.2 and 2.3); if two parameters are known, the rest of the system is constrained and the remaining parameters can be calculated as long as SST, salinity, and pressure are also known (also PO_4^{3-}, NO_3^-, SiO_4^{2-} concentrations, Park 1969).

Analysis	Method	Precision	Accuracy	citation
pCO_2	Infrared	0.5 µatm	2 µatm	Wanninkhof & Thoning, 1993
TA	potentiometric	1 µmol/kg	3 µmol/kg	Millero et al. 1993
DIC	coulometric	1 µmol/kg	1 µmol/kg	Johnson et al. 1993
pH	spectrophotometric	0.0004	0.002	Byrne, 1987
pH	ISFET	0.004	0.02	Martz et al. 2010

Table 2.1 Methods used to measure the CO_2-carbonic acid system variables and their uncertainties

In CO_2-carbonic acid system calculations, the uncertainties in the two measured parameters (Table 2.1) and in the apparent equilibrium constants are propagated to the calculated parameters. Therefore the choice of input parameters and apparent equilibrium constants in part determines the uncertainty in the calculated parameters (Table 2.2 and 3.3). Table 2.1 lists the common analytical methods used to measure pH, pCO_2, TA, and DIC, and their generally accepted analytical uncertainties.

The uncertainty in pK'_1 (the negative logarithm of K'_1) ranges from 0.003 to 0.007, and the uncertainty in pK'_2 from 0.002 to 0.02 (Millero 2007). Table 2.2 shows the uncertainty in the calculated parameters caused by uncertainties in pK'_1 and pK'_2. The TA–DIC pair causes the largest uncertainty in pCO_2 (~ 6 µatm). Theoretically, the combination of pH–TA or pH–DIC gives the most accurate calculation of pCO_2. The apparent equilibrium constants in Equation 2.2 and 2.3 have been determined in many experiments; some were carried out in artificial seawater (Hansson 1973; Goyet & Poisson 1989;

Roy et al. 1993) and others in natural seawater (Mehrbach et al. 1973; Mojica Prieto & Millero 2002; Millero et al. 2006). The data from these original experiments have also been refitted (Dickson & Millero 1987; Lueker et al. 2000). In order to make reliable comparisons between different studies, Dickson et al. (2007) recommended a standard procedure of using the constants of Mehrbach et al. (1973), refitted by Dickson & Millero (1987) on the total pH scale for all seawater CO_2-carbonic acid calculations. The choice of this set of constants was based on the internal consistency studies of Wanninkhof et al. (1999) and Lee et al. (1996), who pointed out that these constants are most reliable if pCO_2 is used as an input parameter or if pCO_2 is calculated. For CO_2-carbonic acid calculations that involve pH, TA, or DIC, however, the constants of Roy et al. (1993) or Goyet & Poisson (1989) were found to be more suitable (Clayton et al. 1995; Lee et al. 1997). In this work, the constants of Mehrbach et al. (1973), refitted by Dickson & Millero (1987) will be used, because they are generally recommended for OA studies and most of our calculations involve pCO_2. Table 2.3 shows the estimated errors in the calculated parameters propagated from the uncertainty in the input parameters, K'_1, and K'_2. Note that K* and K' both refer to apparent equilibrium constants and these notations are used interchangeably here. In the literature, however, the K* notation is often used for the solubility product of a solid (e.g. K_{sp} of $CaCO_3$) and the K' notation for the dissociation constant of a dissolved species (e.g. K'_2 for HCO_3^-).

The pair that has been recommended as the preferable input parameters for CO_2-carbonic acid system calculations is DIC and TA (Riebesell et al. 2010). The advantages of using TA and DIC as input parameters are that there are well developed analytical methods and certified reference materials (CRM's) available for these parameters (Dickson et al. 2007) and the samples can easily be preserved and stored for later analysis. Many coral reef carbonate chemistry studies use TA and DIC to calculate the CO_2-carbonic acid system (e.g. Shamberger et al. 2011; Albright et al. 2013; Shaw & McNeil 2014; Venti et al. 2014; Yeakel et al. 2015). The combination of pCO_2 with pH is considered to be the worst pair of input parameters because of their high covariance (Dickson & Riley 1978; Millero 2007), which results in large uncertainties in the calculated parameters. The pCO_2 and pH, however, are currently the only two

that can be measured autonomously with commercially available instruments (Dickson et al. 2007) and, therefore, is often the pair of choice in continuous monitoring studies, although progress has been made recently on autonomous DIC technology (Sayles & Eck 2009; Liu et al. 2013; Fassbender et al. 2015; Wang et al. 2015) and autonomous TA analyzers (Martz et al. 2006; Spaulding et al. 2014).

input	parameter	pK_1^*	pK_2^*	both[a]	exptl error
pH−TA	f_{CO_2} (μatm)	1.5−7.6	0.9−1.3	1.7−7.7	2.1
pH−TCO_2		1.5−6.6	0.5−0.6	1.6−6.6	1.8
TA−TCO_2		1.4−4.7	2.5−8.2	2.9−9.4	5.7
f_{CO_2}−TCO_2	pH	0.002	0.0004	0.002	0.0025
f_{CO_2}−TA		0.002	0.0006	0.002	0.0026
TA−TCO_2		0.0003	0.005	0.004	0.0062
pH−TA	TCO_2 (μmol kg^{-1})	0.1−0.2	2.4−0.9	2.4−0.9	3.8
f_{CO_2}−TA		1.0−0.4	1.8−0.8	2.1−0.9	3.2
pH−TCO_2	TA (μmol kg^{-1})	0.04−0.2	2.6−0.8	2.6−0.8	2.7
f_{CO_2}−TCO_2		1.3−0.4	2.3−0.7	2.6−0.8	3.4

[a] The total error is the square root of the sum of the squared errors due to pK_1^* and pK_2^*.

Table 2.2 Estimated probable errors in the calculated parameter of the carbonate system caused by errors in pK'_1(0.002) and pK'_2 (0.005) using various input measurements (Millero, 2007).

Input	ΔpH	ΔTA ($\mu mol\ kg^{-1}$)	ΔDIC ($\mu mol\ kg^{-1}$)	ΔfCO_2 (μatm)
pH, TA	-	-	± 3.8	± 2.1
pH, DIC	-	± 2.7	-	± 1.8
pH, fCO_2	-	± 18	± 15	-
fCO_2, DIC	± 0.0023	± 3.0	-	-
fCO_2, TA	± 0.0021	-	± 3.4	-
TA, DIC	± 0.0062	-	-	± 5.8

[a]The following accuracies were assumed: DIC: $\pm 2\ \mu mol\ kg^{-1}$, TA: $\pm 4\ \mu mol\ kg^{-1}$, pH: 0.002, fCO_2: 2 μatm (compare Millero, 1995).

Table 2.3 Estimated total errors in the calculated parameters of the carbonate system using various input measurements (Zeebe & Wolf-Gladrow, 2001)

2.2 Methods

At four coral reef sites around the island of Oahu, Ala Wai, Kilo Nalu, CRIMP-2, and Kaneohe (Figure 2.1, and described in more detail in Chapter 3), CO_2, pH, SST, salinity, pressure, and dissolved oxygen (DO) data were collected using autonomous sensors. The mole fraction (xCO_2) of seawater was measured with a LICOR-820 infrared CO_2 sensor after drying, and seawater pCO_2 was calculated from dry xCO_2 according to the method of Weiss & Price (1980). DO was measured using a Sea-Bird Electronics 63 Optical DO sensor. SST and conductivity (salinity) were measured using a Sea-Bird Electronics sensor (16plus V2 SeaCAT or 37 SMP MicroCAT). The pH was measured with an ion sensitive field effect transistor type sensor (SeaFET or SeapHOx). Discrete water samples were collected and analyzed in the laboratory for TA and DIC. TA was measured using an open cell potentiometric titration method (Dickson et al. 2007) on a Metrohm Titrando 905, and DIC was measured using a coulometric titration method (Dickson et al. 2007) on a Marianda Vinta 3D instrument. The accuracies of DIC and TA measurements were established with certified reference materials (CRM) obtained from Andrew Dickson at Scripps Institution of Oceanography. The uncertainty of the pCO_2 measurement is

considered to be ±2 µatm (Sutton et al. 2014). The precision of the SeaFET pH sensor is 0.003 and the accuracy is 0.02. Because the factory calibration of the SeaFET sensor was not verified, the uncertainty of the pH data is conservatively estimated to be 0.03. The SeapHOx calibration was verified and the uncertainty of the pH is estimated to be 0.003 (Bresnahan et al. 2014).

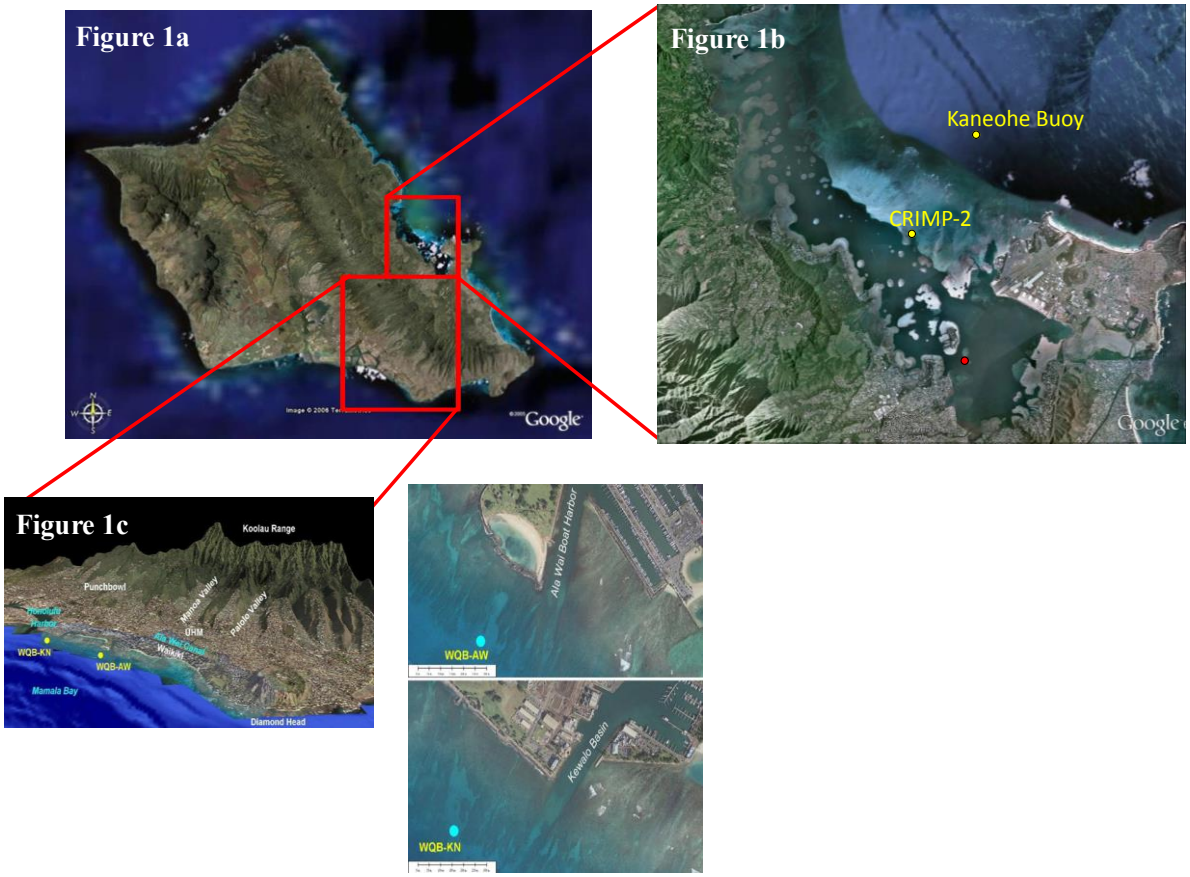

Figure 2.2 The island of Oahu, highlighting Kaneohe Bay on the windward (east) coast and the Honolulu watershed on the southern coast; b) Kaneohe Bay, highlighting the CRIMP-2 buoy on the back reef and the new Kaneohe buoy on the deeper fore-reef; c) Two buoys are located 200 m offshore of urban Honolulu above fringing reefs. Ala Wai buoy (AW) is located near the mouth of the Ala Wai canal, which drains the Honolulu city watersheds. Figure by Pat Drupp.

Parameters of the CO_2-carbonic acid system were calculated in CO2SYS using equilibrium constants of Mehrbach et al. (1973), refitted by Dickson & Millero (1987) on a "Total" scale for pH (Dickson et al. 2007). The uncertainty of the calculated parameters, propagated from the uncertainty in

the measured input parameters, was estimated by running the CO2SYS program for a combination of the two input parameters ± 1 standard deviation (std). There are three values of each input parameter: mean, mean + std, and mean – std. Three combinations of two input parameters results in $3^2 = 9$ unique combinations of input values, and therefore the error propagation calculation in CO2SYS provides 9 different values. Of these 9 values, the difference between the highest and lowest outcome is the "range", and the "standard deviation" of the calculated parameter is defined as half the range (eq. 2.10):

$$\frac{(\text{highest observed value} - \text{mean}) + (\text{lowest observed value} - \text{mean})}{2} \quad (2.10)$$

Equation 2.8 estimates the uncertainty in the calculated parameters by propagating the uncertainty in the measured parameters, but it should be noted that the uncertainties in K'_1 and K'_2 are not taken into account in this error calculation.

Evaluating the internal consistency of the CO_2-carbonic acid data involves examination of the agreement between calculated and measured values and determining which pair of CO_2 input parameters results in the most accurate estimate. For example, a measured parameter is referred to as "measured X", and the parameter calculated as a function of Y and Z is referred as "X(Y–Z)". The residual (ΔX) is the difference between the calculated and measured value of a parameter (e.g. $\Delta pCO_2 = pCO_2(TA–DIC)$ - measured pCO_2). If the residual is within the uncertainty of the measured and calculated value, the system is deemed to be internally consistent. The following definitions and statistical tests are used in this chapter:

I. Residual: $\Delta X = X(Y–Z)$ – measured X is the difference between the calculated and measured value of a parameter. The mean of the residuals is a measure of accuracy and the standard deviation of the residuals are an indication of precision.

II. Percent (%) difference = $\Delta X / X_{\text{in situ}} * 100$. The relative difference between the measured and calculated value.

III. Slope of linear fit: a measure of linearity of the relationship between X(Y–Z) and measured X.

2.3 Case Studies

2.3.1 Case study 1: Four parameters over a diurnal cycle

In this experiment the internal consistency of the pCO_2–pH–TA–DIC data was evaluated by measuring all four parameters over a 24 hour period (diurnal cycle). Each parameter was then calculated from a unique combination of input parameters and this calculated value compared to the measured one. Data were collected at the CRIMP-2 site on 8-9 December, 2015. Sampling was carried out 12 times over the diurnal cycle on somewhat irregular intervals, ranging from one to four hours. The pH was measured hourly and pCO_2 on three hour intervals, both using autonomous sensors. If pCO_2 was not available at the time of discrete sampling for TA and DIC, the value was interpolated from a smooth sinusoidal curve between measured values. We found no difference in accuracy between CO2SYS calculations based on measured or interpolated data points, and therefore assume that the interpolation of pCO_2 data is reliable.

Results

Time-series plots for each parameter, measured and calculated from each unique combination of two input parameters, are shown in Figure 2.3 (pH and pCO_2) and Figure 2.4 (TA and DIC). The blue curve in each graph represents measured data. The error bars represent one standard deviation, and the shaded region in the plot illustrates night time. For pH and pCO_2, the calculated values are all close to the measured values, although values calculated from the TA–DIC do not follow a smooth curve (Fig. 2.2). For DIC and TA, the calculated values are also close to measured values, except when the pCO_2–pH was used as input parameters (Fig. 2.3). Not only are the error bars large, but the data points do not follow a

smooth curve over the diurnal cycle like the measured values or those calculated from other pairs of input parameters. The large error bars for TA(pCO_2–pH) and DIC(pCO_2–pH) are in part because we did not recalibrate the pH sensor after factory calibration. Table 2.4 summarizes the measured and calculated values and their uncertainties (± 1 std) for each parameter. Table 2.5 displays the average residuals for each parameter and the percent offset of the calculated parameter relative to the measured one. All calculated values are within 3% of the measured values, except for pCO_2(TA–DIC), which is 6% off. Note that the large standard deviation of the residuals, especially for TA(pCO_2–pH) and DIC(pCO_2–pH), indicates a poor precision. This poor precision is also very evident in the time-series plots (Fig. 2.3).

	pCO_2 (µatm)	TA (µmolkg^{-1})	DIC (µmolkg^{-1})	pH (total scale)	Ω Ar
Measured	461 ± 2	2226 ± 3.12	1954 ± 0.71	7.98 ± 0.03	-
Calculated from:					
pCO_2– pH	-	2221 ± 187	1961 ± 156	-	2.91 ± 0.42
pCO_2–TA	-	-	1965 ± 3.4	7.98 ± 0.002	2.92 ± 0.02
pCO_2–DIC	-	2213 ± 1.9	-	7.98 ± 0.002	2.89 ± 0.01
pH–TA	462 ± 39	-	1965 ± 19	-	2.91 ± 0.16
pH–DIC	459 ± 35	2213 ± 18	-	-	2.89 ± 0.18
TA–DIC	437 ± 7	-	-	8 ± 0.006	3.02 ± 0.04

Table 2.4 Descriptive statistics of measured and calculated values (mean ± 1 standard deviation and the uncertainty (std) ± 1 standard deviation (n=12) over a diurnal period on December 8-9, 2016 at CRIMP-2. Values in bold on the top row are measured, other values are calculated using CO2SYS as a combination of two measured input variables (column 1)

Measured	Input variables	Residual (Calc. - Meas)	% offset
pCO_2 (µatm)	DIC–TA	-25 ± 20	6%
	DIC–pH	-2 ± 14	2%
	TA–pH	1 ± 16	3%
TA (µmolkg^{-1})	DIC–pCO_2	-13 ± 10	1%
	DIC–pH	-12 ± 11	1%
	pCO_2–pH	-5 ± 75	3%
DIC (µmolkg^{-1})	TA–pCO_2	11 ± 8	1%
	TA–pH	11 ± 10	1%
	pCO_2–pH	7 ± 64	2%
pH (total scale)	DIC–TA	0.021 ± 0.019	0.27%
	DIC–pCO_2	-0.002 ± 0.002	0.12%
	TA–pCO_2	0.001 ± 0.013	0.12%

Table 2.5 Residuals, defined as the value calculated - measured value (mean ± 1 standard deviation) as a function of two input variables. Data were collected over a diurnal period on December 8-9, 2016 at CRIMP-2.

Ω Aragonite	Input variables for calcualtion	Residual (Calc - Meas)	% offset
Ω (pCO_2–DIC)	pH–DIC	0.01 ± 0.08	2%
	pH–TA	0.02 ± 0.07	2%
	pCO_2–TA	0.03 ± 0.02	1%
	pH–pCO_2	0.02 ± 0.18	4%
	TA–DIC	0.14 ± 0.11	5%

Table 2.6 Aragonite saturation state residuals (mean ± 1 standard deviation), defined as the value calculated as a function of two input variables - Ω (pCO_2-DIC) . Ω is not measured directly and therefore the calculated values cannot be compared to measured data. Values are compared to Ω (pCO_2-DIC) because this pair shows the smoothest curve, and the curve of the input variables is also smooth with small error bars.

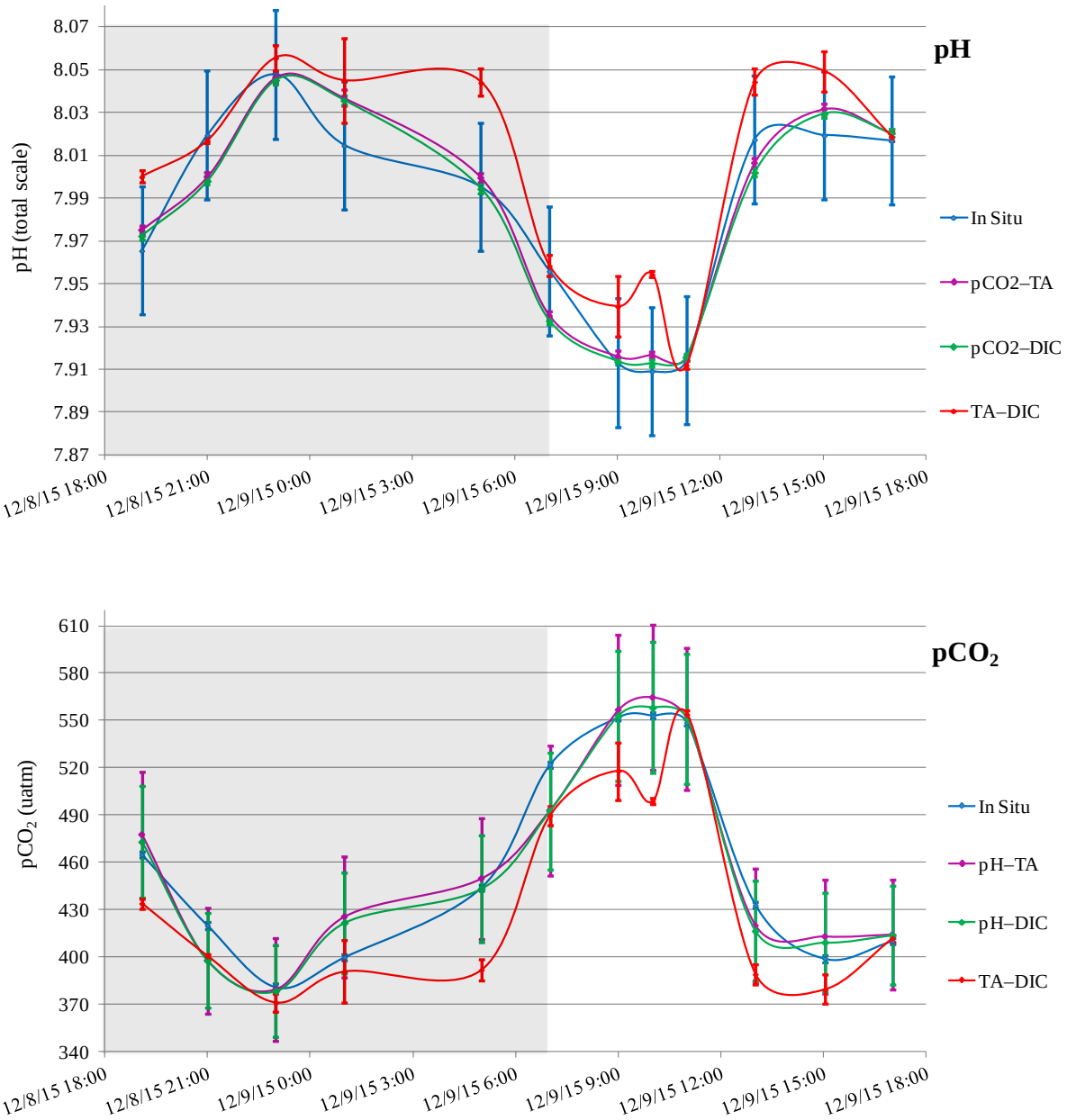

Figure 2.3 Time-series of pH (top) and pCO_2 over a diurnal cycle on 8-9 March 2015 at CRIMP-2. Measured (blue curve) and calculated from a combination of two input variables (mean ± 1 standard deviation). The shaded regions illustrate night time.

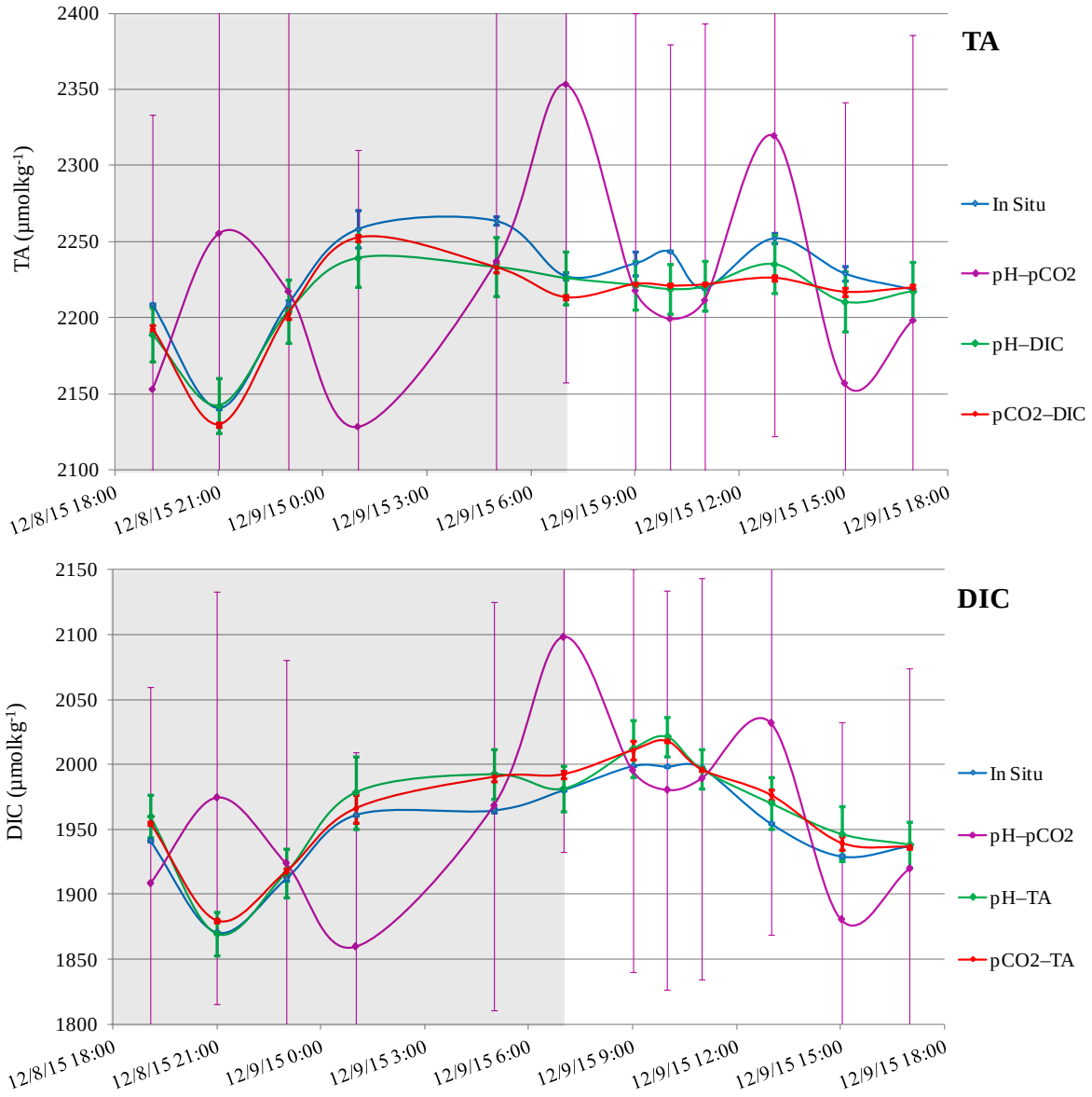

Figure 2.4 Time-series of TA (top) and DIC over a diurnal cycle on 8-9 March 2015 at CRIMP-2. *M*easured (blue curve) and calculated from a combination of two input variables (mean ± 1 standard deviation). The shaded regions illustrate night time.

Figure 2.5 displays a time series of Ω_{Ar}, the degree of saturation with respect to Aragonite, calculated from each combination of two input parameters. Because Ω_{Ar}, is not measured directly, we do

not know the "true" value, and therefore Ω_{Ar} (pCO_2–DIC) data are used to compare estimates of Ω_{Ar} from other pairs for two reasons; (1) this curve is the "smoothest", and (2) the curves of the input parameters, pCO_2 and DIC, are smooth and have small error bars (Fig. 2.2 and 3.3). The descriptive statistics of the calculated data are shown in Table 2.4 and the residuals for Ω_{Ar} are summarized in Table 2.6. All calculations of Ω_{Ar} are very close to each other, and the largest offset is 5% between Ω_{Ar} (TA–DIC) and Ω_{Ar} (pCO_2–DIC).

It should be noted that this study was based on only 12 data points for each parameter, from the CRIMP-2 site during the winter season (December). This is a small sample size and these results should be verified by duplicating this experiment under the same conditions, as well as under different conditions such as a different season (summer) or another study site.

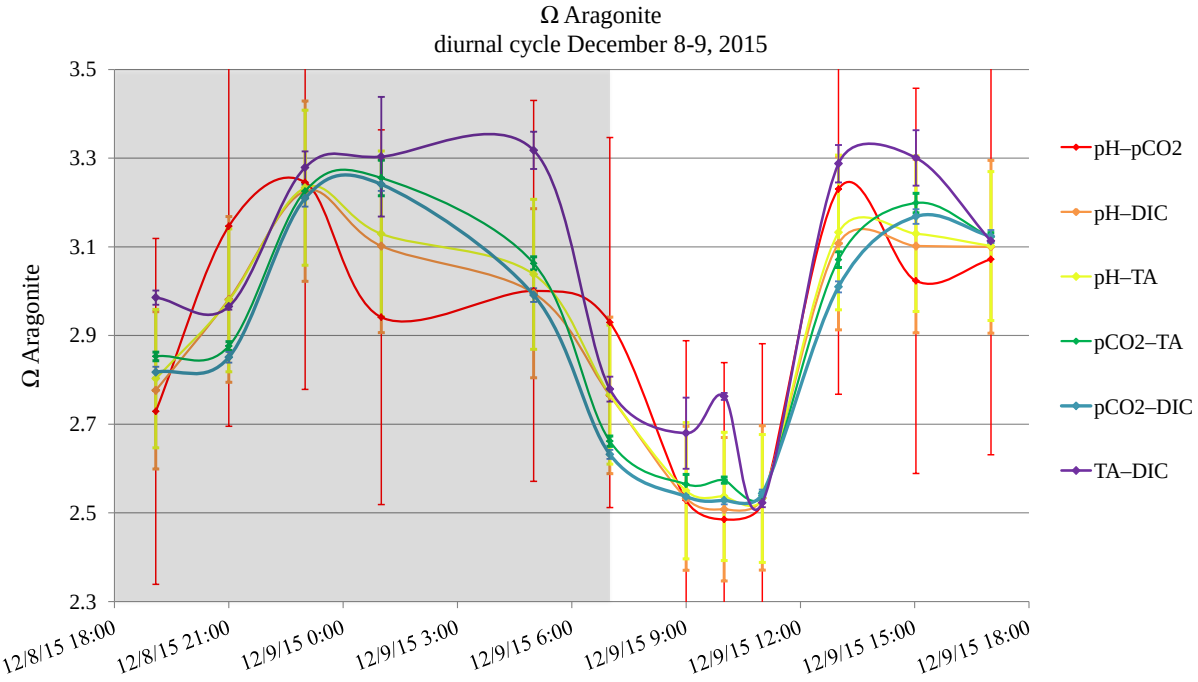

Figure 2.5 Time-series of the aragonite saturation state (Ω_{Ar}) over a diurnal cycle on 8-9 March 2015 at CRIMP-2. Measured (blue curve) and calculated from a combination of two input variables (mean ± 1 standard deviation). The shaded regions illustrate night time.

2.3.2 Case study 2: TA and DIC to verify autonomously collected pCO_2

As part of NOAA PMEL's mooring quality control and assurance, "validation samples" should be taken at least four times a year at all $MAPCO_2$ sites (InteragencyOADataMgmtPlan_June2012-20). "Validation samples" refers to samples used for the analysis of inorganic carbon parameters that cannot yet routinely be measured autonomously such as DIC and TA, and to verify the autonomously collected pCO_2 data. Here the autonomously measured pCO_2 data are compared to pCO_2 values calculated from TA and DIC bottle samples.

Results

Table 2.7 presents a summary of the measured (pCO_2, TA, and DIC) and calculated (pCO_2 (TA–DIC)) values and their uncertainties. Data from the samples collected at each site are also depicted in scatter plots (Fig. 2.6) to evaluate the linearity and spread of the data. The slope of the linear fit through the data is close to one for all sites, which indicates a linear relationship between measured and calculated values that is the same over the range of pCO_2 in this study (~300-700 µatm). Table 2.8 shows the residuals (measured – calculated) and the percent offset. The mean residual is roughly zero at each site but the standard deviation is large and ranges from 21 µatm at Kilo Nalu, 41 µatm at Ala Wai, to 67 µatm at CRIMP-2. The Kaneohe site has only three data points and will not be discussed until more data are available.

There was no correlation between the magnitude of the residual and the values of salinity, pCO_2, or SST, or with the date of analysis. It should be noted that the number of data points at each site ranges from 12 to 34, which is quite small for a statistical evaluation of the internal consistency. Additionally, some discrete TA and DIC samples were not collected at the exact time of autonomous pCO_2, SST, and salinity sampling, and therefore the corresponding values for pCO_2 were interpolated to the time of discrete TA and DIC sampling.

	n	pCO_2 (µatm) mean	std	TA (µmolkg^{-1}) mean	std	DIC (µmolkg^{-1}) mean	std	pCO_2 (TA–DIC) mean	std
Kilo Nalu	34	384 ± 21	2 ± 0	2320 ± 15	2.5 ± 1.8	1999 ± 9	1.1 ± 1.0	383 ± 21	5.5 ± 3.2
Ala Wai	12	410 ± 40	2 ± 0	2314 ± 15	2.4 ± 1.9	2005 ± 18	1.7 ± 1.5	400 ± 19	7.0 ± 3.7
CRIMP-2	23	454 ± 82	2 ± 0	2227 ± 31	2.4 ± 2.9	1962 ± 39	1.1 ± 1.2	454 ± 83	7.1 ± 6.3
Kaneohe	3	400 ± 36	2 ± 0	2203 ± 12	1.0 ± 0.2	1933 ± 75	0.7 ± 0.3	448 ± 52	3.4 ± 1.2

Table 2.7 Descriptive statistics for measured values of pCO_2, TA, and DIC, and pCO_2(TA-DIC) (mean ± 1 standard deviation) and the uncertainties in the measurement (mean ± 1 standard deviation). Samples were collected at various times between 2010 and 2016 at the Kilo Nalu, Ala Wai, CRIMP-2, and Kaneohe sites.

	n	Residual (Calc - Meas)	% offset
Kilo Nalu	34	-0.6 ± 21	4%
Ala Wai	12	-0.5 ± 41	5%
CRIMP-2	23	-0.2 ± 67	9%
Kaneohe	3	48 ± 37	12%

Table 2.8 Descriptive statistics comparing measured and calculated values of data, collected between 2010 and 2016 at Kilo Nalu, Ala Wai, CRIMP-2, and Kaneohe sites. Residuals, defined as the pCO_2(TA-DIC) - measured pCO_2 (mean ± 1 standard deviation) and the % offset defined as the residual / measured pCO_2 * 100%.

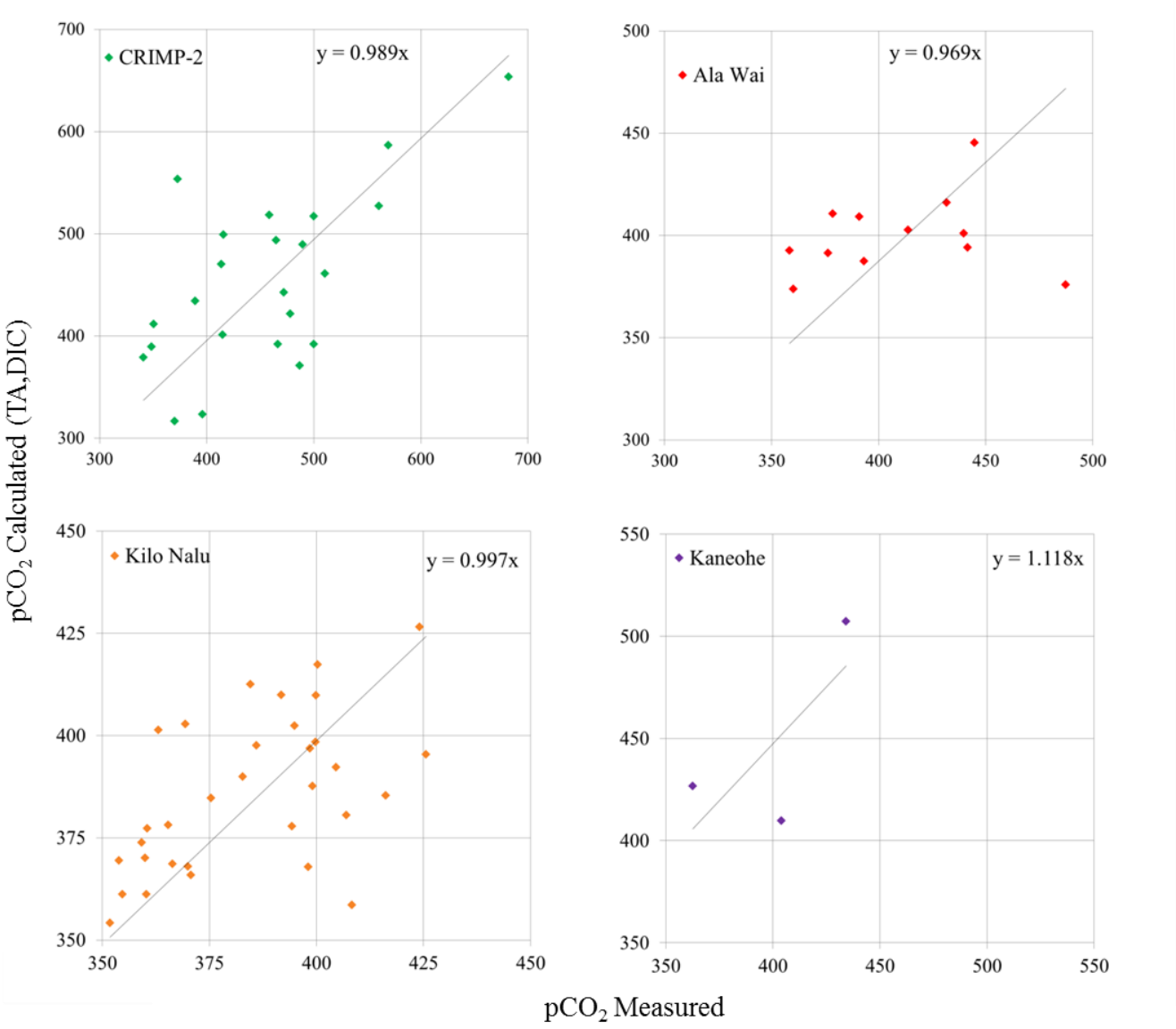

Figure 2.6 Scatter plot of measured pCO_2 (horizontal axis) and pCO_2 (TA-DIC) (vertical axis) at CRIMP-2, Ala Wai, Kilo Nalu, and Kaneohe. Samples were collected at various times between 2010 and 2016 at the Kilo Nalu, Ala Wai, CRIMP-2, and Kaneohe sites. The line of best fit is forced through zero. If the slope of the linear fit is less than 1, measured values are greater than calculated values on average, and vice versa.

2.3.3 Case study 3: Three-month time-series of autonomous pH and pCO_2

A SeapHOx sensor was deployed on the MAPCO_2 mooring at the CRIMP-2 site from December 2013 through February 2014 as part of a larger commercial instrument evaluation under the auspices of the Alliance for Coastal Technology (ACT). This instrument is a combined pH and dissolved oxygen sensor developed by the Martz group at Scripps Institution of Oceanography (SIO, Bresnahan et al. 2014). In this case study, autonomously collected pH and pCO_2 data are used to calculate DIC and TA over a three month period. Because only two parameters of the CO_2-carbonic acid system were measured (pCO_2 and pH), we did not "over-constrain" the system, and the internal consistency cannot be evaluated by comparing calculated and measured values. Instead, the pH data are compared to data from a parameter that is expected to co-vary with pH, such as DO and pCO_2, to evaluate the reliability of the autonomous pH data (Martz 2015). The internal consistency between pH, pCO_2, DO, and the Apparent Oxygen Utilization (AOU, e.g. Li et al. 2000; Park 1969) is evaluated by determining how well these parameters correlate. Also, DIC(pCO_2–pH) and TA(pCO_2–pH) calculated in this study are compared to TA and DIC measured from bottle samples collected at the CRIMP-2 site between 2010 and 2016 (validation samples described in case study 2).

Results

Scatter plots with correlation coefficients between parameters (pH, pCO_2, DO, AOU, TA(pCO_2–pH), and DIC(pCO_2–pH)) are shown in Figure 2.7. There was a strong correlation between pH and pCO_2 (R^2 = 0.90) and between DO and pH (R^2 = 0.73). The descriptive statistics of each parameter are summarized in Table 2.9. Briefly, measured pCO_2 was 475 ± 68 µatm, measured pH was 7.98 ± 0.06, calculated TA(pCO_2–pH) was 2225 ± 112 µmolkg^{-1}, and calculated DIC(pCO_2–pH) was 2003 ± 88 µmolkg^{-1}. The mean values of calculated TA and DIC agree well with the mean values of measured TA and DIC (Table 2.7, case study 2): mean measured TA at was 2227 µmolkg^{-1} (Table 2.7) and TA(pCO_2–

pH) in this study was 2225 µmolkg^{-1} (Table 2.9). Mean measured DIC was 1962 µmolkg^{-1} (Table 2.7) and DIC(pCO_2–pH) in this study was 2003 µmolkg^{-1}. The standard deviation for the calculated TA and DIC values was much greater than that of the measured values (112 vs. 29 for DIC and 88 vs. 31 for TA). The spread of the calculated TA and DIC is thus somewhat unrealistic.

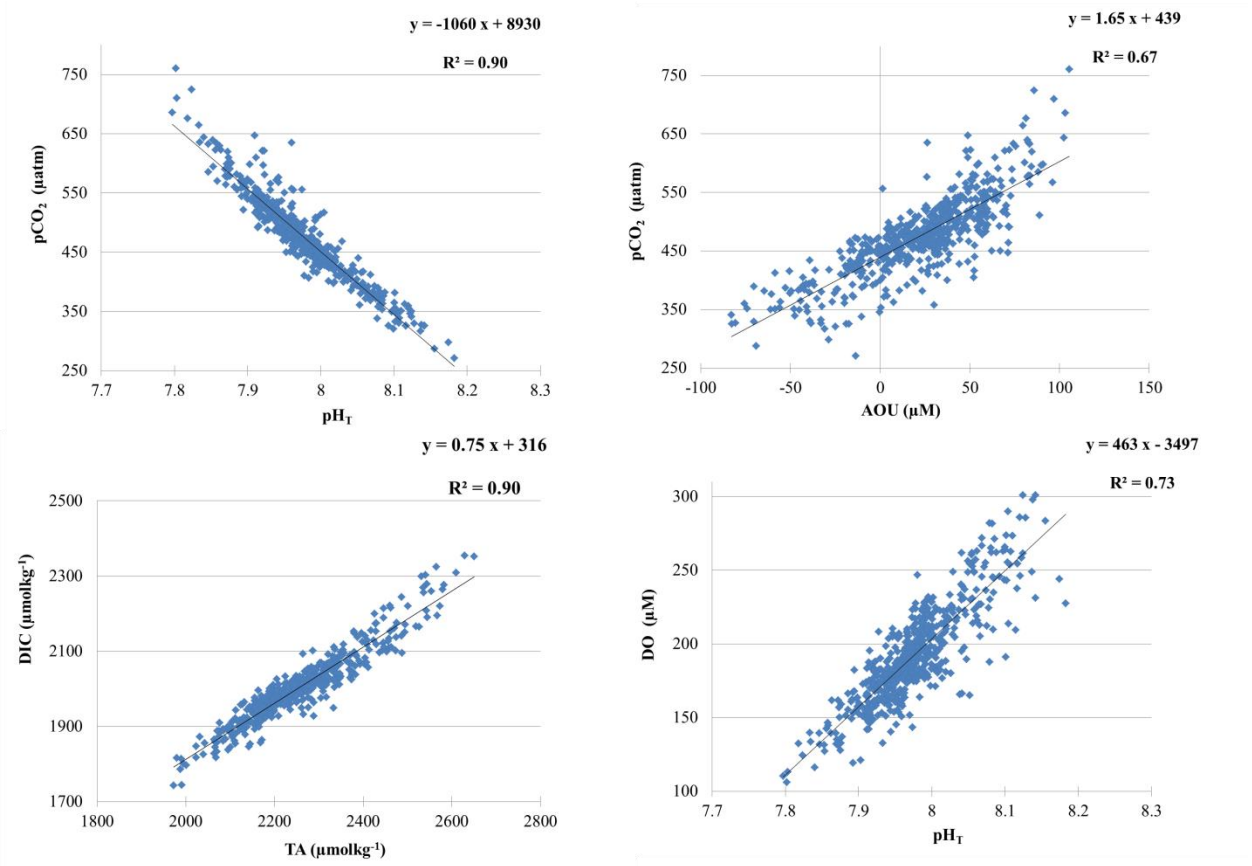

Figure 2.7 Scatter plots of measured pCO_2, pH, and DO, and calculated TA(pCO_2-pH), DIC(pCO_2-pH), the Apparent Oxygen Utilization (AOU). Data were collected at the CRIMP-2 site from December 2013 to February 2014. The equations of a linear fit, and the correlation coefficient (R^2) is shown for each scatter plot.

	Input Variables	mean	std
pCO_2 (µatm)	measured	475 ± 68	2 ± 0
pH (total scale)	measured	7.98 ± 0.06	0.03 ± 0
TA ($\mu mol kg^{-1}$)	pH–pCO_2	2225 ± 112	27 ± 2.5
DIC ($\mu mol kg^{-1}$)	pH–pCO_2	2003 ± 88	23 ± 1.9

Table 2.9 Descriptive statistics (mean ± 1 standard deviation) of measured pCO_2 and pH, and calculated TA(pCO_2–pH) and DIC(pCO_2–pH) at CRIMP-2 for 2/20/2013 – 3/1/2014.

2.4 Discussion

In three case studies described above, measured values for pCO_2, pH, DIC, and TA were compared to values calculated from two measured input parameters using CO2SYS (Lewis & Wallace 1998). What pair of parameters is best for calculating the full CO_2-carbonic acid system (pH, pCO_2, TA, DIC, and Ω) of particular interest. The main findings of the three case studies are discussed below.

2.4.1 Covariance between pCO_2–pH

Using the pH–pCO_2 pair for calculations of TA and DIC resulted in the greatest residuals (calculated – measured values) in the diurnal experiment (case study 1, Table 2.5). The large standard deviation indicates that the calculation was not very precise. This imprecision in calculations from the pH–pCO_2 pair is generally attributed to their strong covariance (Dickson & Riley 1978) and therefore a small error in either pCO_2 or pH has a large effect on calculated TA and DIC values. This is explained in detail by Cullison Gray et al. (2011).

In case study 3 the CO_2-carbonic acid system was not over-constrained and therefore TA and DIC

calculated from the pH–pCO_2 pair (Table 2.9) were compared to measured TA and DIC from bottle samples collected at CRIMP-2 between 2010 and 2016 (Table 2.7). The standard deviation of the mean was 112 for calculated TA (pH–pCO_2) (Table 2.9), but only 31 for measured TA (Table 2.7), which is a 3.5-fold difference in the standard deviation. The standard deviation of the mean for calculated DIC (pH–pCO_2), was 88 (Table 2.9), but only 39 for measured DIC (Table 2.7), which is a 2.3 fold difference in the standard deviation. To compare, the standard deviation of the mean measured pCO_2 in Tables 2.7 and 2.9 only differs by 12%. In summary, TA and DIC values calculated from the pH–pCO_2 pair span a much greater range than measured TA and DIC, as indicated by the difference in the standard deviations. This large spread in calculated TA and DIC data indicates that the pH–pCO_2 pair is not well suited for calculating the CO_2-carbonic acid system.

2.4.2 Ω_{Ar} calculations

The use of the pCO_2–pH pair in CO_2-carbonic acid system calculations creates large uncertainties and inaccurate values for TA and DIC (Fig. 2.4), but aragonite saturation state (Ω_{Ar}) calculations are not affected in the same way (Fig. 2.5). The Ω_{Ar} values calculated as a function of each pair of input parameters were all within 5% of each other, which corresponds to a difference of 0.14 in Ω_{Ar}. (Table 2.6). Because the Ω_{Ar} is directly proportional to the carbonate ion concentration (CO_3^{2-}, Eq.2.9), and CO_3^{2-} is only a small portion (~1%) of the total CO_2 (DIC) at the average pH of seawater (~8), small errors in pH and pCO_2 do not affect CO_3^{2-} as much as they affect DIC (e.g. Cullison Gray et al. 2011). The average Ω_{Ar} in our diurnal experiment was 2.92 ± 0.05 (case study 1, Table 2.4), which is close to the value of 2.84 reported by Shamberger et al. (2011) for Ω_{Ar} of the Kaneohe Bay barrier reef in winter, and is within the 95 % confidence interval of our Ω_{Ar} estimate (95% CI= 2.82 – 3.02)[1].

[1]The 95 % confidence interval (CI) was defined as the mean ± 1.96 times the standard deviation

2.4.3 Calculations of pCO_2 and Ω_{Ar} from the TA–DIC pair

The TA–DIC pair caused the greatest offset in Ω_{Ar} (5%), relative to Ω_{Ar} calculated from the DIC–pCO_2 pair, which is still quite small (Table 2.6). The use of the TA–DIC pair also produces the largest offset in pH and pCO_2 compared to the use of other pairs in our diurnal experiment (Fig. 2.3 and Table 2.6). Calculations from TA–DIC tend to underestimate measured pCO_2 and overestimate measured pH. It is well known that TA–DIC is not the ideal pair for CO_2-carbonic acid system calculations, especially if a measure of pCO_2 is required (Dickson & Riley 1978; Millero 2007). Patsavas et al. (2015) examined the internal consistency of the CO_2-carbonic acid system during two cruises off the west coast of the U.S. near the aragonite saturation horizon ($\Omega_{Ar} \approx 1$). They found differences in Ω_{Ar} on the order of 10% based on the use of the TA–DIC pair relative to the pH–DIC, pCO_2–DIC, and pCO_2–pH pairs. A 10% difference near the saturation horizon can be the difference between supersaturated or undersaturated (i.e., dissolution of aragonite minerals) and the authors stress the importance of including either pH or pCO_2 in Ω_{Ar} calculations. Although most coral reefs are highly supersaturated with respect to aragonite (Kleypas et al. 1999b), an accurate calculation of Ω_{Ar} is important. If possible, pH or pCO_2 should be included in the calculations. Currently, however, most coral reef CO_2-carbonic acid system experiments use the TA–DIC pair to calculate pH, pCO_2, and Ω_{Ar} (e.g. Shamberger et al. 2011; Albright et al. 2013; Shaw & McNeil 2014; Venti et al. 2014; Yeakel et al. 2015). Perhaps TA–DIC has been the pair of choice because it has been recommended in the guide to best practices for OA research and data reporting (Riebesell et al. 2010). There are some distinct advantages to measuring TA and DIC: samples can be stored for later analysis; the analytical methods with CRM's are highly developed (Dickson et al. 2007); and DIC and TA are state variables (independent of SST and pressure) that often can be used to separate the influence of biogeochemical processes from physical mixing.

2.4.4 Organic contribution to Total Alkalinity

The internal consistency between measured pCO_2 and pCO_2 calculated from the TA–DIC pair was different at each $MAPCO_2$ buoy site; the offset between measured and calculated values seems to increase at sites with greater biological productivity. For example, Kilo Nalu largely reflects open ocean conditions, and has less biological productivity than Ala Wai and CRIMP-2, and shows the greatest internal consistency (4% offset, table 2.8). Ala Wai is subject to land-derived inputs of nutrients and organic matter, which increase productivity relative to Kilo Nalu, and slightly decrease the internal consistency (5% offset). CRIMP-2 is a shallow reef environment with much greater productivity as well as calcification than the other sites, and has the lowest internal consistency (9% offset).

The observed offsets between calculated and measured values of pCO_2 mentioned above could be due to inaccuracies in the analytical measurements of DIC and TA. From the diurnal time-series of TA and DIC (Figure 2.4), it is evident that calculated values generally underestimate the measured TA — the curve of measured data (blue curve) is above the calculated data— and the calculations generally overestimate measured DIC. It is worth noting that this is not true for calculations from the pCO_2–pH pair, which follow no particular trend and have large error bars. If the calculated DIC values are correct, this would imply that measured DIC is systematically too low. Incomplete titration of the carbonate species in the water samples could cause low values for measured DIC. Although this is a plausible explanation from an analytical point of view, our sample data are verified with CRM's that are accurate to ± 1 µmol kg^{-1}. Unless CRM's are systematically off, which is not likely, DIC should not be underestimated in our measurements.

Measured TA could be overestimated in the analytical measurement; if there are proton acceptors (weak bases) present in the seawater sample that are not accounted for in the CO2SYS calculation, the alkalinity of these proton acceptors will be attributed to CO_2-carbonate system species. As described in the introduction of this chapter, HCO_3^- and CO_3^{2-} are the main proton acceptors in seawater. Boric acid

($B(OH)_3$), borate ($B(OH)_4^-$), hydroxide (OH^-), and conjugate bases of phosphoric acid and nitrate also contribute significantly, and are taken into account in the CO2SYS calculation. The concentrations of other (organic) weak acids and bases in seawater are assumed to be negligible. If the weak bases are not negligible, they will be titrated and their alkalinity is attributed to the main proton acceptors of the carbonate system, HCO_3^- and CO_3^{2-}. This results in an overestimation of measured Carbonate Alkalinity. CRM's do not correct for the presence of these species because CRM's are made from open-ocean water with negligible concentrations of additional acid-base species. Based on the diurnal experiment (case study 1), and the fact that the internal consistency decreases with increasing biological productivity at the study sites (case study 2), it could be concluded that inconsistencies in the CO_2-carbonic acid system calculations are due to inaccurate CA based on measured TA, and attributable to unidentified proton acceptors in the samples. It should be noted, however, that the sample size is small, only 12 data points in case study one and 12-34 data points at each site in case study two, and thus more data are needed to test this hypothesis. Yet, other studies have found similar results. Cai and Wang, (1998) found that humic materials can significantly affect total alkalinity in different estuarine waters in Georgia (USA). Kim et al. (2006) found that active surface sites (proton acceptors) on phytoplankton and bacteria added up to 5 µmol kg^{-1} to TA for unfiltered samples. In the Northern Gulf of California, organic base concentrations of greater than 50 µmolkg^{-1} were found (Hernández-Ayon et al. 2007). Helmuth et al. (2016), in their internal consistency study of the North Sea CO_2-carbonic acid system, observed a lower internal consistency of CO_2-carbonic acid system data in water with a higher fraction of Baltic seawater compared to open ocean water, and they attributed this to the high contribution of organic alkalinity in Baltic seawater, which is not accounted for in the CO_2-carbonic acid system calculations.

2.5 Conclusion and recommendations

CO_2-carbonic acid system calculations are least accurate (greatest difference between calculated and measured values) when the pCO_2–pH pair is used as input parameters due to their high co-variance. TA and DIC should therefore not be calculated from the pCO_2–pH pair. However, calculations of Ω_{Ar} are much less sensitive to pCO_2–pH errors and could potentially be made reliably from autonomous pCO_2–pH data. Unfortunately, pH and pCO_2 are the only parameters currently measured autonomously on a routine basis, and often are the only CO_2-carbonic acid system data available; yet TA and DIC should not be calculated from these parameters.

Calculations of pCO_2 (and Ω_{Ar}) are least accurate when the TA–DIC pair is used; therefore this pair is not well suited to "validate" autonomously measured pCO_2 data. Instead, pH (ideally measured spectrophotometrically) should be included in the calculation for "validating" autonomous pCO_2 data. Besides the pCO_2–pH or TA–DIC pairs, any other combination of two parameters results in reliable CO_2-carbonic acid system calculations.

The "best" pair of input parameters depends on the sampling location and the analytical instrumentation available. In an environment with terrestrial input or high productivity, DIC should be used instead of TA, because unknown organic acid-base species could negatively affect the TA measurement, and DIC should be used. Potentiometric pH measurements are prone to the drift of electrodes, and unless pH can be measured spectrophotometrically, pCO_2 (even autonomous) is probably more accurate. For sampling at our study sites, the pCO_2–DIC pair is recommended for the above reasons. To verify the autonomous pCO_2 data, DIC with spectrophotometric pH is the preferred pair of measured parameters. The quality and reliability of the autonomous pCO_2 data as well as other CO_2-carbonic system data (pH, TA, and DIC) collected by our research group was examined in Chapter 2.

This investigation of the CO_2-carbonic acid system data collected by our research group has improved our understanding these data as well as the associated uncertainty. Seawater pCO_2 trends on

Hawaiian coral reefs are discussed in the next chapter. Here we showed that the autonomous pCO_2 data, collected using the LICOR sensors on the $MAPCO_2$ system, are accurate and reliable.

CHAPTER III: CLIMATOLOGY AND TRENDS OF SEAWATER CO_2 DYNAMICS ON HAWAIIAN CORAL REEFS

3.1 Introduction

Since the start of the industrial revolution, atmospheric CO_2 concentrations have been increasing steadily from 280 ppm in preindustrial times and now exceed 400 ppm (Keeling et al. 1976; Keeling et al. 2001; Bender et al. 2005; Tans & Keeling 2016). Through the process of air-sea gas exchange, the oceans take up approximately one-quarter of the anthropogenic CO_2 emissions and have taken up about 50% of total emissions since the industrial revolution (Keeling & Garcia 2002; Takahashi et al. 2002; Gloor et al. 2003; Quay et al. 2003; Bender et al. 2005; Lerman & Mackenzie 2005). The trend of rising atmospheric CO_2 concentrations has been well documented for several decades now in multiple locations (Keeling et al. 1976; Thoning et al. 1989; Keeling et al. 2001; Chamard et al. 2003), but the uptake of CO_2 by the ocean, and subsequent decrease in seawater pH (Ocean Acidification, OA), and the consequences for the marine environment have only more recently become a topic of study (Kleypas et al. 1999; Caldeira & Wickett 2003; Hoegh-Guldberg et al. 2008; Doney et al. 2009; Dore et al. 2009; Andersson & Gledhill 2013). Although we now have good high temporal resolution records of the atmospheric CO_2 concentrations, high-resolution monitoring of the seawater CO_2-carbonic acid system is still in its nascent stages (See NOAA/PMEL CO_2 monitoring program). Additionally, work to date (Drupp et al. 2011; Yan et al. 2011; Massaro et al. 2012; De Carlo et al. 2013; Bates et al. 2014; Shaw & McNeil 2014; Sutton et al. 2014; Yan et al. 2016) has shown that, in order to characterize short-term variability and identify long-term trends, it is necessary to gain better insight into the processes that control marine CO_2 concentrations, hence the direction and magnitude of the air-sea CO_2 flux.

Although there has been abundant research to date on air-sea CO_2 gas exchange rates and air-sea CO_2 fluxes in the open ocean (Key et al. 2004; Sabine et al. 2004; Feely et al. 2008; Lenton et al. 2013; Sarma et al. 2013; Ishii et al. 2014), coastal systems remain relatively understudied. Quantifying air-sea CO_2 fluxes in the coastal ocean and, in particular in coral reef ecosystems, is much more difficult than in the open ocean due to a variety of factors. One important reason is the high temporal variability of the CO_2-carbonic acid system parameters in coastal systems that is often associated with rapid changes in other water quality parameters (e.g. Drupp et al. 2011; Shamberger et al. 2011; Drupp et al. 2013). Although great strides have been made over the past few years in adding time-series stations in coral reefs and other coastal environments, there are still only a relatively small number of sites that have successfully monitored current biogeochemical conditions in waters on coral reefs for extended periods of time, making it difficult to attribute observed changes to OA.

In an effort to characterize coastal and open ocean CO_2 dynamics on short and long time scales, the NOAA Pacific Marine Environmental Laboratory (PMEL) developed a global network of carbon dioxide time-series observing stations. Moored Autonomous CO_2 platforms ($MAPCO_2$ buoys) were deployed at various open ocean locations in the Pacific, Atlantic, and the Indian Ocean, to measure atmospheric boundary layer and surface ocean pCO_2 at a three hour resolution, leading to a better understanding of CO_2 dynamics (temporal and spatial CO_2 variability and the processes affecting this) in such open ocean environments (Sutton et al. 2014; http://www.pmel.noaa.gov/co2/story/Buoys+and+Autonomous+Systems). Late in 2005, NOAA/PMEL and University of Hawaii scientists teamed up to establish the first coastal $MAPCO_2$ monitoring station in Kaneohe Bay. A buoy was deployed in southern Kaneohe Bay and dubbed the Coral Reef Instrumented and CO_2 Monitoring Platform (CRIMP-CO_2). Since that time our collaborative group has deployed three $MAPCO_2$ buoys on different coral reef sites, and a fourth $MAPCO_2$ buoy just offshore of Kaneohe Bay, Oahu, Hawaii. The buoys are equipped with instruments that collect high temporal resolution CO_2 and water quality data that are suitable for time-series analysis to assess the scales over which these

biogeochemical parameters vary. The array for four $MAPCO_2$ buoys around Oahu provides a unique opportunity to assess the influence of local climatic, geographic, and biogeochemical differences on CO_2 dynamics. Another mooring operated by the Woods Hole Oceanographic Institution (WHOI) was deployed in July 2007, 100 km North of Oahu, near the HOT site, where ocean observations have been made for over 25 years. The data acquired between 2008 and now at the coastal sites allow a realistic comparison between coastal ocean CO_2 dynamics and those in the North Pacific Subtropical Gyre.

The biogeochemistry of Hawaii's coastal waters is strongly influenced by land-derived nutrient inputs (e.g. Ringuet & Mackenzie 2005; Hoover et al. 2006; De Carlo et al. 2007) which drive primary productivity and impact the CO_2-carbonic acid system parameters (e.g Shamberger et al. 2011; Drupp et al. 2011, 2013; Massaro et al. 2012). After rain storms, freshwater with a high nutrient content enters coastal waters, typically causing increased phytoplankton growth and subsequently leading to a drawdown of pCO_2 (Fagan & Mackenzie 2007; Drupp et al. 2011; Massaro et al. 2012). Intense rainfall episodes can also deliver dissolved and particulate organic matter, which through enhanced microbial respiration, increases pCO_2 as well as nutrient concentrations in bay waters. In the latter case, extended plankton blooms can be triggered, with their duration depending partly on physical processes such as water residence time and mixing (e.g. De Carlo et al. 2007; Tomlinson et al. 2011) and biotic effects such as predation (e.g. Hoover et al. 2006). Hawaii's first $MAPCO_2$ buoy was originally deployed in Southern Kaneohe Bay (CRIMP http://www.pmel.noaa.gov/co2/story/crimp) near Lilipuna from November 2005 through June 2008 (Drupp et al. 2011; Massaro et al. 2012). In June 2008, the CRIMP buoy was relocated from its relatively deep lagoon site in Southern Kaneohe Bay to a shallow location along the landward edge of the barrier reef in the central part of the bay (CRIMP-2, Figure 3.1b, http://www.pmel.noaa.gov/co2/story/CRIMP-2). Two other moorings were also installed at the same time off Honolulu on Oahu's south shore (Fig. 3.1c). One buoy was placed several hundred meters offshore of the outlet of the Ala Wai canal (Ala Wai http://www.pmel.noaa.gov/co2/story/Ala+Wai), the other, dubbed Kilo Nalu, was placed at a similar distance offshore of Kewalo Basin

(http://www.pmel.noaa.gov/co2/story/Kilo+Nalu). Drupp et al. (2013) described CO_2 dynamics and variations in water quality over three years at these locations (Ala Wai, Kilo Nalu, and CRIMP-2). In 2011, an additional $MAPCO_2$ buoy was deployed outside of the barrier reef of Kaneohe Bay, Oahu (Kaneohe http://www.pmel.noaa.gov/co2/story/Kaneohe). Because this buoy has only provided limited data so far, largely owing to several relatively long periods during which it was subjected to repairs and an inability to return it to operation due to weather, no data from this station will be described in this thesis.

This chapter builds on prior work by our research group and utilizes an additional four years of data that have not been previously described to develop a climatology and carry out more extensive data and trend analysis. Our stations represent the longest running nested $MAPCO_2$ time series dataset in coastal waters of our planet. The nearly eight years of high-resolution data are sufficient to begin to develop a detailed description and statistical analysis of the variability of seawater CO_2 and the water quality of Oahu's coastal waters. Additionally, a comparison can now be made between CO_2 dynamics at the coral reef $MAPCO_2$ buoys, and the open ocean WHOTS buoy, located in the North Pacific Subtropical gyre. The results of this study contribute to our understanding of the behavior of the tropical coastal ocean with respect to the CO_2-carbonic acid system and provide a basis to begin to define the coastal CO_2 budget regionally and globally. Additionally, it is anticipated that our observations and interpretation will help agency managers and decision makers by providing a basis on which to help make better coastal resource management decisions.

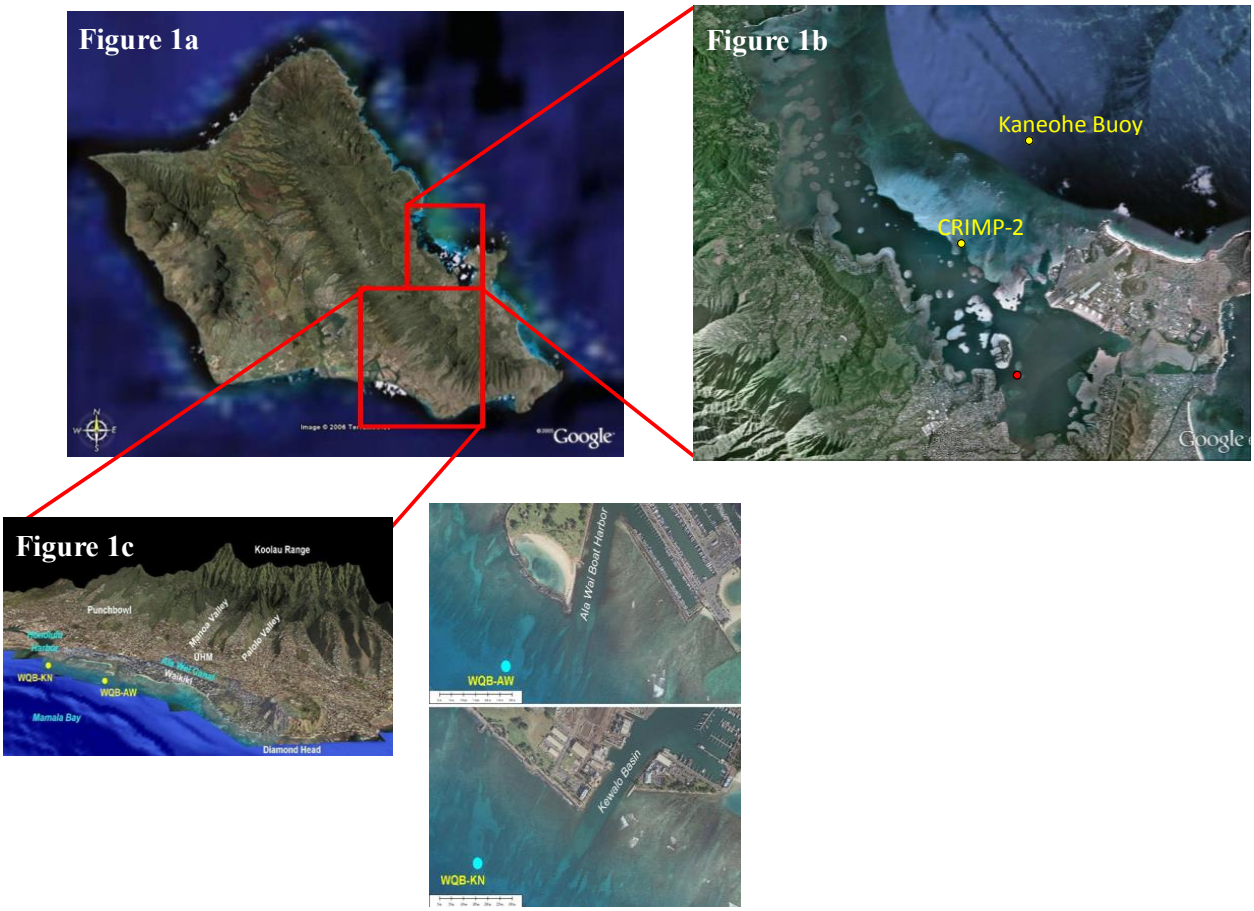

Figure 3.1 The island of Oahu, highlighting Kaneohe Bay on the windward (east) coast and the Honolulu watershed on the southern coast; b) Kaneohe Bay, highlighting the CRIMP-2 buoy on the back reef and the new Kaneohe buoy on the deeper fore-reef; c) Two buoys are located 200 m offshore of urban Honolulu above fringing reefs. Ala Wai buoy (AW) is located near the mouth of the Ala Wai canal, which drains the Honolulu city watersheds. Figure by Pat Drupp.

3.2 Methods

3.2.1 Environmental setting

The CRIMP-2 buoy was deployed in June 2008. It is located above a sandy bottom in three meters of water depth on the landward edge of the barrier reef of Kaneohe Bay (Fig. 3.1b). Kaneohe bay is the largest semi-enclosed water body on Oahu and is located on the windward side of the island, where northeasterly trade winds blow most of the year (Giambelluca et al. 2013). The entire bay is relatively

shallow, with a mean depth of 9.5 m, and the depth of the barrier reef is quite variable with a significant area characterized by approximately 2 m water depth. Water at the CRIMP-2 location is characterized by relatively long water residence time (hours to days), compared to water from the two locations on the south shore of Oahu. Water reaching the CRIMP-2 buoy crosses the barrier reef, enters a deep lagoon and moves back outwards towards through a relatively shallow Sampan Channel (Lowe et al. 2009). A small fraction of the water leaving the bay through this channel during outgoing tides can be recirculated over the barrier reef, depending on wind and wave conditions (e.g. Lowe et al. 2009). Two other buoys are located near fringing reefs offshore of Honolulu in Mamala Bay on the south shore of Oahu (Fig. 3.1c). Compared to the CRIMP-2 location, this coastline is relatively unprotected, is affected significantly by tides and winds, and is also directly exposed to open ocean swells from the south, especially during the spring and summer. The water on the reefs is thought to have a short residence time and exchanges freely with the open ocean. The Kilo Nalu buoy (WQB-KN in Fig. 3.1) offshore of Kewalo Harbor is not directly affected by stream input, although urban runoff enters the coastal zone in this area through multiple storm drains and via overland runoff. The other mooring on the south shore of Oahu, the Ala Wai buoy (WQB-AW in Fig. 3.1) is located several hundred meters offshore the mouth of the Ala Wai Canal and receives both direct urban runoff as well as a significant discharge from several streams draining into the canal that often contains high nutrient and sediment loads (e.g Carlo et al. 2004; Tomlinson et al. 2011).

The Woods Hole Oceanographic Institution (WHOI) Hawaii Ocean Time Series station buoy (WHOTS) is an open ocean MAPCO$_2$ system located approximately 100 km north of Oahu. The WHOTS buoy is co-located with the Hawaii Ocean Time-series (HOT) site (http://uop.whoi.edu/projects/whots/whots.html). The primary intent of the WHOTS station is to provide long-term, high-quality air-sea CO_2 fluxes as a coordinated part of the HOT program and contribute to the HOT goals of observing heat, momentum, fresh water and chemical fluxes at a site representative of the oligotrophic North Pacific Ocean. Ocean acidification has been well documented at this site by Dore et al.

(2009) and this mooring serves as a deep ocean reference site for the current study because its chemistry is largely unaffected by coastal processes.

3.2.2 Measurements

All buoys are equipped with a LICOR-820 infrared (IR) sensor to measure CO_2. Besides the CO_2 analyzer, the CRIMP-2 buoy has a MaxtechMax-250 series sensor to measure dissolved oxygen (DO), a Sensiron humidity sensor, and a Sea-Bird Electronics 37 SMP (SBE 37), collecting data at 3-hour intervals (Drupp et al. 2013; Massaro et al. 2012). The Ala Wai and Kilo Nalu buoys also have a Sea-Bird Electronics SeaCat16 v2plus instead of an SBE 37. This instrument measures sea surface temperature (SST), conductivity (salinity), DO, chlorophyll-a, and turbidity at 20-minute intervals. More recently, the buoys have also been equipped with SeaFET pH meters, although insufficient data currently exist to carry out time-series analysis of this parameter. The WHOTS buoy is equipped with a Microcat temperature and conductivity sensor, and a humidity sensor.

Discrete water samples were collected at the buoy sites (Ala Wai, Kilo Nalu, CRIMP-2) at various times between 2010 and 2016, and analyzed for Total Alkalinity (TA) and Dissolved Inorganic Carbon (DIC) following methods described by Dickson et al. (2007).

3.2.3 Ancillary data

Wind data needed for air-sea CO_2 flux calculations were obtained from various sources. Data for the south shore buoys were obtained from NOAA - National Ocean Service Station OOUH1 in Honolulu. Wind data for the CRIMP-2 buoy were obtained from the Hawaii Institute for Marine Biology weather station on Moku o Loʻe (Coconut Island) in South Kaneohe Bay. Wind data for the WHOTS buoy are collected on site by an ASIMet logger. Pacific Decadal Oscillation data are from (https://www.ncdc.noaa.gov/teleconnections/pdo/), North Pacific Gyre Oscillation data are from

(http://www.o3d.org/npgo/npgo.php), and the Nino 3.4 SST anomalies are from (http://www.esrl.noaa.gov/psd/data/correlation/nina34.datal).

3.2.4 Calculations

The pCO_2 of air and seawater is calculated from the LICOR-820 CO_2 data (dry xCO_2) following the method of Weiss & Price (1980). Air-sea CO_2 fluxes are calculated from the gas transfer (or piston) velocity (Ho et al. 2006) and the air-sea pCO_2 difference (Weiss 1974; Liss 1983; Wanninkhof 1992). Air-sea fluxes were determined according to equation 3.1.

(3.1) $$F = k \alpha \Delta pCO_2,$$

where k is the gas transfer velocity, α is the solubility of CO_2 in seawater at a specified salinity and SST, and Δ pCO_2 the difference between seawater and air pCO_2 concentrations. The wind speed parameterization of Ho et al. (2006) was used to calculate the gas transfer velocity k (Eq. 3.2)

(3.2) $$k(600) = 0.266 (U_{10})^2,$$

where the k(600) coefficient is a scaling factor for the gas transfer velocity and U_{10} is the wind speed at 10 m altitude above the water surface. The uncertainty in the flux (1 SD) was calculated by error propagation of 2 µatm uncertainty in the pCO_2 measurement (Sutton et al. 2014) and an uncertainty of 0.019 in the gas transfer velocity k (Ho et al. 2006). In order to remove the SST effect from the observed pCO_2, the observed values were normalized to the mean pCO_2 at each buoy over the full study period, using Equation 3.3. The effect of SST changes on pCO_2 has been computed by perturbing the mean annual pCO_2 with the difference between the mean and observed SST (Takahashi et al. 2002)

(3.3) $$pCO_2n = pCO_{2obs} * \exp (0.0423 * (T_{mean} - T_{obs})),$$

where T is the SST in °C and the subscripts ‘‘mean’’ and ‘‘obs’’ indicate the annual average and observed values, respectively. Monthly climatologies were made separating data collected during the study period based on the month, and these were visualized in box plots using the MATLAB “box plot” function. Weekly and monthly means were estimated by applying a moving average filter to the data (MATLAB’s

"smooth" function: A lowpass filter with filter coefficients equal to the reciprocal of the span), smoothing 56 and 240 data points for weekly and monthly averages, respectively. Anomalies of monthly mean pCO_2sw were calculated by subtracting the climatological monthly mean over the entire study period from the mean of that particular month (no filter, actual mean).

3.3 Results

3.3.1 Eight year time-series dataset at CRIMP-2, Ala Wai, Kilo Nalu, and WHOTS

Seawater pCO_2

Figure 3.2 displays seawater pCO_2 (pCO_2sw) over the study period from June 2008 through March 2016. The top panel shows the pCO_2sw at all four sites, and the bottom panel shows the same data for Kilo Nalu and WHOTS on a y-axis that spans a smaller pCO_2sw range. A seasonal trend in pCO_2sw was observed at all buoys with, in general, higher pCO_2sw in summer (May through October) and lower pCO_2sw in winter (November through April). The dashed grey line at 382 µatm in the top Figure represents mean air pCO_2 (pCO_2air) over the study period at all sites. If pCO_2sw is above this line, the site is a source of CO_2 to the atmosphere, and if pCO_2sw is below this line, seawater at the site is a sink for atmospheric CO_2. It should be noted that instantaneous air-sea CO_2 fluxes reported here are calculated from pCO_2air measured at the time of the seawater pCO_2sw measurement, rather than from the mean pCO_2air, and the dashed grey line in Figure 3.2 serves as an average boundary between source and sink behavior. Figure 3.2 and Table 3.1 also illustrate the differences in short-term (diurnal) variability between sites. At the CRIMP-2 site, diurnal pCO_2sw variability is greatest but considerably reduced variability is observed at the Ala Wai and Kilo Nalu sites. Compared to these coastal sites, however, diurnal pCO_2sw variability at the open ocean WHOTS buoy is minimal.

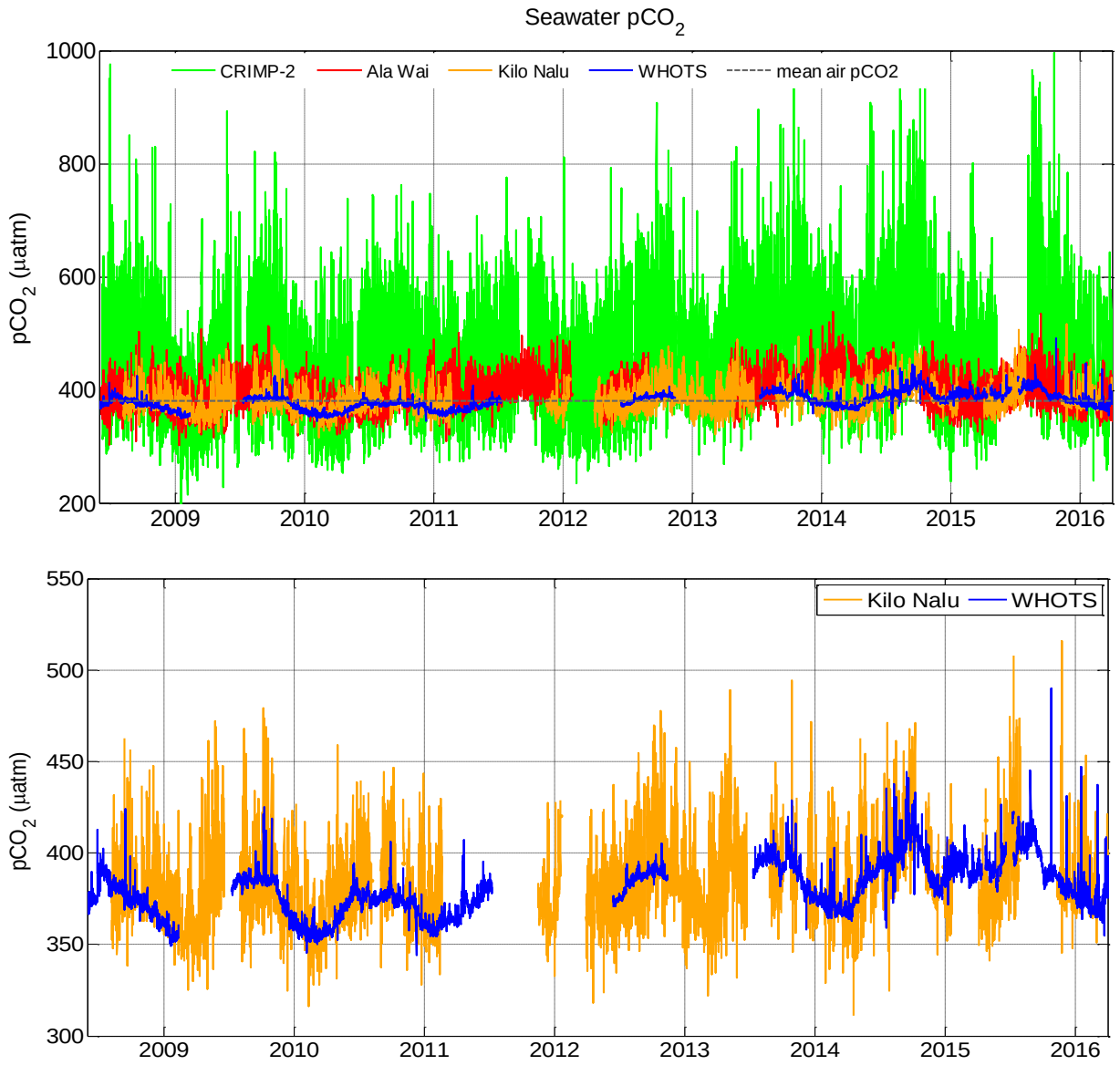

Figure 3.2 Time-series of in situ (3-hourly) pCO_2sw at CRIMP-2, Ala Wai, Kilo Nalu, and WHOTS from June 2008 through March 2016 (top). Mean air pCO_2 is represented by the dashed grey line at 382 µatm, to indicate whether the site was a source or a sink for atmospheric CO_2. The bottom Figure shows the same time-series for Kilo Nalu and WHOTS only, on a y-axis with a smaller range of pCO_2sw.

Table 3.1 summarizes the descriptive statistics of pCO_2sw at each site. Average pCO_2sw values at CRIMP-2, Ala Wai, Kilo Nalu, and WHOTS were 460 ± 91, 397 ± 29, 384 ± 19, and 379 ± 14 µatm, respectively. At CRIMP-2, the mean pCO_2sw was at least 60 µatm higher than at the other sites. The

greater variability at CRIMP-2 compared to the other sites is evident from the range and standard deviation shown in Table 3.1. For example, the overall range of pCO_2sw values at CRIMP-2 (801 µatm) is more than three times greater than at Ala Wai (249 µatm) and Kilo Nalu (205 µatm), and nearly eight times greater than at WHOTS (102 µatm). Mean pCO_2sw at WHOTS is only 5 µatm lower than at Kilo Nalu but the range of pCO_2 at Kilo Nalu is almost twice as large as that at WHOTS. Minimum observed pCO_2sw values at Ala Wai and Kilo Nalu only differ by 6 µatm, but the mean and maximum at Ala Wai are 15 and 33 µatm greater, respectively.

To evaluate short-term variability and elucidate its causes, the diurnal range (maximum – minimum value on a specific day) of pCO_2sw was calculated for each day at all sites (Table 3.2). The mean diurnal ranges in pCO_2 were 194, 51, 31, and 6 µatm at CRIMP-2, Ala Wai, Kilo Nalu, and WHOTS, respectively. The mean diurnal range at CRIMP-2 was nearly four times as large as at Ala Wai and Kilo Nalu, and more than an order of magnitude greater than at WHOTS.

pCO_2 (µatm)	Min	Max	Mean	Standard Deviation	Range
CRIMP-2	196	997	460	91	801
Ala Wai	300	549	397	29	249
Kilo Nalu	306	516	384	19	210
WHOTS	344	446	379	14	102

Table 3.1 Descriptive statistics for seawater pCO_2 at CRIMP-2, Ala Wai, Kilo Nalu, and WHOTS for the entire study period (June 2008 through March 2016).

Diurnal Range pCO_2 (µatm)	Min	Max	Mean	Standard Deviation
CRIMP-2	20.0	556	194	78
Ala Wai	0.20	146	51	22
Kilo Nalu	0.25	124	31	20
WHOTS	0.23	103	6	6

Table 3.2 Descriptive statistics for seawater pCO_2 at CRIMP-2, Ala Wai, Kilo Nalu, and WHOTS for the entire study period (June 2008 through March 2016). Diurnal range is defined as the maximum – minimum

To provide a sense of biogeochemical and physical conditions at each site, Table 3.3 presents the mean values for a series of water parameters; these include SST, sea surface salinity (SSS), pCO_2sw, pCO_2air, the air-sea CO_2 difference (ΔpCO_2 = pCO_2sw- pCO_2air), wind speed (U10), and air-sea CO_2 fluxes (Flux).

Mean SST values were similar at all sites — 25.2°C at CRIMP-2 and WHOTS, and 25.5°C at Kilo Nalu and Ala Wai — although the variability of SST (as expressed by the standard deviation of the mean) was greater at CRIMP-2 (1.6°C) than at WHOTS, Ala Wai, or Kilo Nalu (1.1-1.2°C). Mean SSS was highest at WHOTS (35.2 PSU) and lowest at Ala Wai (34.9 PSU). The standard deviation was much greater at CRIMP-2 (0.6 PSU) compared to Kilo Nalu, WHOTS (0.2 PSU) and Ala Wai (0.3 PSU). Mean pCO_2air was 381 µatm at CRIMP-2 and WHOTS, and 382 µatm at Ala Wai and Kilo Nalu. These values are identical within the uncertainty of the measurement (± 2 µatm). Mean ΔpCO_2 between air and seawater was greatest at CRIMP-2 (80 µatm) owing to the significantly higher pCO_2sw at this site. Mean ΔpCO_2 was negative at WHOTS (-2.7 µatm), near zero at Kilo Nalu (1.4 µatm), but positive at Ala Wai (14 µatm). Mean wind speed at Ala Wai and Kilo Nalu — on the leeward side of the island — was relatively low and consistent (2.3 ± 1.3 ms^{-1}). Note that the wind speed is identical at these sites because of the use of a single source of weather data for the South Shore sites. At CRIMP-2 — on the windward side of the island — mean wind speed was twice as high as on the leeward side and much more variable

(5.1 ± 2.5 ms^{-1}). The mean wind speed was greatest at the open ocean WHOTS site (6.6 ms^{-1}). Air-sea CO_2 fluxes, driven by ΔpCO_2 and wind speed, are discussed in the next section.

	SST	SSS	pCO_2air	pCO_2sw	ΔpCO_2	U10	Flux
CRIMP-2	25.2 ± 1.6	35.0 ± 0.6	381 ± 9	460 ± 91	80 ± 91	5.1 ± 2.5	1.236 ± 2.29
Ala Wai	25.5 ± 1.1	34.9 ± 0.3	382 ± 9	397 ± 29	14 ± 29	2.3 ± 1.3	0.046 ± 0.24
Kilo Nalu	25.5 ± 1.2	35.1 ± 0.2	382 ± 10	384 ± 19	1.4 ± 22	2.3 ± 1.3	0.000 ± 0.21
WHOTS	25.2 ± 1.2	35.2 ± 0.2	381 ± 7	379 ± 14	-2.7 ± 14	6.6 ± 2.1	-0.169 ± 0.57

Table 3.3 Descriptive statistics (mean ± 1 standard deviation) of SST (˚C), SSS, air and seawater pCO_2 (µatm), ΔpCO_2 ($pCO_2sw - pCO_2air$, in µatm), wind speed (U10 in ms^{-1}), and air-sea CO_2 flux (Flux in mol C m^{-2} yr^{-1}) at CRIMP-2, Ala Wai, Kilo Nalu, and WHOTS from June 2008 through March 2016.

Air-Sea CO_2 fluxes

Figure 3.3 displays instantaneous air-sea CO_2 fluxes in units of mol C m^{-2} yr^{-1} from June 2008 through March 2016. A positive value indicates that seawater is a source of CO_2 to the atmosphere and vice versa. The top panel of Figure 3.3 shows fluxes at all four sites, and the bottom panel shows only the Kilo Nalu and WHOTS data, plotted for ease of view on a y-axis that spans a smaller range of air-sea CO_2 fluxes. A seasonal trend is observed at all sites with, in general, more positive flux values in summer. The seasonal cycle is most pronounced at the WHOTS buoy, where the flux is consistently positive in summer and becomes negative in winter. Average air-sea CO_2 fluxes were 1.24 ± 2.29 mol C m^{-2} yr^{-1} at CRIMP-2, 0.05 ± 0.24 mol C m^{-2} yr^{-1} at Ala Wai, 0.00 ± 0.21 mol C m^{-2} yr^{-1} at Kilo Nalu, and -0.17 ± 0.57 mol C m^{-2} yr^{-1} at WHOTS. On average, the sea to air CO_2 flux is positive (source) at CRIMP-2, close to zero at Ala Wai and Kilo Nalu, and negative (sink) at WHOTS. The variability, represented by the standard deviation of the mean, is an order of magnitude greater at CRIMP-2 (2.29) than at Ala Wai (0.24) and Kilo Nalu (0.21). The variability in the flux at WHOTS (0.54) was much lower than at CRIMP-2 but more than twice the variability of Ala Wai and Kilo Nalu.

The estimated annualized air-sea CO_2 fluxes over the entire study period were 1.24 ± 0.07 at CRIMP-2, 0.05 ± 0.02 at Ala Wai, 0.00 ± 0.01 at Kilo Nalu, and -0.17 ± 0.09 mol C m^{-2} yr^{-1} at WHOTS, where the standard deviation represents the uncertainty of the flux estimate, propagated from the uncertainty in the gas transfer parameter (± 0.019) and the pCO_2 measurements (± 2 µatm). Note that the estimated annualized flux is equal to the average flux because the average flux is presented here in units of mol C m^{-2} yr^{-1}.

3.3.2 A closer look at one month of data at the CRIMP-2 site

A one-month period at the CRIMP-2 site was selected from the eight-year dataset, and is described in more detail in this section to illustrate variability in pCO_2 and air-sea CO_2 fluxes on diurnal to weekly time scales. Dissolved Oxygen (DO) and pH data, collected with a SeapHOx as part of a sensor test deployment, were also available for this period. The full dataset of the three-month SeapHOx test deployment can be found in the supplementary material "chapter 2 case study 3". Note that these data were collected in the winter season and that mean values as well as the amplitudes of temporal changes in parameters vary between seasons, but the general diurnal to biweekly pattern is the same throughout the entire study period.

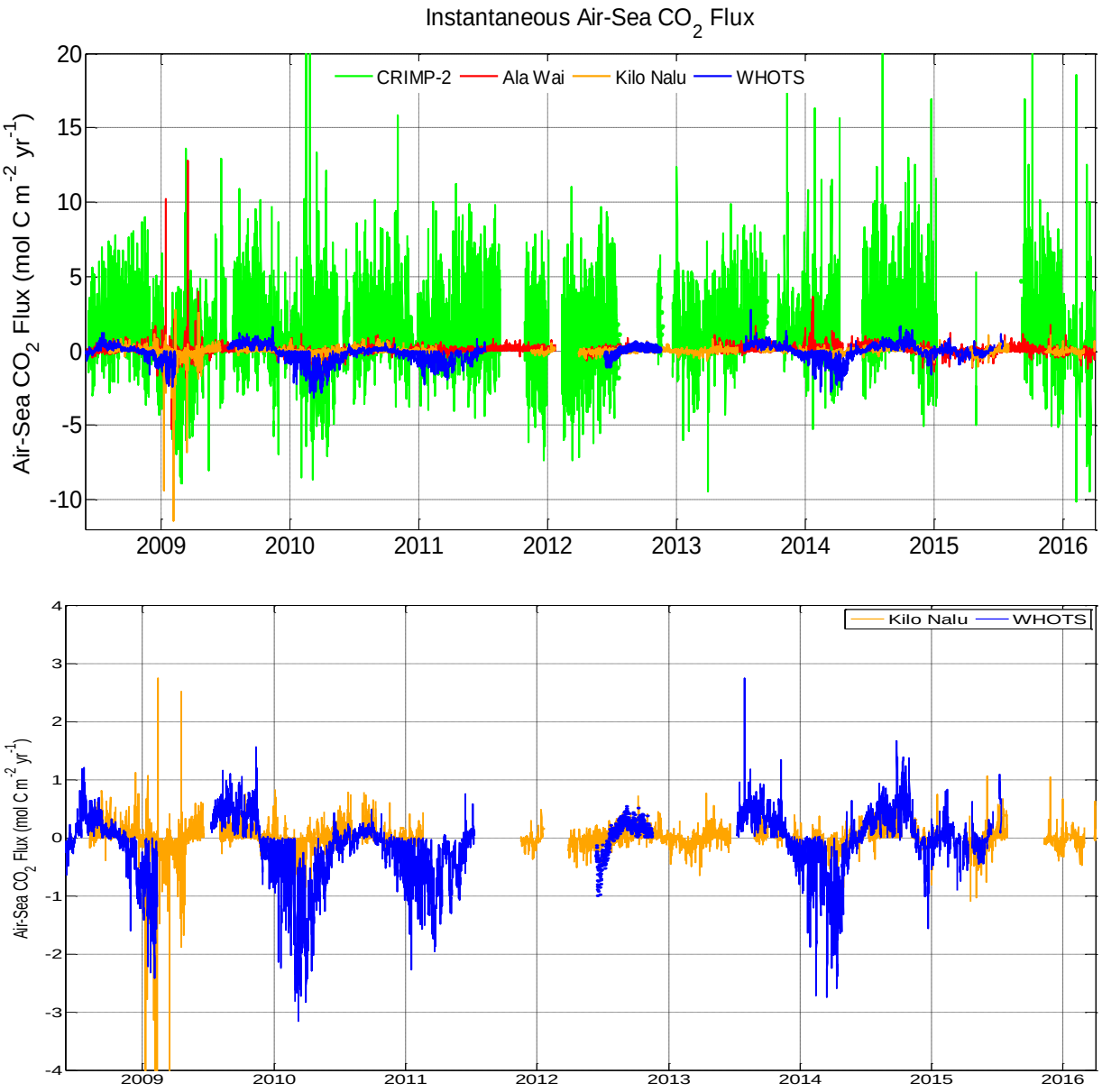

Figure 3.3 Time-series of *in situ* (3-hourly) air-sea CO_2 fluxes at CRIMP-2, Ala Wai, Kilo Nalu, and WHOTS from June 2008 through March 2016 (top) in units of mol C m^{-2} yr^{-1}. Positive values indicate a source of CO_2 to the atmosphere. The bottom Figure shows the same time-series for Kilo Nalu and WHOTS only, on a y-axis with a smaller range of air-sea CO_2 fluxes.

Biweekly scale variability

Figure 3.4 displays tidal range (Tide), pCO_2, pH, DO, DO percent saturation (DO %Sat), SST, and wind speed at the CRIMP-2 site from 19 December 2013 to 18 January 2014. The diurnal range of biogeochemical and physical properties of seawater (pCO_2, pH, DO, and DO%sat) appear to be influenced by the tidal range and the 14-day cycle of neap/spring tides. A smaller diurnal cycle in water properties occurs when the tidal range is greatest (spring tide) and a larger diurnal range of changes occurs during neap tides (small tidal range). DO%sat of seawater fluctuates between super-saturation during the day (>100%) and under saturation during the night, but during spring tide (large tidal range), seawater remains under-saturated the majority of the time. The diurnal SST range was also smaller during spring tide than during neap tide, but there is also lower frequency variability in the SST record. SST decreases gradually from an average daily SST of 25˚C in December to 22.5˚C during the first half of January, and then increases again to approximately 24˚C on 18 January, 2014. Wind speed data did not show a diurnal or biweekly pattern that correlated with the tidal range variability.

Diurnal scale variability

A week-long time-series (Fig. 3.5) at the CRIMP-2 site (23-29 December, 2013) is used to illustrate diurnal variability of pCO_2 (air and seawater), tidal height, SSS, SST, pH, DO, CO_2 flux, and wind speed. Mean diurnal ranges were calculated from the three months of available SeapHOx data: 19 December 2013 to 1 March 2014. Photosynthesis decreases pCO_2sw during the day, while increasing DO and pH. Minimum pCO_2sw was reached at ~ 17:00 hours, and a maximum occurs in the early morning ~ 05:00 hours, with a mean diurnal range of 160 µatm. Compared to pCO_2sw, the diurnal variability in pCO_2air at CRIMP-2 is small, with a mean diurnal range of 12 µatm, and does not follow a distinct diurnal cycle. Hawaii's waters are subject to mixed semi-diurnal tides with a mean tidal range of 1.97 feet. These semidiurnal tides also affect the semidiurnal signal in pH and DO. The mean diurnal ranges of pH and DO were 0.137 and 84 µM, respectively. The mean diurnal range of SSS was 0.41 PSU and did

not correlate with tidal height, nor was there any lagged correlation. Wind speed, although highly variable, generally increases during the day peaking in the early afternoon, and decreases throughout the night, with a mean diurnal range of 4 m s^{-1}. The air-sea CO_2 flux for the study period shows a mean diurnal range of 3.17 mol C m^{-2} yr^{-1} (which corresponds to 8.69 mmol C m^{-2} d^{-1}). As pCO_2sw decreases throughout the day, the flux of CO_2 from seawater to the atmosphere decreases and can even become negative (CO_2 flux from the atmosphere to seawater). The mean SST range is 0.92 ˚C, and SST increases throughout the day and decreases throughout the night.

Correlation among parameters

Table 3.4 shows the Pearson's correlation coefficients (R values) between SSS, SST, pH, DO, pCO_2air, pCO_2sw, CO_2 flux, wind speed (U10), and tidal height at the CRIMP-2 site. These R values are based only on the evaluation of the three months of data collected between 19 December 2013 and 1 March 2014. At CRIMP-2, pCO_2sw correlated strongly with the CO_2 flux (0.77), nearly perfectly anti-correlated with pH (-0.98) and DO (-0.82), and weakly anti-correlated with SST (-0.53). The flux of CO_2 from seawater to the atmosphere is anti-correlated with pH (-0.79), and anti-correlated with DO (-0.67) and SST (-0.61). The pH and DO are highly correlated (0.88).

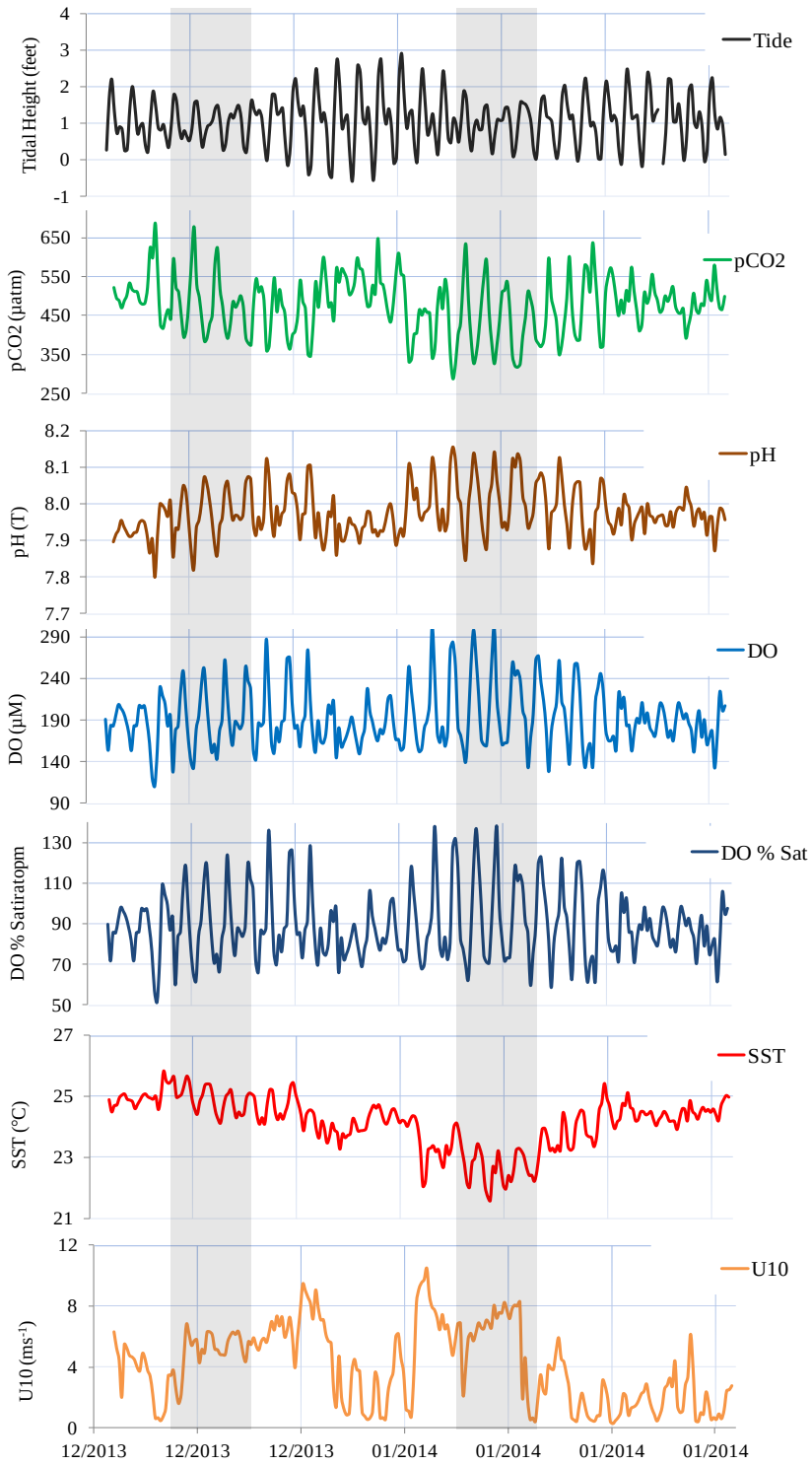

Figure 3.4 A month long time-series — at CRIMP-2 from 19 December, 2013 to 18 January, 2014 — of tidal range (feet), pCO_2sw (uatm), pH (total scale), DO (µmolkg^{-1}), DO%sat (%), SST ˚C, and U10 (ms^{-1}). This figure illustrates the effect of the lunar cycle on the tidal range, which in turn affects the diurnal amplitude of biogeochemical and physical parameters. The shaded regions represent a smaller diurnal tidal amplitude (neap tide).

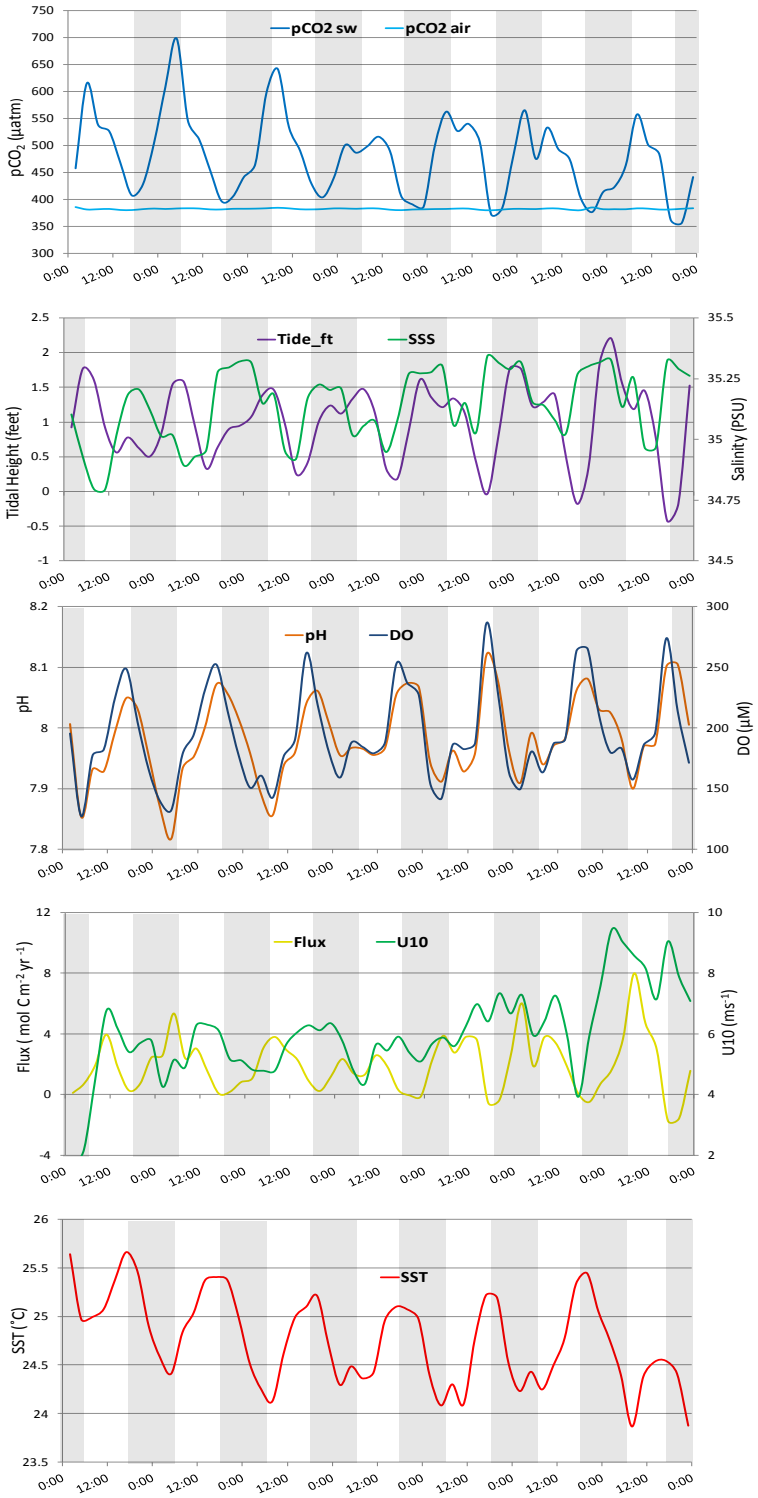

Figure 3.5 A time-series of (from top to bottom) pCO_2 and pCO_2air (µatm), tidal height (feet), SSS, pH, DO (µM), Flux (mol C m^{-2} yr^{-1}), U10 (ms^{-1}), and SST at CRIMP-2 from December 23 to 29, 2013.

	SST	SSS	pH	DO	pCO_2air	pCO_2sw	Flux	U10	Tide_ft
SST	1.00								
SSS	-0.05	1.00							
pH	**0.55**	**0.50**	1.00						
DO	**0.64**	0.25	**0.88**	1.00					
pCO_2air	-0.37	-0.01	-0.38	-0.47	1.00				
pCO_2sw	**-0.53**	-0.49	**-0.98**	**-0.82**	0.37	1.00			
Flux	**-0.61**	-0.33	**-0.79**	**-0.67**	0.29	**0.77**	1.00		
U10	-0.29	0.26	0.26	0.17	-0.19	-0.28	0.21	1.00	
Tide_ft	-0.43	-0.04	**-0.52**	**-0.65**	0.40	0.48	0.46	-0.03	1.00

Table 3.4 Pearson's correlation coefficients (R) between SST, SSS, pH, DO, pCO_2air, pCO_2sw, flux, wind speed (U10), and tidal height at CRIMP-2 from December 19 2013 to March 1 2014.

3.4 Discussion

3.4.1 Diurnal to biweekly variability in pCO_2 and air-sea CO_2 fluxes

Diurnal variability

Diurnal variability in pCO_2sw and the air-sea CO_2 flux are driven by a combination of biogeochemical and physical processes, and the relative importance of these processes can be inferred from the Pearson's correlation coefficients (R values) of the measured parameters with pCO_2sw and the air-sea CO_2 flux (Table 3.4).

The strong anti-correlation between pCO_2sw and DO at the CRIMP-2 site (R = -0.82) indicates that organic carbon metabolism, photosynthesis/respiration, was the main driver of the diurnal pCO_2sw cycle at CRIMP-2, because DO is produced/consumed during these processes. DO is not involved

directly in the inorganic carbon metabolic cycle of calcification/dissolution of calcium carbonate. Day-time photosynthesis decreases pCO_2sw while increasing DO (Fig. 3.5), reaching maximum DO concentrations between 14:00 and 17:00 hrs. Respiration at night increases pCO_2sw, reaching maximum values in the early morning between 04:00 and 07:00 hrs, as previously shown by Drupp et al. (2013). In three 48-hour synoptic studies, Shamberger et al. (2011) showed that calcification is strongly coupled with photosynthesis on the Kaneohe bay barrier reef; the uptake of CO_2 during photosynthesis increases $\Omega_{aragonite}$ during the day, which in turn facilitates calcification. The observed diurnal pCO_2sw cycle is the net effect of photosynthesis/respiration and calcification/dissolution (Kayanne et al. 1995; Kleypas et al. 1999; Drupp et al. 2011; Shamberger et al. 2011; De Carlo et al. 2013). The weaker correlation between pCO_2sw and physical parameters SST (R = -0.53), SSS (R = -0.49), wind speed (R = -0.28), and tidal height (R = 0.48) indicates that physical processes were not the main drivers of diurnal pCO_2sw variability.

The air-sea CO_2 flux (from here on referred to as CO_2 flux) at CRIMP-2 follows the same diurnal pattern as pCO_2sw (Fig. 3.5); increasing (source of CO_2 to the atmosphere) throughout the day and decreasing at night. The CO_2 flux, which is parameterized as a function of ΔpCO_2 (pCO_2sw - pCO_2air) and wind speed, had a strong correlation with pCO_2sw (0.77) but a much weaker correlation with pCO_2air (0.29) and wind speed (0.21) (Table 3.4). These R-values indicate that on diurnal time-scales, pCO_2 is the main driver of flux variability. This can be explained in part by the differences in diurnal variability between pCO_2sw and pCO_2air. For the time period discussed here, the diurnal range of pCO_2sw (160 µatm) is much greater than that of pCO_2air (12µatm), and therefore ΔpCO_2 is determined mainly by pCO_2sw. The negative correlation between wind speed and the CO_2 flux is the result of their opposite diurnal patterns; wind speed generally peaks in the early afternoon and decreases at night, whereas the flux increases at night because pCO_2sw increases. The relatively weak correlation between wind speed and the CO_2 flux is likely due to the following two reasons. First, wind speed affects the rate of gas transfer across the air-sea interface, and thus only the magnitude of the flux. The direction (source or sink

for atmospheric CO_2) is determined by ΔpCO_2. Second, there is significant random variability in wind speed which does not follow a diurnal pattern, and this reduces the strength of the correlation.

Variability in pCO_2sw at the other sites — Ala Wai, Kilo Nalu, and WHOTS — is driven by the same processes as at CRIMP-2, but the diurnal range differs according to local climatic, geographic, and biogeochemical drivers. The mean diurnal ranges of pCO_2sw over the entire study period were 194 µatm at CRIMP-2, 51 µatm at Ala Wai, 32 µatm at Kilo Nalu, and 6 µatm at WHOTS.

Biological productivity is the main driver of diurnal pCO_2sw variability. The CRIMP-2 site is located on the inside edge of the Kaneohe bay barrier reef in ~3 m deep water, and the observed large diurnal pCO_2 fluctuations at this site are due to high rates of photosynthesis, respiration, and calcification on the reef flat. The sites on Oahu's South shore, Ala Wai and Kilo Nalu, are located in ~12 m deep water on sand patches within fringing reefs, about 200 m offshore of the Honolulu coast line (Fig. 3.1). Productivity is significantly lower at these sites and calcification does not appear to play a major role in pCO_2sw variability (Drupp et al. 2013). Biological productivity is strongly affected by the availability of nutrients (and organic matter) for photosynthesis (and respiration) (Ringuet & Mackenzie 2005; Hoover et al. 2006; De Carlo et al. 2007; Fagan & Mackenzie 2007). The effects of nutrient and OM availability on pCO_2sw can be illustrated by comparing data from Ala Wai and Kilo Nalu. The primary difference between the two sites is that the Kilo Nalu site receives no direct riverine input, whereas (diluted) riverine input from the Ala Wai canal passes by the Ala Wai site. The Ala Wai canal drains approximately one third of urban Honolulu and delivers water that is enriched in nutrients and dissolved and particulate OM to the Ala Wai site (De Carlo et al. 2004; De Carlo et al. 2007; Drupp et al. 2011; Tomlinson et al. 2011), thereby raising productivity which results in an 19 µatm greater mean diurnal range at Ala Wai compared to that at Kilo Nalu.

Residence time is an important physical factor that impacts pCO_2sw variability. If the residence time of water at a site is long, a water parcel is exposed to photosynthesis, respiration, calcification, and dissolution by the biological community for a relatively long time, which allows for changes in pCO_2sw

to accumulate and results in a stronger "biogeochemical signal". The residence time of water is controlled by physical forcings such as wind speed, waves, and to some extent by tidal fluctuations. The water at Ala Wai and Kilo Nalu is thought to have a short residence time and exchanges freely with the open ocean. The water residence time at CRIMP-2 is relatively long, and can range from a few hours to more than a day during periods of light winds (Lowe et al. 2009; Shamberger et al. 2011).

Water depth also controls the extent to which biogeochemical processes affect pCO_2sw. The CRIMP-2 site is relatively shallow (~3 m) and the volume of water on the reef that is affected by benthic and water column productivity is relatively small, therefore the "biogeochemical signal" is more concentrated and pCO_2sw fluctuations are greater. The Ala Wai and Kilo Nalu sites are deeper than CRIMP-2 (~12 m) and the volume of water is greater, therefore the "biogeochemical signal" is diluted and the pCO_2sw fluctuations are smaller. Benthic processes at the WHOTS site cannot affect surface water pCO2sw, because of its depth (4.8 km). The mean five-fold greater diurnal fluctuation in pCO_2sw at Kilo Nalu (32 μatm) compared to that at WHOTS (6 μatm), despite the fact that tidal and wind-driven circulation delivers predominantly oligotrophic water to the Kilo Nalu site, may simply reflect a greater benthic and water column productivity than in the open ocean, likely due to slightly enhanced nutrient concentrations and benthic community production in the near shore zone.

Transient events such as storms strongly affect pCO_2sw variability for a period ranging from hours to days. After rain storms, freshwater with a high nutrient content enters coastal waters, typically causing increased phytoplankton growth and subsequently leading to a drawdown of pCO_2sw (Fagan and Mackenzie, 2007; Drupp et al, 2011; Massaro et al, 2012). Intense rainfall episodes can also deliver dissolved and particulate organic matter, which through enhanced respiration can increase pCO_2sw as well as nutrient concentrations in bay waters. In the latter case, extended plankton blooms can be triggered, with their duration depending partly on physical processes such as water residence time and mixing (e.g. De Carlo et al., 2007; Tomlinson et al. 2011) and biotic effects such as predation (e.g. Hoover et al., 2006).

Weekly-biweekly variability

The range of the diurnal cycle of pCO_2sw and other seawater parameters is affected by changes in the diurnal tidal range over time scales of 14 days. Hawaii generally has mixed tides, which means that the two high and two low tides that occur each day are of different heights. In Kaneohe Bay, the mean tidal range is 68 cm d^{-1} and the maximum range is ~110 cm d^{-1} (Jokiel 1991). Figure 3.4 displays a month-long time-series — from 19 December 2013 to 18 January 2014 — of tidal height at Moku o Loe (Coconut Island) in Kaneohe Bay (top panel) and data from various parameters at the CRIMP-2 site (lower panels). Over the course of this time-series, the minimum tidal range was 31 cm d^{-1} (neap tide), and the maximum was 109 cm d^{-1} (spring tide, shaded regions in Fig. 3.4). The pCO_2sw, pH, and DO clearly exhibit much smaller diurnal amplitudes when the tidal range is greater, and larger amplitudes when the tidal range is smaller. This difference in amplitude is caused by a combination of factors. During a rising tide, there is a greater rate of advection of water across the reef and thus a shorter water residence time, which results in less build-up of the reef "biogeochemical signal" (see also section 3.4.1). A greater tidal range also results in a greater change in the volume of water on the reef, which results in a more diluted (high tide, large volume of water) or more concentrated (low tide, small volume of water) biogeochemical signal.

Atmospheric heating or cooling changes the SST as water travels across the reef, and will either increase or decrease the water temperature, depending on the time of year (winter/summer) and time of day (day/night). The data displayed in Figure 3.4 were collected in winter (December), and therefore lower atmospheric temperatures cooled the water as it travelled across the reef. In summer, the opposite is generally observed; higher atmospheric temperatures warm the water as it travels across the reef. During small tidal cycles, water residence time is longer, and the degree of heating and cooling of water on the reef is greater and therefore the SST amplitude is greater than during larger tidal cycles. In the time-series (Fig. 3.4), DO saturation fluctuated between super-saturation during the day and under-saturation at night, driven by the diurnal photosynthesis and respiration cycle. During spring tide (large tidal range),

however, the water seems to be under-saturated the majority of the time. Atmospheric cooling of the water might be driving this under-saturation. Because O_2 solubility increases in colder water, the same amount of DO will leave cooler water under-saturated. During spring tide advection is stronger and the water might be moving too fast for DO to reestablish equilibrium with the atmosphere, leaving the water relatively under-saturated with respect to O_2. Wind speed was highly variable, and its variability does not seem to be related to tidal variability.

3.4.2 Monthly to seasonal variability in pCO_2 and air-sea CO_2 fluxes

To visualize monthly, seasonal, and longer-term variability, weekly mean values of pCO_2sw, air-sea CO_2 fluxes, and SST at each site were calculated as shown in Figure 3.6. To approximate weekly means, a running average filter was applied over 56 data points (measurements are taken on 3-hourly intervals, which translates to 56 data points per week).

Seasonal cycle

Weekly mean pCO_2sw increases during the summer and decreases during the winter (Figure 3.6, top panel). The seasonal pCO_2sw cycle can be explained for the most part by the effect of SST on the solubility of CO_2 in seawater. CO_2 solubility decreases with increasing SST because the partial pressure of CO_2 in seawater (pCO_2sw) increases by about 4.23% for every °C increase in SST (Takahashi et al. 2002). Pearson's correlation coefficients between weekly mean SST, SSS, pCO_2sw, pCO_2air, ΔpCO_2, wind speed, and the air-sea CO_2 flux at CRIMP-2 are shown in Table 3.5. Pearson's correlation coefficients at Ala Wai, Kilo Nalu, and WHOTS are not summarized in a table, although some important correlations between parameters at these sites are shown in parenthesis throughout this text. The strong correlation between weekly mean SST and pCO_2sw (R = 0.79) is

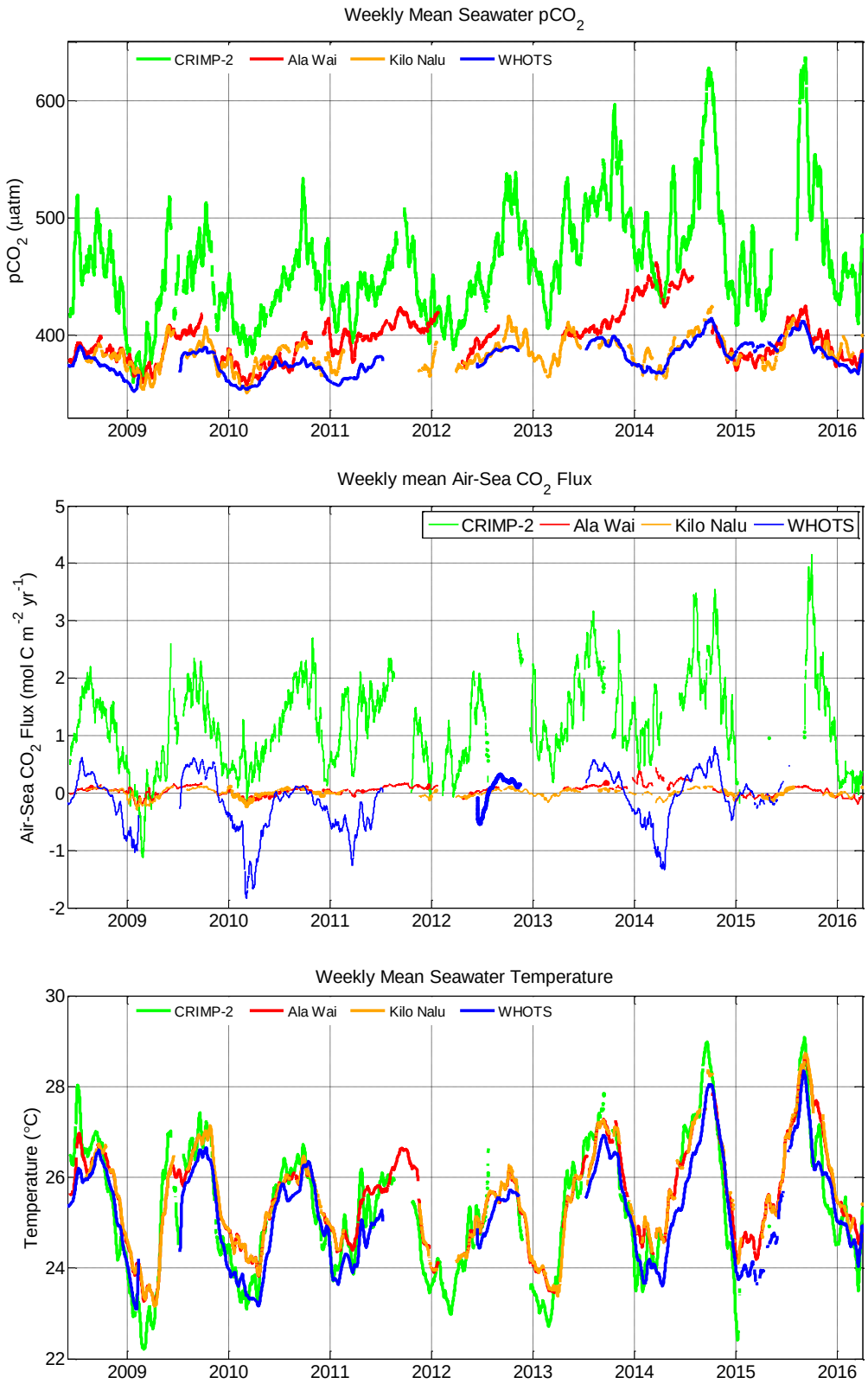

Figure 3.6 Time series of weekly mean pCO_2 (top), air-sea CO_2 fluxes (middle), and SST (bottom) at CRIMP-2, Ala Wai, Kilo Nalu, and WHOTS from June 2008 to March 2016.

consistent with the idea that SST drives the seasonal trend in pCO_2sw (Massaro et al. 2012). Note that on diurnal time-scales SST and pCO_2sw were negatively correlated (R = -0.53, Table 3.4) because of their opposite diurnal patterns; at night SST decreases but night time respiration increases pCO_2sw (Figure 3.5, see also section 3.4.1). Seasonal changes in productivity have been shown to either amplify or dampen the seasonal pCO_2 cycle, because rates of biological processes of photosynthesis/respiration and calcification/dissolution generally increase with increasing SST (Jokiel & Coles 1977; Coles & Jokiel 1978; Marshall & Clode 2004; Langdon & Atkinson 2005). At CRIMP-2, calcification and dissolution most likely contribute significantly to pCO_2sw variability, therefore higher rates of calcification during the summer further elevate pCO_2sw, thereby amplifying the seasonal pCO_2sw cycle (Drupp et al. 2013; Shamberger et al. 2011). Seasonal changes in productivity at Ala Wai and Kilo Nalu have the opposite effect on pCO_2sw because photosynthesis and respiration mainly drive pCO_2sw, and calcification and dissolution are likely to be less important. Decreased SST during the winter reduces primary production but respiration from autotrophs remains significant, which leads to a slight increase in pCO_2sw. Additionally, inputs of OM rich runoff water from the Ala Wai canal in winter can enhance respiration and result in periods of elevated pCO_2sw. The much lower correlation between SST and pCO_2sw at Ala Wai (R = 0.41) compared to CRIMP-2 and Kilo Nalu (R = 0.73) suggests that the effect of productivity (OM respiration increasing pCO_2sw in winter) is out of phase with the effect of SST (lower SST decreases pCO_2) and therefore dampens the seasonal pCO_2sw cycle at Ala Wai.

The weekly mean air-sea CO_2 flux also shows a strong seasonality (Figure 3.6, middle panel). During the summer the weekly mean CO_2 flux is positive (source of CO_2 to the atmosphere). During the winter when SST and pCO_2sw decrease, the CO_2 flux becomes a smaller source (e.g. CRIMP-2) or even switches to being a sink (e.g. WHOTS). The seasonality of the CO_2 flux is further enhanced albeit to a slight extent by the seasonal cycle in pCO_2air. In Hawaii and throughout the Northern Hemisphere, pCO_2air is higher in winter and lower in the summer owing to the Northern Hemisphere terrestrial respiration/photosynthesis cycle (e.g. Keeling et al. 1976). The seasonal pCO_2air cycle mirrors that of

pCO_2sw, which results in a strong seasonality of ΔpCO_2 and thus in the CO_2 flux. The dynamics of the CO_2 flux at coastal sites and the open ocean are somewhat different, however, owing to both differences in ΔpCO_2 variability and wind speed. In the oligotrophic open ocean, productivity in the water column is low and diurnal variability in pCO_2sw is small and generally does not affect the sign of ΔpCO_2 (Figure 3.3, bottom panel). Therefore, ΔpCO_2 remains generally consistent throughout the season (positive in summer and negative in winter), and the direction of the flux is also seasonally determined (a source in summer and a sink in winter). At the coastal sites, the sign of ΔpCO_2 switches often due to highly variable rates of productivity in the water column that either draw down pCO_2sw (photosynthesis) or increase pCO_2sw (respiration, calcification) which leads to variability in the direction of the flux (Figure 3.3), even within a diurnal cycle (Figure 3.5).

Wind speed is an important driver of the CO_2 flux, and the relatively strong consistent trade winds in the open ocean enhance the CO_2 flux, despite the small ΔpCO_2 (Table 3.3). The average wind speed during the study period at WHOTS was 6.6 ± 2.1 m s^{-1}, which is approximately three times greater than at Kilo Nalu (2.3 ± 1.3 m s^{-1}). The mean magnitude of the CO_2 flux at WHOTS was large (0.41 mol C m^{-2} yr^{-1}), owing to the greater gas transfer velocity at higher wind speeds (e.g. Ho et al. 2006). In contrast, the mean magnitude of the CO_2 flux at Kilo Nalu was much smaller (0.08 mol C m^{-2} yr^{-1}) due to the much lower wind speed. The CO_2 flux at CRIMP-2 was large and positive year-round, primarily due to the ~ 60 µatm higher mean pCO_2sw (Table 3.1) and greater variability on the barrier reef, but also in part due to higher wind speed on the windward side of Oahu (mean wind speed = 5.1 ± 2.5 ms^{-1}).

Weekly mean SST increases during the summer (May – October) and decreases during the winter (November – April) with a seasonal amplitude of ~ 3-5 ˚C (Figure 3.6, top panel). Mean SST values were similar at all sites, and ranged from 25.2 to 25.5 °C (Table 3.3). The significantly longer residence time and the shallow nature of the site, however, make CRIMP-2 more subject to atmospheric heating (and cooling) in summer (and winter), which results in a 1.5 times greater seasonal amplitude relative to the other sites, as previously described by Drupp et al. (2013), and overall greater SST variability as

illustrated by the greater standard deviation of the mean SST (± 1.6 °C) compared to the other sites (± 1.1-1.2 °C).

	SST	**SSS**	**pCO_2**	**pCO_2air**	**ΔpCO_2**	**U10**	**CO_2 flux**
SST	1						
SSS	-0.05	1					
pCO_2	**0.79**	-0.22	1				
pCO_2air	-0.36	-0.31	0.00	1			
ΔpCO_2	**0.84**	-0.17	**0.99**	-0.17	1		
U10	-0.13	0.28	-0.39	-0.16	-0.35	1	
CO_2 flux	**0.72**	0.00	**0.68**	-0.24	**0.71**	0.23	1

Table 3.5 Pearson's correlation coefficients (R values) of weekly mean SST, SSS, pCO_2sw, pCO_2air, ΔpCO_2, wind speed (U10), and the CO_2 flux at CRIMP-2 for the entire study period from June 2008 to March 2016

Monthly Climatologies

Monthly climatological statistics were calculated for SST, SSS, seawater and air pCO_2, temperature normalized pCO_2sw (pCO_2n), wind speed, and air-sea CO_2 fluxes at CRIMP-2, Ala Wai, and Kilo Nalu. These climatological data are illustrated in box plots, each of which is based on approximately 23,000 time-series measurements made between June 2008 and March 2016. In this section we will discuss the climatologies of pCO_2sw and air-sea CO_2 fluxes. The climatologies of SST, SSS, pCO_2air,

pCO_2n, and wind speed are summarized in Appendix A.

Figure 3.7 displays the monthly pCO_2sw climatologies for Ala Wai (red), Kilo Nalu (orange), and CRIMP-2 (green). Note that the range of the y-axis is greater for the box plot for CRIMP-2 (200 – 800 µatm) than for Ala Wai and Kilo Nalu (300-500 µatm). High productivity on the shallow reef flat combined with the relatively long water long residence time resulted in a range of pCO_2 at CRIMP-2 (801 µatm) that was at least three times greater than at Ala Wai (249 µatm) and Kilo Nalu (210 µatm). Each site reveals a similar yet distinct seasonal trend in mean pCO_2sw values, which is discussed on pages 55-56. The range of pCO_2sw variability, which is illustrated by the size of the boxes and the length of the whiskers, also shows strong seasonality. At CRIMP-2, greater variability was observed during the summer (May through October) because higher SST and increased solar radiation increase rates of photosynthesis/respiration and calcification/dissolution (Drupp et al. 2013; Shamberger et al. 2011). In contrast to CRIMP-2, pCO_2sw variability at Ala Wai was greatest during the winter season (November through April), potentially reflecting enhanced coastal productivity driven by increased fluvial nutrient and OM inputs during the wet season (e.g Tomlinson et al. 2011; Hoover et al. 2006; Ringuet & Mackenzie 2005). The relatively low variability in winter at Kilo Nalu compared to Ala Wai reflects the general lack of nutrient rich runoff water reaching this site. Instead, the greatest variability in pCO_2sw at Kilo Nalu is observed in May and October, which are the "transition months" between the relatively wet winter season to the drier summer season. Depending on the year, these months can be either relatively warm and dry (higher pCO_2sw), or relatively cold and rainy (lower pCO_2sw). The frequency and severity of "extreme" events is illustrated by the difference between the mean and median, because the latter is unaffected by extreme values. For example, the mean pCO_2sw was significantly greater than the median at Ala Wai from January to March, indicating that extreme events of high pCO_2sw took place. January - March are relatively wet winter months with increased frequency of storm events, and these high pCO_2sw events could be caused by respiration of pre-formed OM delivered from the Ala Wai canal during intense rainfall (see section 3.4.1).

Figure 3.8 displays the monthly air-sea CO_2 flux climatologies at Ala Wai (red), Kilo Nalu (orange), and CRIMP-2 (green). Note that the range of the y-axis is more than an order of magnitude greater for the box plot for CRIMP-2 (-4 to 8 mol C m^{-2} yr^{-1}) than for Ala Wai and Kilo Nalu (-0.5 to 0.5 mol C m^{-2} yr^{-1}). The dashed blue line represents a flux of zero, and positive values indicate a flux of CO_2 from seawater to the atmosphere (source) and vice versa. Net calcification and oxidation of organic matter at CRIMP-2 makes this site, on average, a source of CO_2 to the atmosphere year-round; with an overall average CO_2 flux of 1.24 ± 2.29 mol C m^{-2} yr^{-1}. Our flux estimate is slightly larger than the CO_2 flux of 1.15 mol C m^{-2} yr^{-1} at CRIMP-2 described by Drupp et al. (2013) based on the same dataset between June 2008 and December 2011. Fagan and Mackenzie (2007) calculated a slightly greater CO2 flux (1.45 mol C m^{-2} yr^{-1}) for the entire Bay. Massaro et al. (2011) estimate a CO_2 flux of 1.80 mol C m^{-2} yr^{-1} at the original CRIMP-CO_2 site located in the southern part of Kaneohe Bay (Fig. 3.1b). The 45% greater flux at CRIMP-CO_2 compared to CRIMP-2 likely reflects the greater water residence time as well as increased riverine input of pre-formed organic matter in Southern Kaneohe Bay. At Ala Wai and Kilo Nalu, the magnitude of the flux is much smaller (Table 3.3) owing to much lower productivity at these sites as well as the deeper water column and shorter water residence time, because this area is nearly continuously flushed by tidal and wave action. The direction of the CO_2 flux shows a strong seasonality and is generally positive during the summer due to elevated seawater pCO_2sw and decreased pCO_2air (page 58), and the opposite is true in winter. At CRIMP-2, like for pCO_2sw, the variability in the CO_2 flux is much greater in the summer. December and January show considerably less variability than the other months, also consistent with the typically lower wind speed during this period of the year, although the actual speed and direction are most variable during these two months.

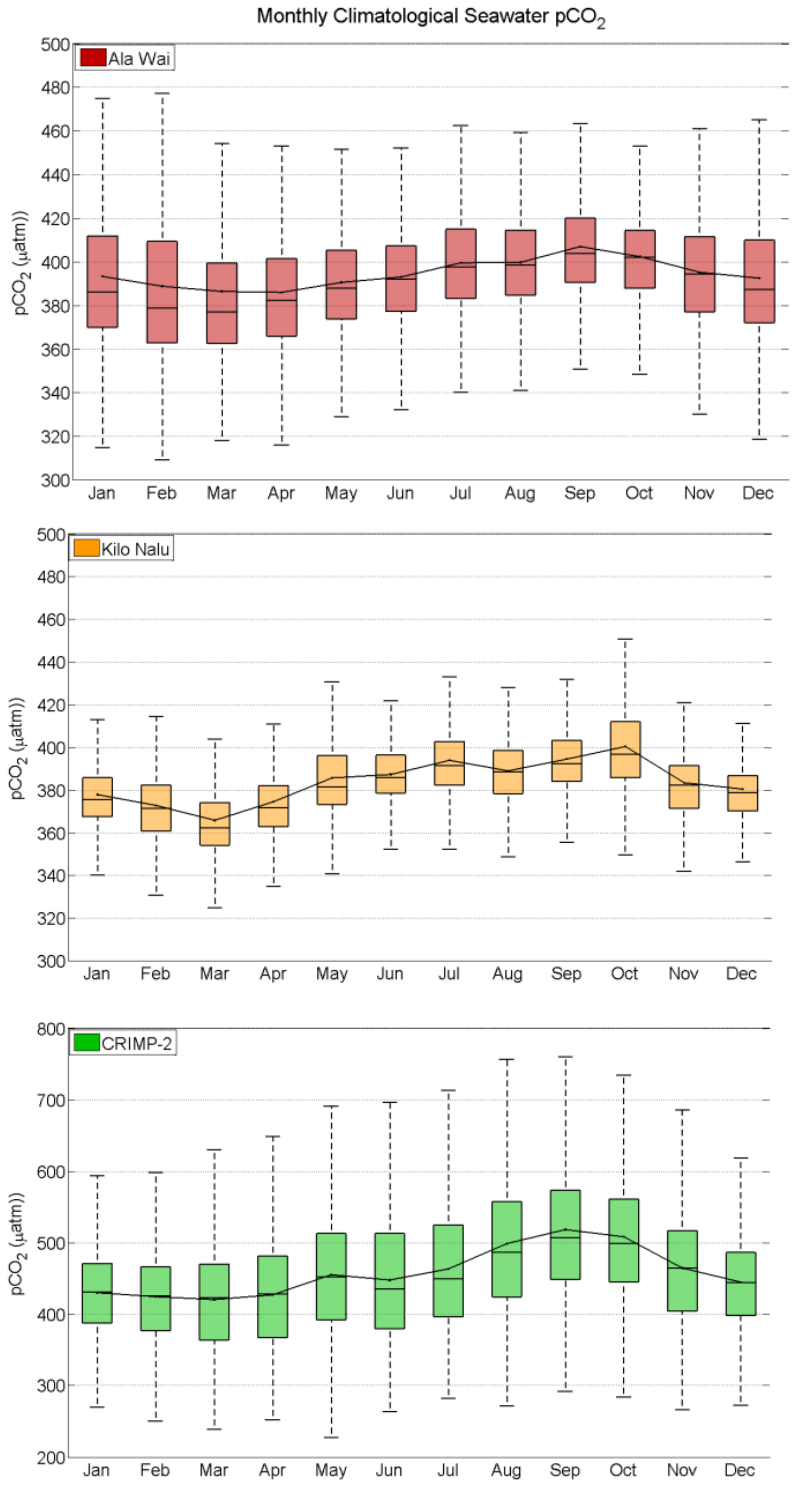

Figure 3.7 Monthly climatological box plots of pCO_2sw at Ala Wai, Kilo Nalu, and CRIMP-2. Box plots show median (line within the box), mean (dot, with a line drawn through the mean of each month), the bottoms and tops of the boxes are the 25^{th} (q_1) and 75^{th} (q_3) percentiles, respectively. The whiskers extend to 1.5 X interquartile range (q_3-q_1), corresponding to approximately ± 2.7 σ or 99.3% of the data (if normally distributed).

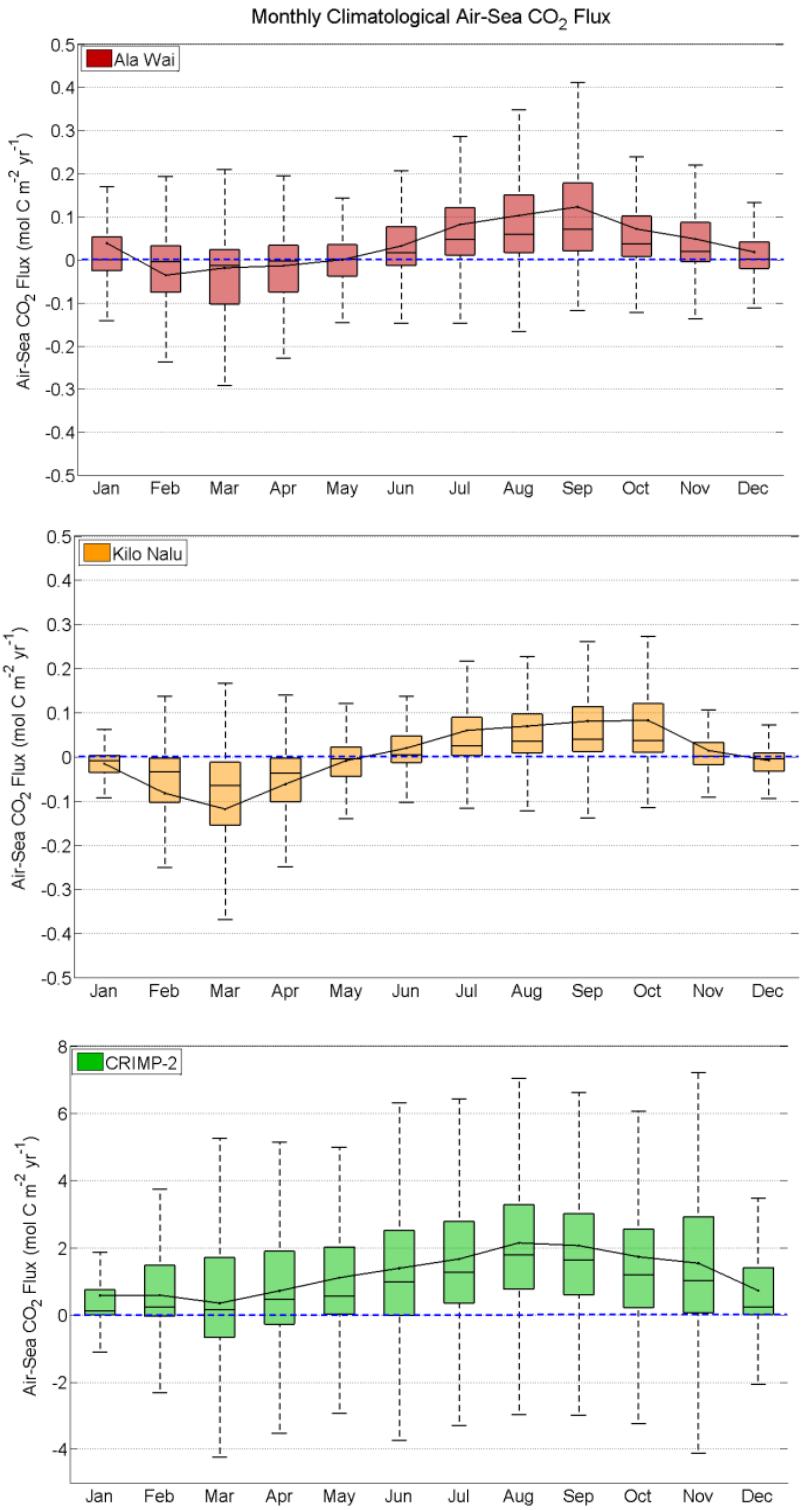

Figure 3.8 Monthly climatological box plots of air-sea CO_2 fluxes at Ala Wai, Kilo Nalu, and CRIMP-2. The blue dashed line illustrates a flux of zero, positive values indicates that the area is a source of CO_2 to the atmosphere.

3.4.3 Inter-annual variability and long term pCO_2 trends

The CRIMP program is the longest running high temporal resolution time-series record of coastal CO_2 chemistry on our planet. The nearly eight-year record of data (June 2008 – March 2016), acquired following the move of the original CRIMP-CO_2 buoy to the barrier reef of Kaneohe Bay, though too short to unequivocally identify a climate change signal, allows an initial examination of inter-annual variability and longer-term trends in pCO_2sw. Over the course of the study period, weekly mean pCO_2sw increased at all sites (Fig. 3.6). A linear fit through these data resulted in an average annual increase of 9.8, 3.9, 1.3, and 2.7 µatm yr^{-1} at CRIMP-2, Ala Wai, Kilo Nalu, and WHOTS, respectively. The inter-annual trend discussion will primarily focus on the CRIMP-2 site because the annual pCO_2sw increase at this site was more than twice that of the other sites.

On inter-annual time-scales, pCO_2sw could be affected by climate change (e.g. Sabine et al. 2004) as well as by climate oscillations such as the El Nino Southern Oscillation (ENSO) (e.g. Sutton et al. 2014). Short-term (i.e. decades to centuries) climate change, the anthropogenic increase of atmospheric CO_2 and the associated global warming, mainly affect pCO_2sw in two ways. First, pCO_2sw should increase due to the flux of anthropogenic atmospheric CO_2 into the ocean to re-establish the air-sea CO_2 equilibrium. Second, global warming should increase SST which then should increase pCO_2sw owing to reduced solubility in warmer water (see section 3.4.2). Basin-wide climate oscillations drive inter-annual changes in ocean-atmosphere circulation patterns as well as SST. These large scale physical changes can affect biological productivity and calcification and therefore should also affect pCO_2sw variability.

Climate change as a driver of the pCO_2sw trend at CRIMP-2

To evaluate if the atmospheric (air) CO_2 trend could be driving the pCO_2sw trend at CRIMP-2, the rates of annual increase of seawater and air CO_2 were compared. Air CO_2 at the CRIMP-2 site is displayed here as the CO_2 concentration in units of parts per million (ppm) instead of the partial pressure

of CO_2 (pCO_2) in micro atmospheres (µatm) so that these data can be more readily compared to the long-term CO_2 record from the Mauna Loa Observatory (e.g. Keeling et al. 1976; Tans & Keeling 2016). Figure 3.9 displays the monthly mean air CO_2 concentration at CRIMP-2 (green), overlaying the monthly mean air CO_2 concentration at the Mauna Loa Observatory (red) and the Mauna Loa trend-line (blue). To determine the annual increase in air CO_2 concentrations at CRIMP-2, a linear fit was done through the monthly mean air CO_2 data displayed in Figure 3.9. The linear fit yielded an average increase of 1.72 ppm yr^{-1} over the course of the study period. The annual increase in pCO_2sw at CRIMP-2 (9.8 µatm yr^{-1}), however, is more than five times greater than the air CO_2 increase, which suggests that the atmospheric CO_2 trend alone cannot explain the observed pCO_2sw trend at CRIMP-2.

Two interesting features of the air CO_2 time-series are the slightly larger seasonal cycle at CRIMP-2 compared to at the Mauna Loa Observatory, largely due to consistently lower values in summer at CRIMP-2, and also the anomalously high air CO_2 at CRIMP-2 during the 2015/2016 winter. The differences in the seasonal CO_2 cycle might be related to the mixing time of CO_2 in the atmosphere, which is on the order of three months within the Northern Hemisphere. The Mauna Loa Observatory is located at 3397 m elevation (as opposed to the CRIMP-2 site at sea level) and the atmosphere might not reach full equilibrium with respect to the CO_2 concentration at this height and therefore the seasonal cycle could be dampened at Mauna Loa. The anomalously high air CO_2 during the 2015/2016 coincided with much lower monthly mean wind speed in Kaneohe Bay (Fig. 3.12). Winters in Hawaii are characterized by much more variability in wind speed and direction. NNE trade winds alternate with low speed south-westerly winds ("Kona Winds"). Kona winds blow across the island of Oahu but are blocked by the high elevation Koolau Ridge before reaching Kaneohe Bay (CRIMP-2 location). Because Kona wind speeds are much lower, the atmosphere is not "flushed" as strongly, and there likely is some build-up of CO_2 that outgassed from seawater to the overlaying atmosphere. This winter pattern also delivers higher air CO_2 concentrations from land respiration and human fossil fuel consumption, the "island effect" to the CRIMP-2 location.

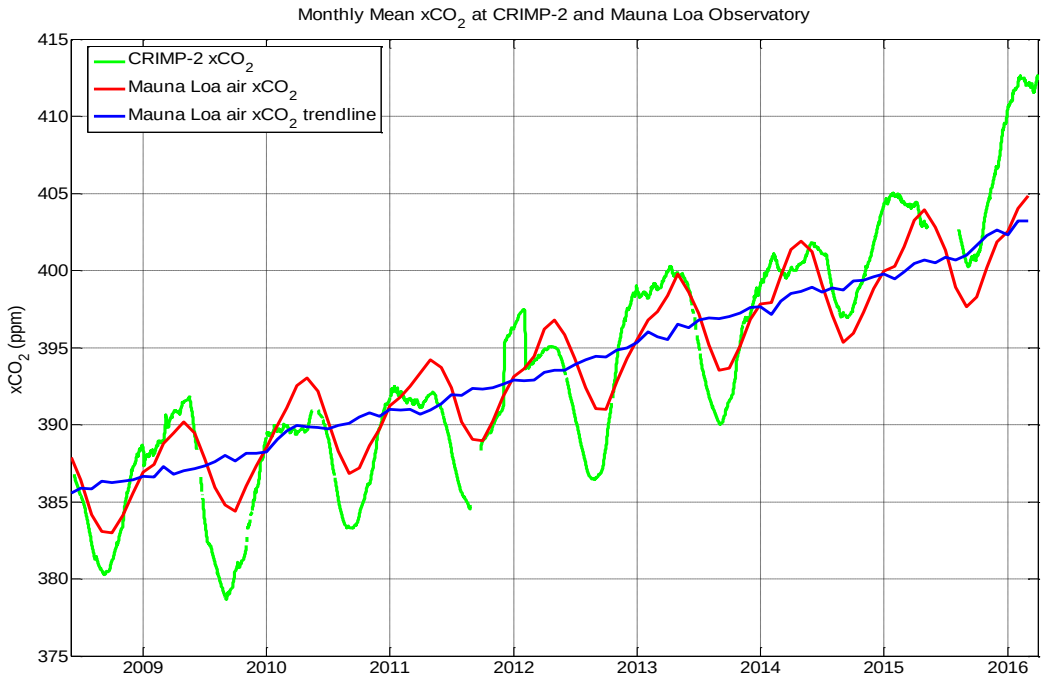

Figure 3.9 Time-series of monthly mean atmospheric CO_2 concentrations at CRIMP-2 (green) and the Mauna Loa observatory (red). The blue line represents the trend line of Mauna Loa CO_2 concentrations.

To evaluate the effect of SST on the long term pCO_2sw trend, pCO_2sw was normalized to the mean SST at each site (Table 3.3). Temperature normalized pCO_2 (pCO_2n) provides an estimate of the "net biology effect", however, this includes both the variability in pCO_2sw due to biogeochemical and physical processes other than SST. Weekly mean pCO_2n at all sites is displayed in Figure 3.10. The annual increase of weekly mean pCO_2n was 8.4 µatm yr^{-1} at CRIMP-2, but there was no apparent trend at the other sites. SST was clearly not the only driver because the annual increase in pCO_2n is still large and SST only accounts for ~1.4 µatm yr^{-1} increase in pCO_2sw (9.8 – 8.4 µatm yr^{-1}), suggesting that biogeochemical and physical processes other than SST are much more important drivers of this trend.

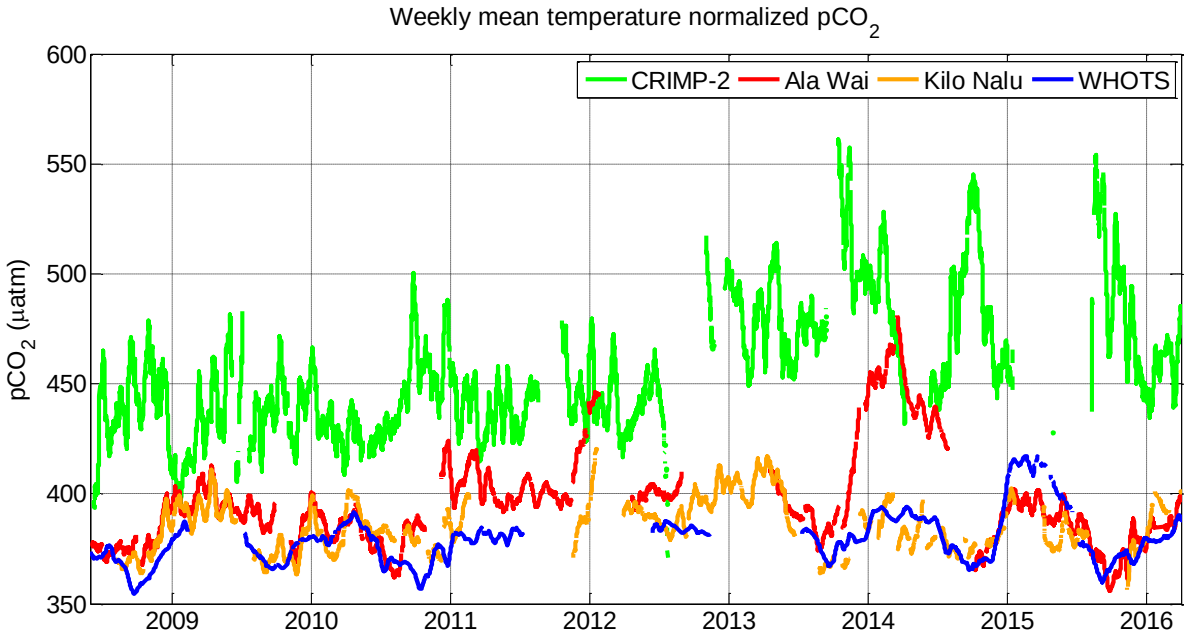

Figure 3.10 Time-series of weekly mean temperature normalized pCO_2sw (pCO_2n) at CRIMP-2, Ala Wai, Kilo Nalu, and WHOTS from June 2008 to March 2016

North (Pacific) climate oscillations and their correlation to the pCO2 trend at CRIMP-2

In the open ocean, i.e., the North Pacific Subtropical Gyre at station ALOHA, inter-annual differences in biological productivity have previously been linked to changing physical processes due to the El Niño Southern Oscillation (ENSO) and the Pacific Decadal Oscillation (PDO) (Karl et al. 2001; Corno et al. 2007). ENSO is a high frequency (1-3 years) recurrent climate pattern of warm (El Niño) and cold (La Niña) SST phases in the equatorial Pacific (Mantua et al. 1997). The PDO is often described as a "long-lived ENSO like pattern" of Pacific climate variability which occurs on time-scales of 10-30 years (Zhang et al. 1997). Although the abovementioned studies linked ENSO and PDO to productivity at station ALOHA, a later study by Dave & Lozier (2010) found no significant correlation between these climate oscillations and productivity at this site, and the absence of correlation might be because the region is a strongly stratified ecosystem and it lacks a sufficiently strong inter-annual forcing. Dave &

Lozier (2010) did find a strong correlation between productivity and the North Pacific Gyre Oscillation (NPGO), a pattern that was discovered only in 2008 by Di Lorenzo et al. (2008). NPGO fluctuations are driven by basin-scale variations in horizontal advection and wind driven upwelling. These physical processes control salinity and nutrient availability, and the latter is important for primary productivity and pCO_2sw variability.

The basin-scale changes in physical processes driven by oceanic climate oscillations may also affect productivity on coral reefs. For example, a recent study by Yeakel et al. (2015) showed that inter-annual changes in biogeochemistry on a Bermuda coral reef may be linked to changes in offshore productivity, which in turn correlated with the North Atlantic Oscillation (NAO) index.

In this section the correlation between the long-term pCO_2sw trend at CRIMP-2 and the ENSO, PDO, and NPGO are examined. The indices of these climate oscillations are expressed as monthly mean anomalies relative to a long-term mean. To illustrate ENSO variability, the Niño 3.4 index was used, which represents the monthly SST anomalies averaged over the Niño 3.4 region in the equatorial Pacific (5°S to 5°N latitude and 170°W to 120°W longitude). For a more appropriate comparison, the pCO_2sw time-series at CRIMP-2 was also expressed in terms of monthly mean anomalies (hereafter referred to as anomalies). The anomalies were calculated by subtracting the long term monthly average (climatological monthly mean, see section 3.4.2) from the individual monthly mean (Fig. 3.11). Negative anomalies indicate a monthly mean pCO_2sw value that was lower than the long-term average. The pCO_2sw anomalies ranged from - 57 µatm in December 2008 to + 91 µatm in August 2016. Figure 3.11 shows a clear increasing trend over the course of the study period, and anomalies are generally negative during the first three years of the time-series (2008-2011) and positive during the last five years of the time-series (2012-2016)

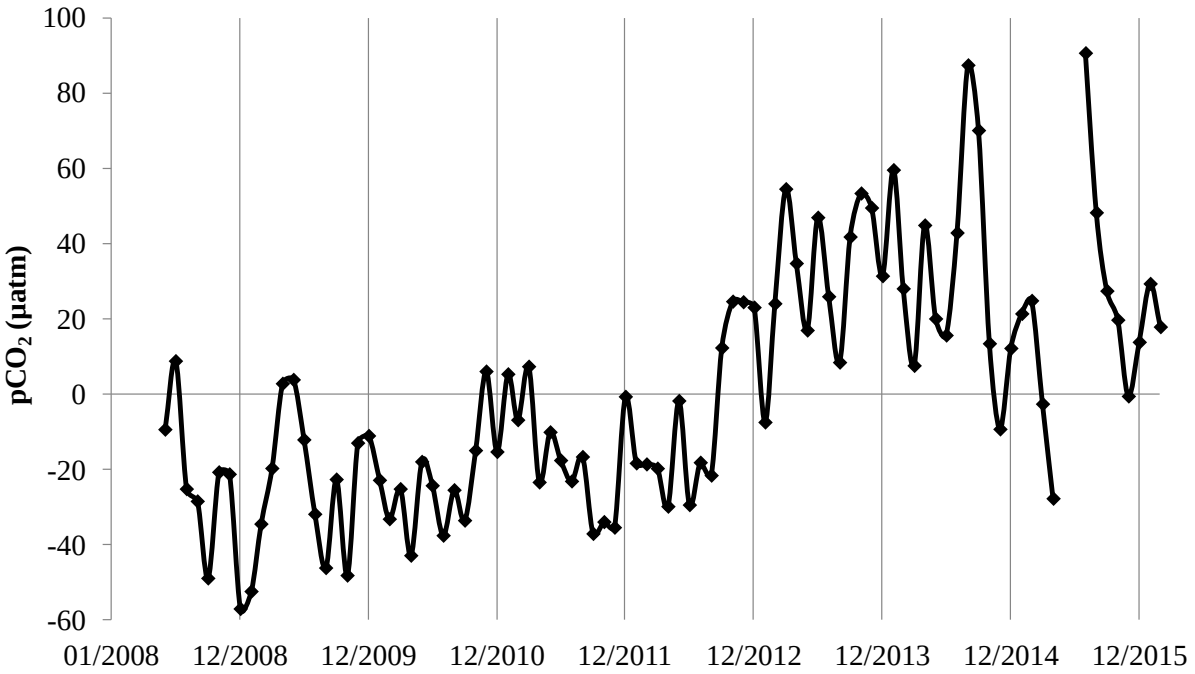

Figure 3.11 Time-series of monthly mean pCO_2sw anomalies at the CRIMP-2 site from June 2008 to March 2016. Anomalies were calculated by subtracting the climatological monthly mean (section 4.2.2) from the monthly mean.

To compare quantitatively the pCO_2sw anomalies to the data of the climate oscillation indices, all data (pCO2sw anomalies in Fig. 3.11 and climate oscillation indices in section 3.2.3) were standardized by converting to z-scores as shown in Equation 3.4.

(3.4) $$z_i = (x_i - \mu) / \sigma,$$

where z_i is the standardized value, x_i is the monthly mean anomaly, and μ and σ are the mean and standard deviation of the time-series, respectively. Each panel in Figure 3.12 displays a time-series of a standardized climate oscillation index (in color) overlaying standardized pCO_2sw anomalies (in black). The Pearson correlation coefficients between the standardized climate oscillation indices and pCO_2sw are summarized in table 3.6. The inverse of the NPGO index is displayed in Figure 3.11 to illustrate better the covariance between the time-series because pCO_2sw and NPGO are anti-correlated. The correlation between pCO_2sw and ENSO (Niño 3.4 index) is relatively weak ($R = 0.28$) and this index fails to explain the observed positive pCO_2sw anomalies between 2012 and 2014. The PDO index has a stronger

correlation with pCO_2sw (R = 0.48) than ENSO, and better captures the pCO_2sw increase from 2010 through 2015. The strongest (although negative) correlation was found between pCO_2sw and the NPGO index (R = -0.57), which captures inter-annual variability in pCO_2sw between 2008 and 2011 as well as the increasing pCO_2sw trend from 2011 through 2015.

The observed correlation between pCO_2sw anomalies at CRIMP-2 and the NPGO index does not explain how NPGO is connected to the observed pCO_2sw; it merely identifies that there might be basin-wide physical patterns that are related to the NPGO as well as to pCO_2sw variability on the reef at CRIMP-2. It should also be noted that these climate oscillations are not independent phenomena. They are strongly driven by large scale atmospheric circulation patterns and also force each other through (atmospheric) teleconnections; the latter refers to a connection between climate patterns that occur over long distances (thousands of kilometers) apart (e.g., see Chhak et al. 2009; http://www.o3d.org/npgo/docs/Decadal-Intro.pdf by Di Lorenzo & Schneider). For example, PDO variability is connected to atmospheric circulation anomalies associated with ENSO (e.g. Alexander et al. 2002; Newman et al. 2003), and the NPGO pattern is driven by SST anomalies associated with the Central Pacific El Niño through an atmospheric teleconnection (Modoki, Ashok & Yamagata 2009). The reader is referred to http://www.o3d.org/npgo/ for a detailed description of North Pacific climate variability and teleconnections. A significant fraction of NPGO variability is driven by atmospheric variability, specifically sea level pressure variability above Hawaii (Chhak et al. 2009). This suggests that the observed pCO_2sw anomalies might be related to an atmospheric circulation pattern as opposed to an oceanic one, and further research should be done to investigate if there exists a correlation between seawater pCO_2 anomalies and atmospheric climate oscillations in the North Pacific such as the East Pacific/ North Pacific Oscillation (EP/NP) and the North Pacific pattern (NP).

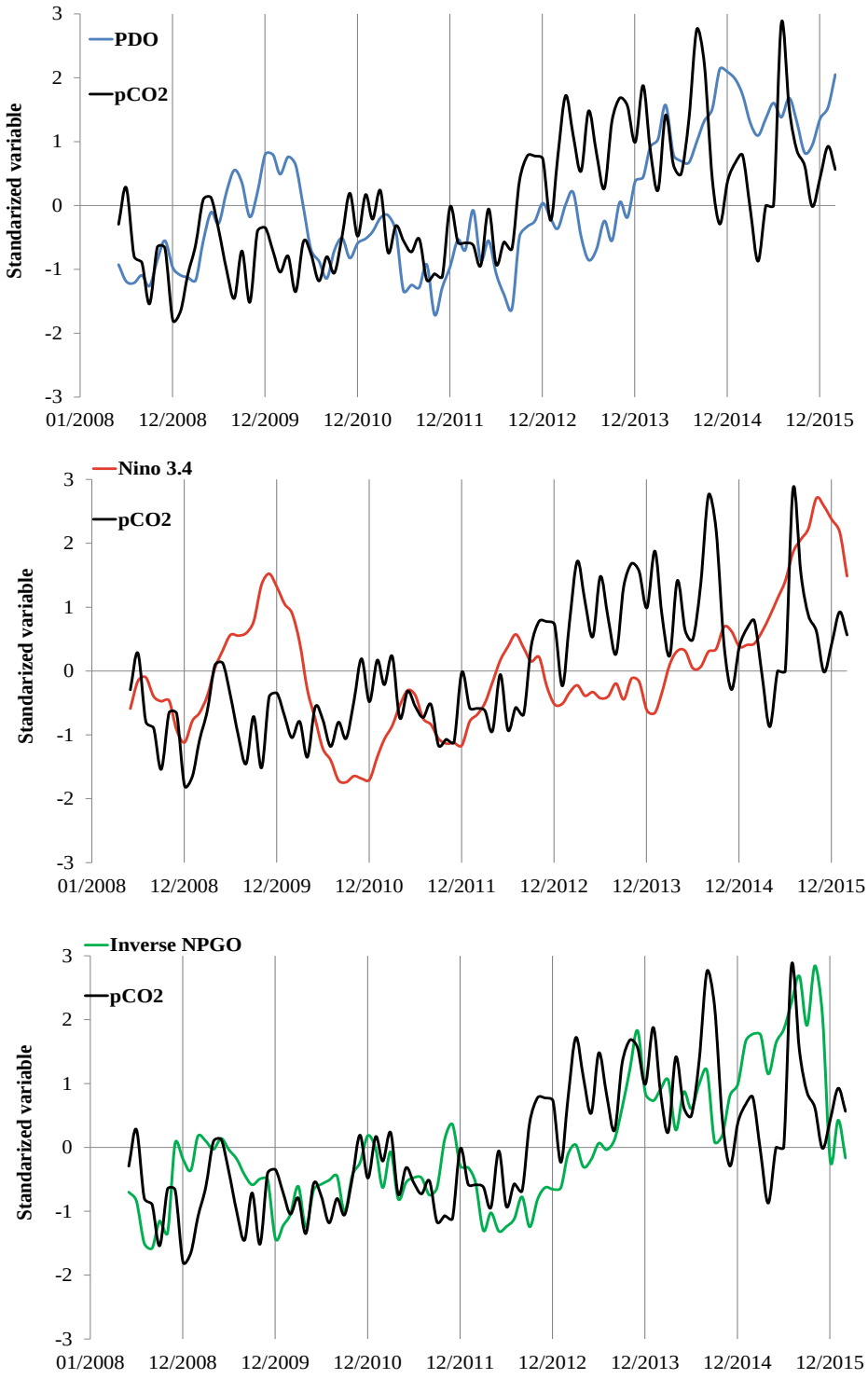

Figure 3.12 Time-series of standardized monthly mean pCO_2sw anomalies at CRIMP-2 with standardized Nino 3.4 index (red), PDO index (blue), and NPGO index (green) from June 2008 to March 2016.

	pCO_2sw CRIMP-2	Nino 3.4	NPGO	PDO
pCO_2sw CRIMP-2	1			
Nino 3.4	0.29	1		
NPGO	-0.59	-0.41	1	
PDO	0.47	0.70	-0.52	1

Table 3.6 Pearson's correlation coefficients (R) between the standardized monthly mean anomalies of pCO_2sw at CRIMP-2, Nino 3.4 index, NPGO index, and PDO index from June 2008 to March 2016.

Possible biogeochemical and physical drivers of the pCO_2sw trend at CRIMP-2

In the previous section a correlation was shown between inter-annual pCO_2sw variability at CRIMP-2 and basin-wide climate oscillations, specifically the NPGO. In this section hypotheses are developed regarding changes in the observed SST and wind speed, which might be driven by basin-wide climate oscillations (NPGO), and how these could have increased pCO_2sw over time through both changes in productivity and water residence time on the barrier reef.

SST affects the relative rates of biological reactions, such as photosynthesis and respiration, and can therefore affect the relative draw down or increase in pCO_2sw, respectively. In section 3.4.2, seasonal SST changes were shown to affect rates of productivity, and it is likely that the inter-annual increase in SST between 2012 and 2016 also increased rates of productivity over these years. Rates of photosynthesis and respiration however, are not affected equally; the photosynthesis/respiration ratio is negatively correlated with increasing SST in plankton and corals in the environmentally relevant SST range of Hawaii (18-31 °C) (e.g. Coles and Jokiel 1977; Hoch Hachka and Somero, 2002). This means that if SST

increases, respiration (which releases CO_2) increases more rapidly relative to photosynthesis (with draws down CO_2), resulting in an overall increase in pCO_2sw. This could be an important contributing factor to the observed rising pCO_2sw trend at CRIMP-2.

Coral bleaching, a stress response of corals that is often induced by sustained high SST's, is the process of degeneration and expulsion of the symbiotic photosynthesizing algae known as zooxanthellae. As a result, the white coral skeleton becomes visible through the transparent coral tissue, and the coral appears bleached (e.g. Hoegh-Guldberg 1999). The loss of zooxanthellae reduces photosynthesis on the reef; however, bleached corals do continue to respire. Coral bleaching could lead to an overall increase in respiration relative to photosynthesis, and thus might increase pCO_2sw. In the summer of 2014, a mass coral bleaching of corals occurred throughout the Hawaiian Islands (Bahr et al. 2015). Although the corals on the barrier reef of Kaneohe Bay were not bleached as severely as some of the fringing reef sites inside the bay, some bleaching did occur and this might have affected relative respiration/photosynthesis rates.

If climate oscillations affect open ocean productivity, the composition of the source water advected to the reef can also change (e.g. Yeakel et al. 2015). Concentrations of organic matter (or nutrients) delivered from the open ocean to the reef could increase rates of respiration (or photosynthesis), and increase (or draw down) pCO_2sw. Although this seems like a plausible process, there is no evidence of significant changes in nutrient concentrations or plankton biomass at the nearby open-ocean time-series site, station ALOHA, during the relevant time period (Dave Karl and Matt Church, personal comm., June 12, 2016).

Increased residence time of water on the reef could further amplify the observed productivity driven changes in pCO_2sw. Figure 3.13 displays a time-series monthly mean wind speed at CRIMP-2 from June 2008 through March 2016. There is a clear trend of decreased wind speed between 2012 and 2014, and sustained lower wind speeds thereafter. What is driving this inter-annual trend in wind speed remains currently unknown, but it might be related to an atmospheric climate oscillation pattern. A

decrease in wind speed will increase residence time of water on the reef through lower wave setup and flow velocities across the reef (Lowe et al. 2009), which results in a build-up of CO_2 in the water, thereby increasing pCO_2sw (Section 3.4.1).

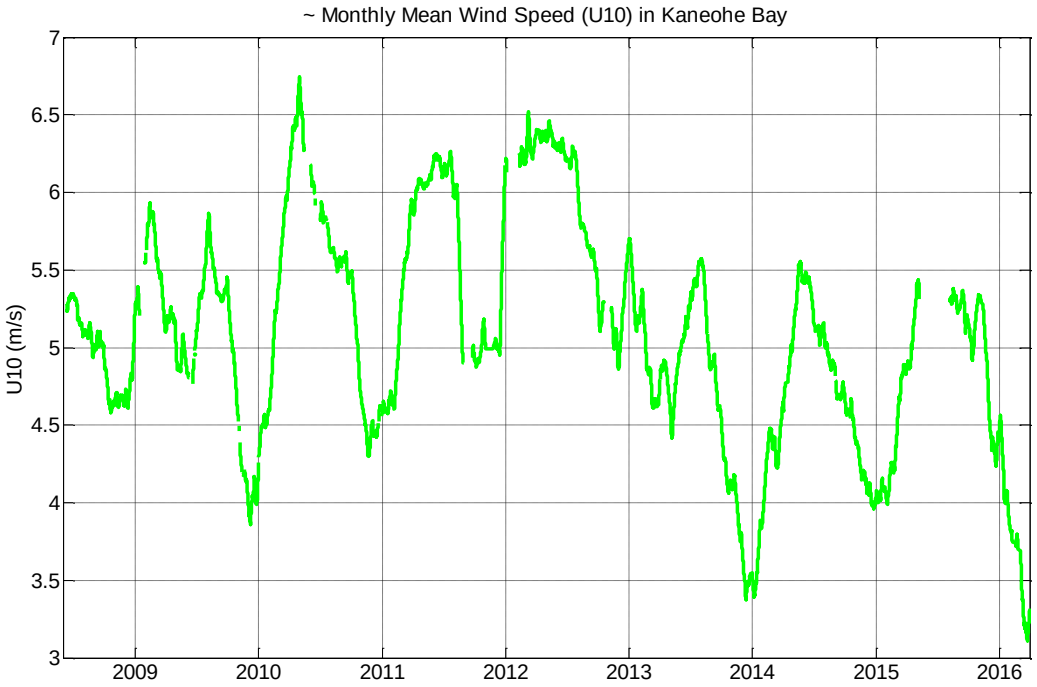

Figure 3.13 Time-series of monthly mean wind speed at Coconut Island, Kaneohe Bay near the CRIMP-2 site. A running average filter over 500 data points (~ 2-monthly means) was applied to remove low frequency variability.

Comparing the CRIMP-2 pCO_2sw trend to other reefs around the world

To put the findings of this study in a more global context, the CRIMP-2 seawater CO_2 time-series was compared to three other coral reef $MAPCO_2$ sites. Two are located in the Atlantic Ocean (Puerto Rico and Bermuda) and one is in the Western Equatorial Pacific (Micronesia) (http://www.pmel.noaa.gov/co2/story/Coral+Reef+Moorings). These three sites were chosen mainly because of their relatively long and continuous CO_2 record and their different geographic locations

(Western equatorial Pacific and Atlantic). Mole fractions of CO_2 in seawater (xCO_2) in ppm were compared instead of pCO_2, because these data are readily availability online for all $MAPCO_2$ sites, and xCO_2 largely follows the same trend as pCO_2.

The top panel of Figure 3.14 displays time-series of weekly mean xCO_2 at CRIMP-2, La Parguera (Puerto Rico), Chuuk K1 (Micronesia), and Crescent reef (Bermuda), from June 2008 to March 2016. The bottom panel of Figure 3.14 displays xCO_2n, which is temperature normalized xCO_2, to illustrate the "net biology effect" on xCO_2 variability. La Parguera and Crescent reef are both located in the North Atlantic Ocean. Crescent reef in Bermuda is a high latitude reef (32.40°N, 64.79°W), where the large seasonal SST cycle drives the observed large seasonal xCO_2 cycle. Neither xCO_2 nor xCO_2n show a strong increasing trend over the course of the study period. The La Parguera site is located within a natural reserve (17.95°N, 67.05°W) on a shallow (1.5-5 m) fore-reef. Interestingly this xCO_2 record overlaps with much of the CRIMP-2 record, although the maxima in summer are roughly 50 ppm higher at CRIMP-2 than at La Parguera, but the mean and amplitude are comparable. The similarity in the CRIMP-2 and La Parguera xCO_2 records disappears after the winter of 2011-12, as the xCO_2 at CRIMP-2 begins to rise significantly. Chuuk K1 is a low latitude (7.46°N, 151.90°E) reef located in Micronesia within a semi-enclosed atoll in ~ 23 m water depth. Here, xCO_2 increases much more slowly than at CRIMP-2, which could be because it is a much deeper site than CRIMP-2 (~ 3 m). Also, Chuuk K1 is located in the Western Equatorial Pacific and is likely affected by climate oscillations in a much different way than Hawaii. The rising pCO_2sw trend at CRIMP-2 was not observed at these other reef sites. We showed that changes in physical processes (SST and wind speed) on inter-annual time scales are likely driving the pCO_2 trend at CRIMP-2. Possibly these changes in wind speed and SST are specific to the Central North Pacific (Hawaii) and might be the result of large scale changes in ocean (and atmospheric) circulation patterns.

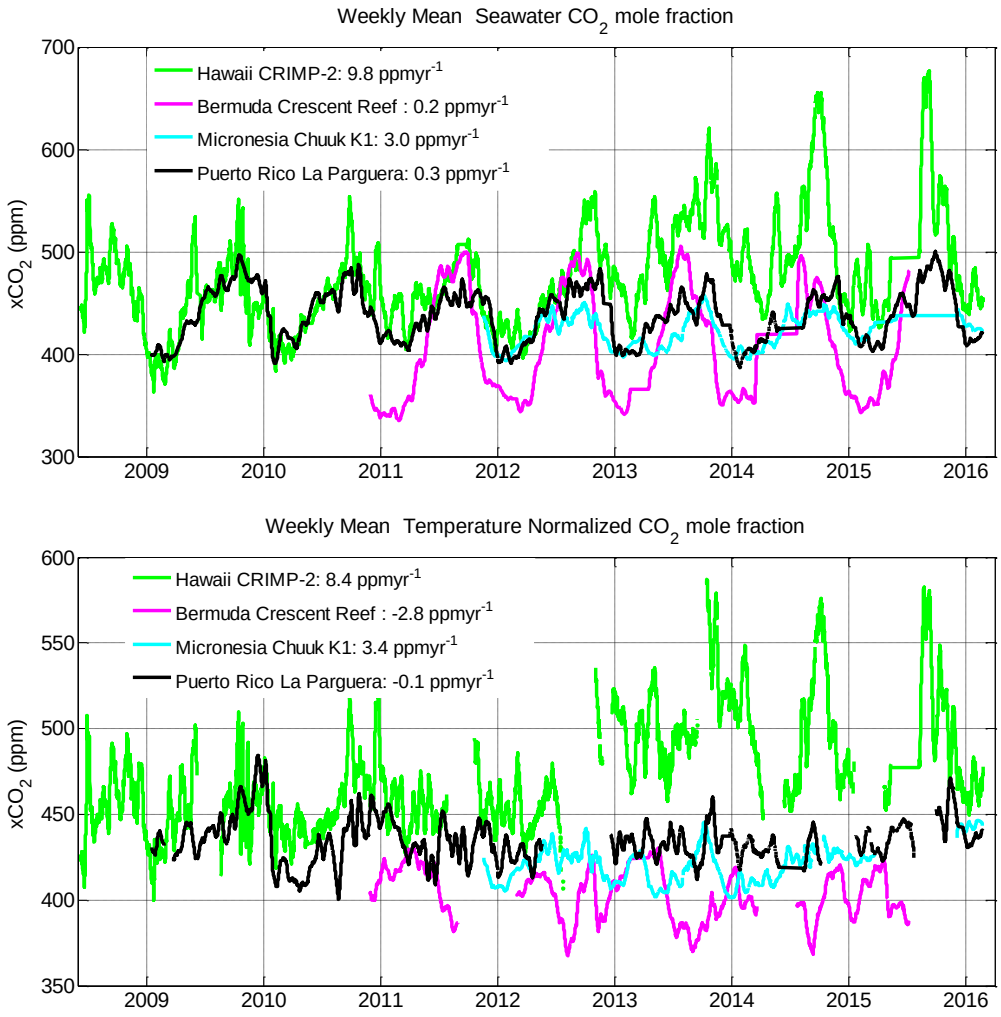

Figure 3.14 Time-series of weekly mean mole fraction of CO_2 (xCO_2, top) and temperature normalized xCO_2 (bottom) at different reef sites for June 2008 – February 2016 Weekly mean values were estimated from 3-hourly data by applying a running-average filter over 56 data points. The rates of change in the legend of the Figure correspond to the slope of a linear regression over the length of the time-series, and are an estimate of the average annual increase. Only the increase at CRIMP-2 was significant.

3.5 Conclusion

In this chapter I examined which processes may be driving variability in pCO_2sw and air-sea CO_2 fluxes on different time-scales. The effect of local geographic and climatic differences between sites was examined using data from $MAPCO_2$ buoys at three different reef sites around the island of Oahu, Hawaii.

Additionally, the nearby open ocean MAPCO_2 site WHOTS, co-located with station ALOHA in the North Pacific Subtropical gyre, provided an unique opportunity to compare open ocean and coastal CO_2 dynamics. Diurnal pCO_2sw variability was mainly driven by benthic and water column biological productivity (photosynthesis/respiration and calcification/dissolution). Diurnal pCO_2sw fluctuations were on average 5-30 times greater at the coastal sites than in the open ocean for three main reasons:

1. In coastal waters, land/ocean interactions increase nutrient availability which increases rates of biogeochemical processes.
2. Benthic biogeochemical processes can contribute to surface water pCO_2sw variability at shallow coastal sites, but not in the open ocean.
3. Water residence time can be long in semi-enclosed areas, such as the CRIMP-2 site in Kaneohe Bay, which allows for a buildup of the biogeochemical signal in seawater.

The overall seasonal pCO_2sw cycle was largely controlled by changes in SST, but seasonal differences in productivity also seemed to play an important role. For example, on the Kaneohe Bay barrier reef (CRIMP-2), higher SST and light availability in summer increased calcification, thereby further elevating summer pCO_2sw. On the other hand, increased rainfall during the winter increased land-derived inputs of nutrients and organic matter to the coastal ocean via the Ala Wai canal, thereby increasing photosynthesis and respiration in winter. In the open ocean, seawater is consistently a source of CO_2 to the atmosphere in summer and a sink for atmospheric CO_2 in winter, because ΔpCO_2 is seasonally determined. In coastal waters, the air-sea CO_2 flux often switches between a source and sink, even within a diurnal cycle, because pCO_2sw is highly variable.

On inter-annual time-scales, pCO_2sw variability might be driven by large-scale climate oscillation patterns, which drive changes in SST and nutrient concentrations on decadal-time scales. The pCO_2sw trend at CRIMP-2 correlated significantly ($R = -0.57$, p-value < 0.01) with the North Pacific Gyre Oscillation (NPGO), which is a climate oscillation that affects oceanic circulation patterns in the North

Pacific Ocean and has previously been linked to changes in open ocean productivity at station ALOHA. Detecting an inter-annual OA signal at coastal sites, however, is likely further complicated as the climate oscillations can mask the long term OA signal.

CHAPTER IV: SUMMARY AND CONCLUSIONS

Understanding the processes that drive pCO_2sw variability in coral reefs on various time scales can provide us with invaluable information on how these ecosystems might respond to climate change. However, datasets that are able to resolve pCO_2 changes on time scales ranging from sub-diurnal to inter-annual are still relatively rare, especially for coral reefs. This thesis provides a synthesis of the longest, nearly continuous, time-series data set of coastal CO_2 dynamics on our planet. Data were collected between 2008 and 2016 at Ala Wai, Kilo Nalu, and CRIMP-2 reef sites around the island of Oahu, Hawaii. These data were compared to a similar time-series data set from the open ocean (WHOTS) in the North Pacific Subtropical gyre. In addition to the time-series data analysis, an internal consistency study of the CO_2-carbonic acid system data that was collected by our research group was carried out to verify the quality of the autonomously collected pCO_2 data.

The quality and reliability of the autonomous pCO_2 data as well as other CO_2-carbonic system data (pH, TA, and DIC) collected by our research group was examined in Chapter 2. In theory, if any combination of two of these four parameters are measured, the full CO_2-carbonic acid system in seawater can be constrained through apparent equilibrium constants. In practice, however, not every combination provides accurate calculations of the other parameters (e.g. Millero et al. 2007). Calculations based on measurements of pH and pCO_2sw are typically less accurate due to the high covariance of these parameters, especially for calculating TA and DIC (Dickson and Riley 1978). Calculations based on measurements of TA and DIC are generally recommended for OA research (Riebesell et al. 2010), although pCO_2sw is actually more accurately calculated from pH in combination with either TA or DIC. In coastal areas where there is a considerable land derived input of organic matter, however, TA measurements could be biased because organic acid-base compounds can contribute to the alkalinity of a sample that is not accounted for in CO_2-carbonic acid calculations. In such areas, DIC should be used in

calculations instead of TA. Overall, the internal consistency study confirms the quality and reliability of the pCO_2 time-series data on which the climatology developed here was based.

We found that daily cycles of photosynthesis/respiration and calcification/dissolution drive diurnal pCO_2sw fluctuations that are on average 5-30 greater at our coral reef sites than in the open ocean (WHOTS). Seasonal changes in pCO_2sw, however, are largely driven by seasonal seawater temperature cycle and, to a lesser extent, by seasonal variations in productivity. Inter-annual trends in pCO_2sw on the Kaneohe Bay barrier reef (CRIMP-2) appear to be influenced by inter-annual changes in physical processes such as SST and wind speed. The increase in pCO_2sw between 2012 and 2016 coincided with increasing SST, which influences the solubility of CO_2 in seawater and also changes the balance of photosynthesis/respiration and calcification/dissolution on the reef. Decreased trade winds between 2012 and 2016 likely decreased air-sea CO_2 gas exchange rates and increased the water residence time thus led to an amplification of the biogeochemical signal. These inter-annual changes in physical processes (SST and wind speed) may be related to basin wide climate oscillation patterns in the North Pacific. For example, the strong 2015/2016 El Niño has been linked to the anomalously high SST in Hawaii. Additionally, anomalies of pCO_2sw at CRIMP-2 correlated significantly with the North Pacific Gyre Oscillation (NPGO, $R = -0.57$), a basin-wide oceanic oscillation pattern that explains changes in circulation in the North Pacific. NPGO affects SST and nutrient concentrations, and has been linked to changes in productivity in the North Pacific Subtropical gyre.

Identifying an ocean acidification trend is much more difficult on coral reefs compared to the open ocean, owing to the large natural pCO_2sw variability in these ecosystems. The anticipated ocean acidification trend of ~ 2 µatm yr^{-1} is overshadowed by inter-annual pCO_2sw trends that are affected by SST and wind speed variations. Projected increases in SST as well as decreased trade wind speeds as a result of climate change might be a more important driver of the inter-annual pCO_2 trend on Hawaiian reefs than Ocean Acidification, at least within the next decade.

LITERATURE

Albright, R., Langdon, C. & Anthony, K.R.N., 2013. Dynamics of seawater carbonate chemistry, production, and calcification of a coral reef flat, central Great Barrier Reef. *Biogeosciences*, 10(10), pp.6747–6758.

Alexander, M.A. et al., 2002. The Atmospheric Bridge: The Influence of ENSO Teleconnections on Air–Sea Interaction over the Global Oceans. *Journal of Climate*, 15(16), pp.2205–2231.

Andersson, A.J. & Gledhill, D., 2013. Ocean acidification and coral reefs: effects on breakdown, dissolution, and net ecosystem calcification. *Annual review of marine science*, 5, pp.321–48.

Ashok, K. & Yamagata, T., 2009. Climate change: The El Niño with a difference. *Nature*, 461(7263), pp.481–484.

Bahr, K.D., Jokiel, P.L. & Rodgers, K.S., 2015. The 2014 coral bleaching and freshwater flood events in Kāneʻohe Bay, Hawaiʻi. *PeerJ*, 3, p.e1136.

Bates, N.R., Amat, A. & Andersson, A.J., 2010. Feedbacks and responses of coral calcification on the Bermuda reef system to seasonal changes in biological processes and ocean acidification. *Biogeosciences*, 7(8), pp.2509–2530.

Bates, R.N. et al., 2014. A Time-Series View of Changing Surface Ocean Chemistry Due to Ocean Uptake of Anthropogenic CO2 and Ocean Acidification. *Oceanography*, 27, pp.126–141.

Bender, M.L. et al., 2005. Atmospheric O2 /N2 changes, 1993-2002: Implications for the partitioning of fossil fuel CO2 sequestration. *Global Biogeochemical Cycles*, 19(4), p.n/a-n/a.

Bresnahan, P.J. et al., 2014. Best practices for autonomous measurement of seawater pH with the Honeywell Durafet. *Methods in Oceanography*, 9, pp.44–60.

Cai, W.-J. & Wang, Y., 1998. The chemistry, fluxes, and sources of carbon dioxide in the estuarine

waters of the Satilla and Altamaha Rivers, Georgia. *Limnology and Oceanography*, 43(4), pp.657–668.

Caldeira, K. & Wickett, M.E., 2003. Oceanography: anthropogenic carbon and ocean pH. *Nature*, 425(6956), p.365.

Chamard, B.P. et al., 2003. Interannual variability of atmospheric CO_2 in the Mediterranean: measurements at the island of Lampedusa. *Tellus*, 55(B), pp.83–93.

Chhak, K.C. et al., 2009. Forcing of Low-Frequency Ocean Variability in the Northeast Pacific*. *Journal of Climate*, 22(5), pp.1255–1276.

Clayton, T.D. et al., 1995. The role of pH measurements in modern oceanic CO2-system characterizations: Precision and thermodynamic consistency. *Deep Sea Research Part II: Topical Studies in Oceanography*, 42(2–3), pp.411–429..

Coles, S.L. & Jokiel, P.L., 1978. Synergistic effects of temperature, salinity and light on the hermatypic coral Montipora verrucosa. *Marine Biology*, 49(3), pp.187–195.

Corno, G. et al., 2007. Impact of climate forcing on ecosystem processes in the North Pacific Subtropical Gyre. *Journal of Geophysical Research*, 112(C4), p.C04021.

Cullison Gray, S.E. et al., 2011. Applications of in situ pH measurements for inorganic carbon calculations. *Marine Chemistry*, 125(1–4), pp.82–90.

Dave, A.C. & Lozier, M.S., 2010. Local stratification control of marine productivity in the subtropical North Pacific. *Journal of Geophysical Research*, 115(C12), p.C12032.

De Carlo, E.H. et al., 2013. Carbonate Chemistry and Air-Sea CO2 Flux in a NW Mediterranean Bay Over a Four-Year Period: 2007-2011. *Aquatic Geochemistry*, 19(5–6), pp.399–442.

De Carlo, E.H. et al., 2007. Impact of storm runoff from tropical watersheds on coastal water quality and productivity. *Applied Geochemistry*, 22(8), pp.1777–1797.

De Carlo, E.H., Beltran, V.L. & Tomlinson, M.S., 2004. Composition of water and suspended sediment in streams of urbanized subtropical watersheds in Hawaii. *Applied Geochemistry*, 19(7), pp.1011–

1037.

Dickson, A.G. & Millero, F.J., 1987. A comparison of the equilibrium constants for the dissociation of carbonic acid in seawater media. *Deep Sea Research Part A. Oceanographic Research Papers*, 34(10), pp.1733–1743.

Dickson, A.G. & Riley, J.P., 1978. The effect of analytical error on the evaluation of the components of the aquatic carbon-dioxide system. *Marine Chemistry*, 6(1), pp.77–85.

Dickson, A.G., Sabine, C.L. & Christian, J.R., 2007. Guide to Best Practices for Ocean CO2 Measurements.

Di Lorenzo, E. et al., 2008. North Pacific Gyre Oscillation links ocean climate and ecosystem change. *Geophysical Research Letters*, 35(8), p.L08607.

Di Lorenzo, E. & Schneider, N., An overview of Pacific Climate Variability. Available at: http://www.o3d.org/npgo/docs/Decadal-Intro.pdf [Accessed August 12, 2016].

Doney, S.C. et al., 2009. Ocean acidification: the other CO2 problem. *Annual review of marine science*, 1, pp.169–92.

Dore, J.E. et al., 2009. Physical and biogeochemical modulation of ocean acidification in the central North Pacific. *Proceedings of the National Academy of Sciences of the United States of America*, 106(30), pp.12235–12240.

Drupp, P. et al., 2011. Nutrient Inputs, Phytoplankton Response, and CO2 Variations in a Semi-Enclosed Subtropical Embayment, Kaneohe Bay, Hawaii. *Aquatic Geochemistry*, 17(4), pp.473–498.

Drupp, P.S. et al., 2013. Comparison of CO2 Dynamics and Air-Sea Gas Exchange in Differing Tropical Reef Environments. *Aquatic Geochemistry*, 19(5–6), pp.371–397.

Fagan, K.E. & Mackenzie, F.T., 2007. Air–sea CO2 exchange in a subtropical estuarine-coral reef system, Kaneohe Bay, Oahu, Hawaii. *Marine Chemistry*, 106(1–2), pp.174–191.

Fassbender, A.J. et al., 2015. Robust sensor for extended autonomous measurements of surface ocean dissolved inorganic carbon. *Environmental science & technology*, 49(6), pp.3628–35.

Feely, R.A. et al., 2008. Evidence for upwelling of corrosive "acidified" water onto the continental shelf. *Science (New York, N.Y.)*, 320(5882), pp.1490–2.

Giambelluca, T.W. et al., 2013. Online Rainfall Atlas of Hawai'i. Available at: http://journals.ametsoc.org/doi/abs/10.1175/BAMS-D-11-00228.1 [Accessed May 25, 2016].

Gloor, M. et al., 2003. A first estimate of present and preindustrial air-sea CO 2 flux patterns based on ocean interior carbon measurements and models. *Geophysical Research Letters*, 30(1), pp.10-1-4.

Goyet, C. & Poisson, A., 1989. New determination of carbonic acid dissociation constants in seawater as a function of temperature and salinity. *Deep Sea Research Part A. Oceanographic Research Papers*, 36(11), pp.1635–1654.

Hansson, I., 1973. A new set of acidity constants for carbonic acid and boric acid in sea water. *Deep Sea Research and Oceanographic Abstracts*, 20(5), pp.461–478.

Hernández-Ayon, J.M. et al., 2007. Estimating the contribution of organic bases from microalgae to the titration alkalinity in coastal seawaters. *Limnology and Oceanography: Methods*, 5, pp.225–232.

Ho, D.T. et al., 2006. Measurements of air-sea gas exchange at high wind speeds in the Southern Ocean: Implications for global parameterizations. *Geophysical Research Letters*, 33(16), pp.1–6.

Hoegh-Guldberg, O., 1999. Climate change, coral bleaching and the future of the world's coral reefs. *Marine and Freshwater Research*, 50(8), p.839.

Hoegh-Guldberg, O. et al., 2008. Coral Reefs Under Rapid Climate Change and Ocean Acidification. *Science*, 318(December 2007), pp.1737–1742.

Hoover, R.S. et al., 2006. Zooplankton response to storm runoff in a tropical estuary: Bottom-up and top-down controls. *Marine Ecology Progress Series*, 318(Wassmann 1998), pp.187–201.

Ishii, M. et al., 2014. Air-sea CO2 flux in the Pacific Ocean for the period 1990–2009. Available at: http://darchive.mblwhoilibrary.org/handle/1912/6672 [Accessed May 25, 2016].

Jokiel, P.L., 1991. *Jokiel's illustrated scientific guide to Kaneohe Bay, Oahu*,

Jokiel, P.L. & Coles, S.L., 1977. Effects of temperature on the mortality and growth of Hawaiian reef

corals. *Marine Biology*, 43(3), pp.201–208.

Karl, D.., Bidigare, R.. & Letelier, R.., 2001. Long-term changes in plankton community structure and productivity in the North Pacific Subtropical Gyre: The domain shift hypothesis. *Deep Sea Research Part II: Topical Studies in Oceanography*, 48(8), pp.1449–1470.

Kayanne, H., Suzuki, A. & Saito, H., 1995. Diurnal changes in the partial pressure of carbon dioxide in coral reef water. *Science (New York, N.Y.)*, 269(5221), pp.214–6.

Keeling, C.D. et al., 1976. Atmospheric carbon dioxide variations at Mauna Loa Observatory, Hawaii. *Tellus A*, 28, pp.538–551.

Keeling, C.D. et al., 2001. Exchanges of atmospheric CO2 and 13CO2 with the terrestrial biosphere and oceans from 1978 to 2000. *Global Aspects, SIO Reference Series. Scripps institution of Oceangraphy, San Diego*, 01–06, pp.83–113.

Keeling, R.F. & Garcia, H.E., 2002. The change in oceanic O(2) inventory associated with recent global warming. *Proceedings of the National Academy of Sciences of the United States of America*, 99(12), pp.7848–53.

Key, R.M. et al., 2004. A global ocean carbon climatology: Results from Global Data Analysis Project (GLODAP). *Global Biogeochemical Cycles*, 18(4), pp.1–23.

Kim, H.-C., Lee, K. & Choi, W., 2006. Contribution of phytoplankton and bacterial cells to the measured alkalinity of seawater. *Limnology and Oceanography*, 51(1), pp.331–338.

Kleypas, J.A. et al., 1999. Geochemical Consequences of Increased Atmospheric Carbon Dioxide on Coral Reefs. *Science*, 284(5411), pp.118–120.

Kleypas, J.A., McManus, J.W., and Meñez, L.A.B., 1999. Environmental Limits to Coral Reef Development: Where Do We Draw the Line? *American Zoologist*, 39(1), pp.146–159.

Langdon, C. & Atkinson, M.J., 2005. Effect of elevated pCO_2 on photosynthesis and calcification of corals and interactions with seasonal change in temperature/irradiance and nutrient enrichment. *Journal of Geophysical Research*, 110(C9), p.C09S07.

Lee, K., Millero, F.J. & Campbell, D.M., 1996. The reliability of the thermodynamic constants for the dissociation of carbonic acid in seawater. *Marine Chemistry*, 55(3–4), pp.233–245.

Lee, K., Millero, F.J. & Wanninkhof, R., 1997. The carbon dioxide system in the Atlantic Ocean. *Journal of Geophysical Research: Oceans*, 102(C7), pp.15693–15707.

Lenton, A. et al., 2013. Sea-air CO2 fluxes in the Southern Ocean for the period 1990-2009. *Biogeosciences*, 10(6), pp.4037–4054.

Lerman, A. & Mackenzie, F.T., 2005. CO2 Air–Sea Exchange due to Calcium Carbonate and Organic Matter Storage, and its Implications for the Global Carbon Cycle. *Aquatic Geochemistry*, 11(4), pp.345–390.

Lewis, E. & Wallace, D., 1998. CO2SYS: Program developed for CO2 system calculations. Available at: http://cdiac.ornl.gov/oceans/co2rprt.html.

Li, Y.-H. et al., 2000. Remineralization ratios in the subtropical north pacific gyre. *Aquatic Geochemistry*, 6(1), pp.65–86.

Liss, P.S., 1983. Gas transfer: experiments and geochemical implications. In P. S. Liss & W. G. N. Slinn, eds. *Air-sea exchange of gases and particles*. Dordrecht: D. Reidel, pp. 241–298.

Liu, X. et al., 2013. In situ spectrophotometric measurement of dissolved inorganic carbon in seawater. *Environmental science & technology*, 47(19), pp.11106–14.

Le Quéré, C. et al., 2015. Global carbon budget 2014. *Earth System Science Data*, 7:47-85. doi 10.5194/essd-7-47-2015

Lowe, R.J. et al., 2009. A numerical study of circulation in a coastal reef-lagoon system. *Journal of Geophysical Research*, 114(C6), p.C06022.

Lueker, T.., Dickson, A.. & Keeling, C.., 2000. Ocean p CO 2 calculated from dissolved inorganic carbon , alkalinity , and equations for K 1 and K 2 : validation based on laboratory measurements of CO 2 in gas and seawater at equilibrium.

Mantua, N.J. et al., 1997. A Pacific Interdecadal Climate Oscillation with Impacts on Salmon Production.

Bulletin of the American Meteorological Society, 78(6), pp.1069–1079.

Marshall, A.T. & Clode, P., 2004. Calcification rate and the effect of temperature in a zooxanthellate and an azooxanthellate scleractinian reef coral. *Coral Reefs*, 23(2), pp.218–224.

Martz, T.R., 2015. *Best Practices for autonomous measurement of seawater pH with the Honeywell Durafet pH sensor*, Available at: http://ftp.sccwrp.org/pub/download/DOCUMENTS/TechnicalReports/861_CCAN_Durafet_Best_Practices_Manual.pdf.

Martz, T.R., Dickson, A.G. & DeGrandpre, M.D., 2006. Tracer monitored titrations: measurement of total alkalinity. *Analytical chemistry*, 78(6), pp.1817–26.

Massaro, R.F.S. et al., 2012. Multiple Factors driving Variability of CO 2 Exchange Between the Ocean and Atmosphere in a Tropical Coral Reef Environment. *Aquatic Geochemistry*, 18(4), pp.357–386.

Mehrbach, C. et al., 1973. Measurement of the apparent dissociation constants of carbonic acid in seawater at atmospheric pressure. *Limnology and Oceanography*, 18, pp.897–907.

Millero, F.J. et al., 2006. Dissociation constants of carbonic acid in seawater as a function of salinity and temperature. *Marine Chemistry*, 100(1–2), pp.80–94.

Millero, F.J., 2007. The marine inorganic carbon cycle. *Chemical reviews*, 107(2), pp.308–41.

Mojica Prieto, F.J. & Millero, F.J., 2002. The values of pK1 + pK2 for the dissociation of carbonic acid in seawater. *Geochimica et Cosmochimica Acta*, 66(14), pp.2529–2540.

Morse, J.W., Arvidson, R.S. & Lüttge, A., 2007. Calcium carbonate formation and dissolution. *Chemical reviews*, 107(2), pp.342–81. Available at: http://dx.doi.org/10.1021/cr050358j [Accessed May 8, 2016].

Newman, M. et al., 2003. ENSO-Forced Variability of the Pacific Decadal Oscillation. *Journal of Climate*, 16(23), pp.3853–3857.

Orr, J.C. et al., 2005. Anthropogenic ocean acidification over the twenty-first century and its impact on calcifying organisms. *Nature*, 437(7059), pp.681–686.

Park, P.K., 1969. Oceanic CO2 system: An evaluation of ten methods of investigation. *Limnology and Oceanography*, 14–2(March), pp.179–186.

Patsavas, M.C. et al., 2015. Internal consistency of marine carbonate system measurements and assessments of aragonite saturation state: Insights from two U.S. coastal cruises. *Marine Chemistry*, 176, pp.9–20.

Quay, P. et al., 2003. Changes in the 13 C/ 12 C of dissolved inorganic carbon in the ocean as a tracer of anthropogenic CO 2 uptake. *Global Biogeochemical Cycles*, 17(1), pp.4-1-4–20.

Riebesell, U. et al., 2010. *Guide to best practices for ocean acidification research and data reporting*, Available at: http://blogs.nwic.edu/briansblog/files/2012/02/Guide-to-best-practices-for-ocean-acidification-research-and-data-reporting.pdf.

Ringuet, S. & Mackenzie, F.T., 2005. Controls on nutrient and phytoplankton dynamics during normal flow and storm runoff conditions, southern Kaneohe Bay, Hawaii. *Estuaries*, 28(3), pp.327–337.

Roy, R.N. et al., 1993. The dissociation constants of carbonic acid in seawater at salinities 5 to 45 and temperatures 0 to 45°C. *Marine Chemistry*, 44(2–4), pp.249–267.

Sabine, C.L. et al., 2004. The oceanic sink for anthropogenic CO2. *Science (New York, N.Y.)*, 305(5682), pp.367–71.

Sarma, V.V.S.S. et al., 2013. Sea-air CO2 fluxes in the Indian Ocean between 1990 and 2009. *Biogeosciences*, 10(11), pp.7035–7052.

Sayles, F.L. & Eck, C., 2009. An autonomous instrument for time series analysis of TCO2 from oceanographic moorings. *Deep Sea Research Part I: Oceanographic Research Papers*, 56(9), pp.1590–1603.

Shamberger, K.E.F. et al., 2011. Calcification and organic production on a Hawaiian coral reef. *Marine Chemistry*, 127(1–4), pp.64–75.

Shaw, E.C. & McNeil, B.I., 2014. Seasonal variability in carbonate chemistry and air-sea CO2 fluxes in the southern Great Barrier Reef. *Marine Chemistry*, 158, pp.49–58.

Silverman, J. et al., 2009. Coral reefs may start dissolving when atmospheric CO2 doubles. *Geophysical Research Letters*, 36(5), pp.1–5.

Spaulding, R.S. et al., 2014. Autonomous in situ measurements of seawater alkalinity. *Environmental science & technology*, 48(16), pp.9573–81.

Sutton, A.J. et al., 2014. A high-frequency atmospheric and seawater pCO_2 data set from 14 open-ocean sites using a moored autonomous system. *Earth System Science Data*, 6(2), pp.353–366.

Sutton, A.J. et al., 2014. Natural variability and anthropogenic change in equatorial Pacific surface ocean pCO2 and pH. *Global Biogeochemical Cycles*, 28(2), pp.131–145.

Takahashi, T. et al., 2002. Global sea-air CO2 flux based on climatological surface ocean pCO2, and seasonal biological and temperature effects. *Deep-Sea Research Part II: Topical Studies in Oceanography*, 49(9–10), pp.1601–1622.

Tans, P.P. & Keeling, C.D., 2016. Trends in atmospheric Carbon Dioxide. Available at: www.esrl.noaa.gov/gmd/ccgg/trends/.

Thoning, K.W., Tans, P.P. & Komhyr, W.D., 1989. Atmospheric carbon dioxide at Mauna Loa Observatory: 2. Analysis of the NOAA GMCC data, 1974–1985. *Journal of Geophysical Research*, 94(D6), p.8549.

Tomlinson, M.S. et al., 2011. Characterizing the Effects of Two Storms on the Coastal Waters of Oahu, Hawaii, Using Data from the Pacific Islands Ocean Observing System. *Oceanography*, 24(2), pp.182–199.

Venti, A., Andersson, A. & Langdon, C., 2014. Multiple driving factors explain spatial and temporal variability in coral calcification rates on the Bermuda platform. *Coral Reefs*, 33(4), pp.979–997.

Wang, Z.A. et al., 2015. In situ sensor technology for simultaneous spectrophotometric measurements of seawater total dissolved inorganic carbon and pH. *Environmental science & technology*, 49(7), pp.4441–9.

Wanninkhof, R., 1992. Relationship between wind speed and gas exchange over the ocean. *Journal of*

Geophysical Research, 97(C5), p.7373.

Wanninkhof, R. et al., 1999. The optimal carbonate dissociation constants for determining surface water pCO2 from alkalinity and total inorganic carbon. *Marine Chemistry*, 65(3–4), pp.291–301.

Weiss, R.F., 1974. Carbon dioxide in water and seawater: the solubility of a non-ideal gas. *Marine Chemistry*, 2(3), pp.203–215.

Weiss, R.F. & Price, B.A., 1980. Nitrous oxide solubility in water and seawater. *Marine Chemistry*, 8(4), pp.347–359.

Yan, H. et al., 2011. Coral reef ecosystems in the South China Sea as a source of atmospheric CO2 in summer. *Chinese Science Bulletin*, 56(7), pp.676–684.

Yan, H. et al., 2016. Seasonal variations of seawater pCO 2 and sea-air CO 2 fluxes in a fringing coral reef, northern South China Sea. *Journal of Geophysical Research: Oceans*, 121(1), pp.998–1008.

Yeakel, K.L. et al., 2015. Shifts in coral reef biogeochemistry and resulting acidification linked to offshore productivity. *Proceedings of the National Academy of Sciences*, 112(47), pp.14512–14517.

Zeebe, R.E. & Wolf-Gladrow, D., 2001. CO2 in Seawater: Equilibrium, Kinetics, Isotopes. *Igarss 2014*, (1).

Zhang, Y. et al., 1997. ENSO-like Interdecadal Variability: 1900–93. *Journal of Climate*, 10(5), pp.1004–1020.

APPENDIX A: CLIMATOLOGICAL MONTHLY BOX PLOTS

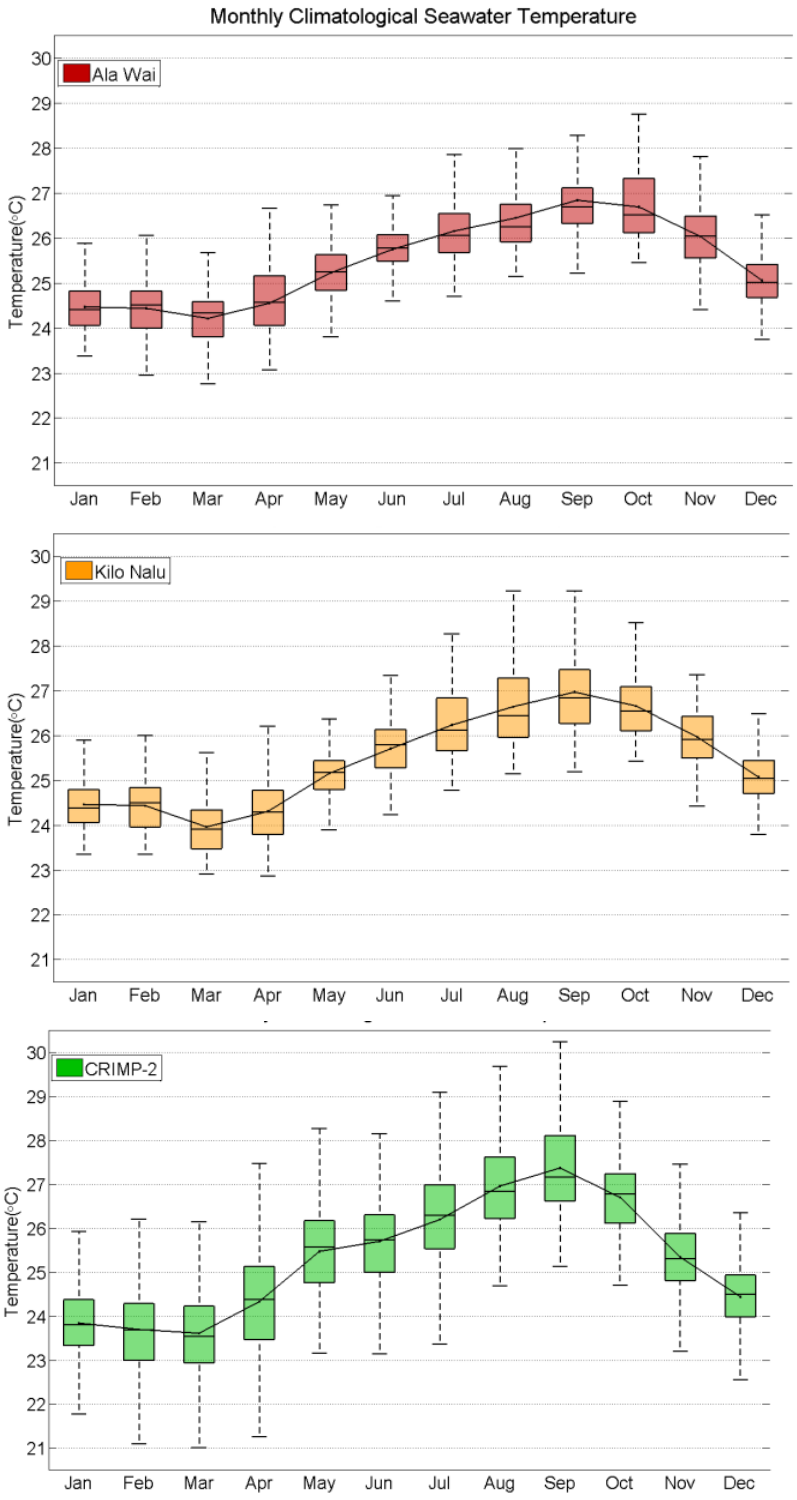

Figure A.1 Climatological monthly box plot of seawater temperature (°C) at Ala Wai (top panel), Kilo Nalu (middle panel), and CRIMP-2 (bottom panel)

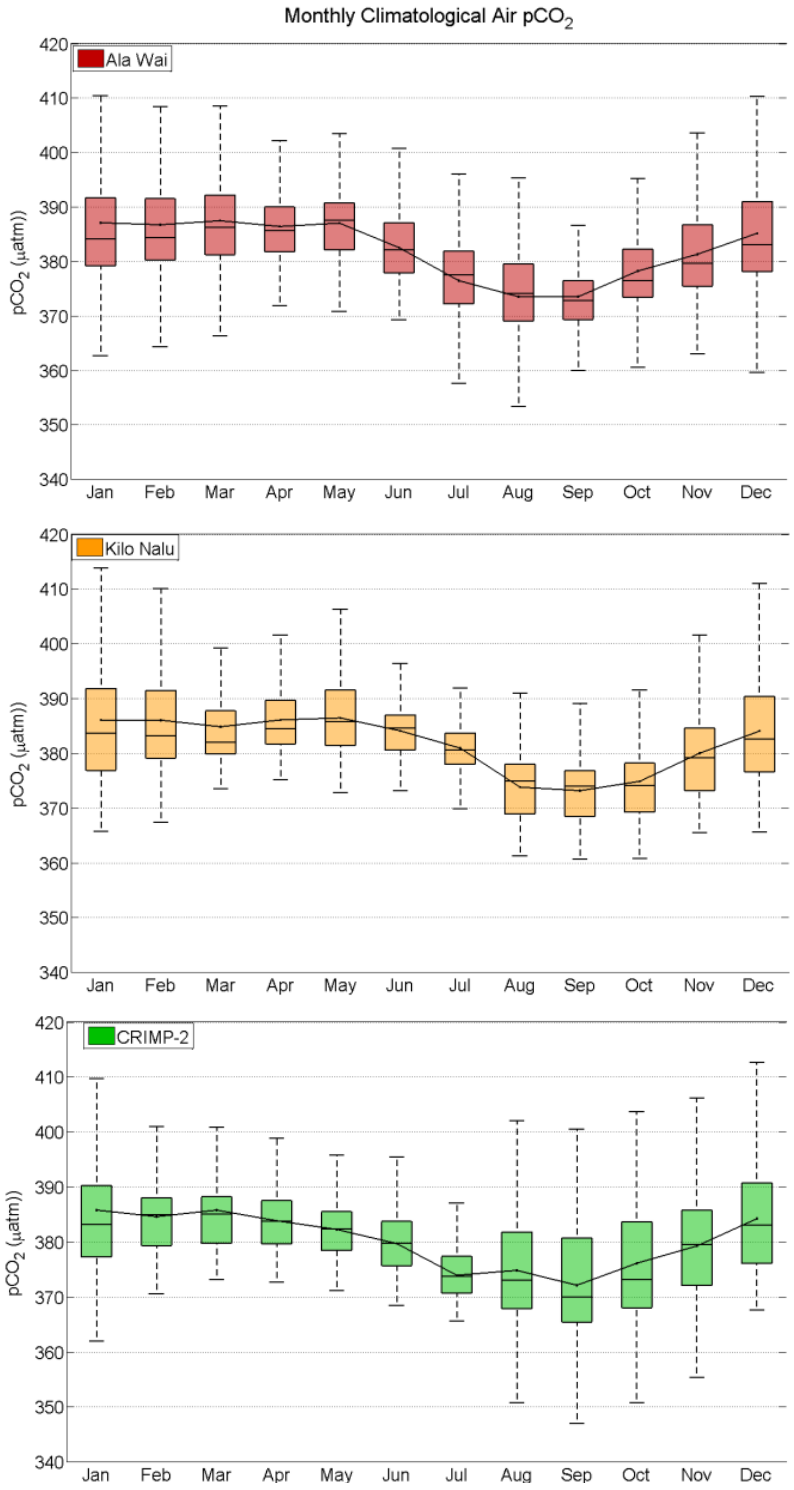

Figure A.2 Climatological monthly box plot of air pCO_2 (µatm) at Ala Wai (top panel), Kilo Nalu (middle panel), and CRIMP-2 (bottom panel)

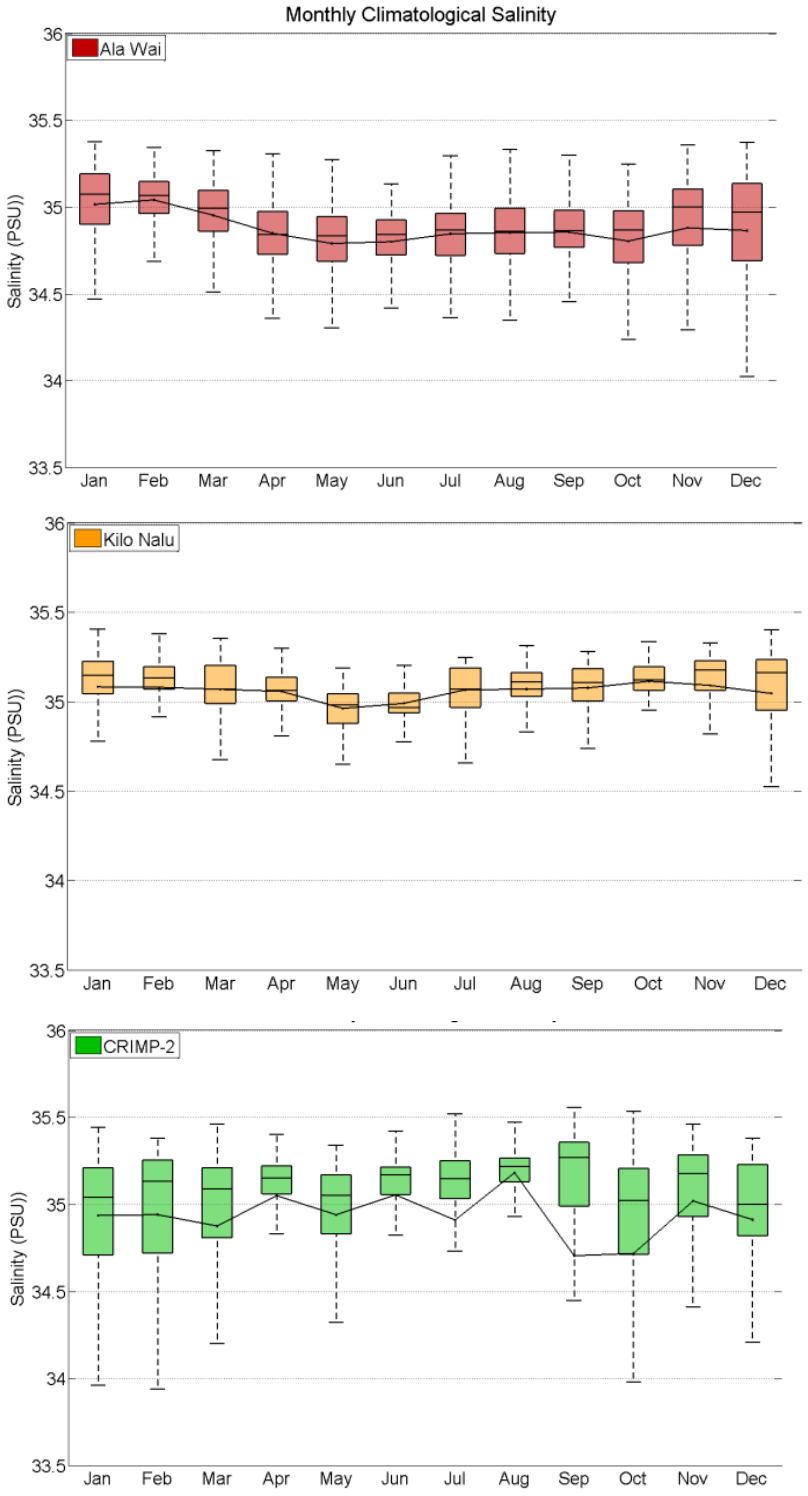

Figure A.3 Climatological monthly box plot of Salinity (PSU) at Ala Wai (top panel), Kilo Nalu (middle panel), and CRIMP-2 (bottom panel)

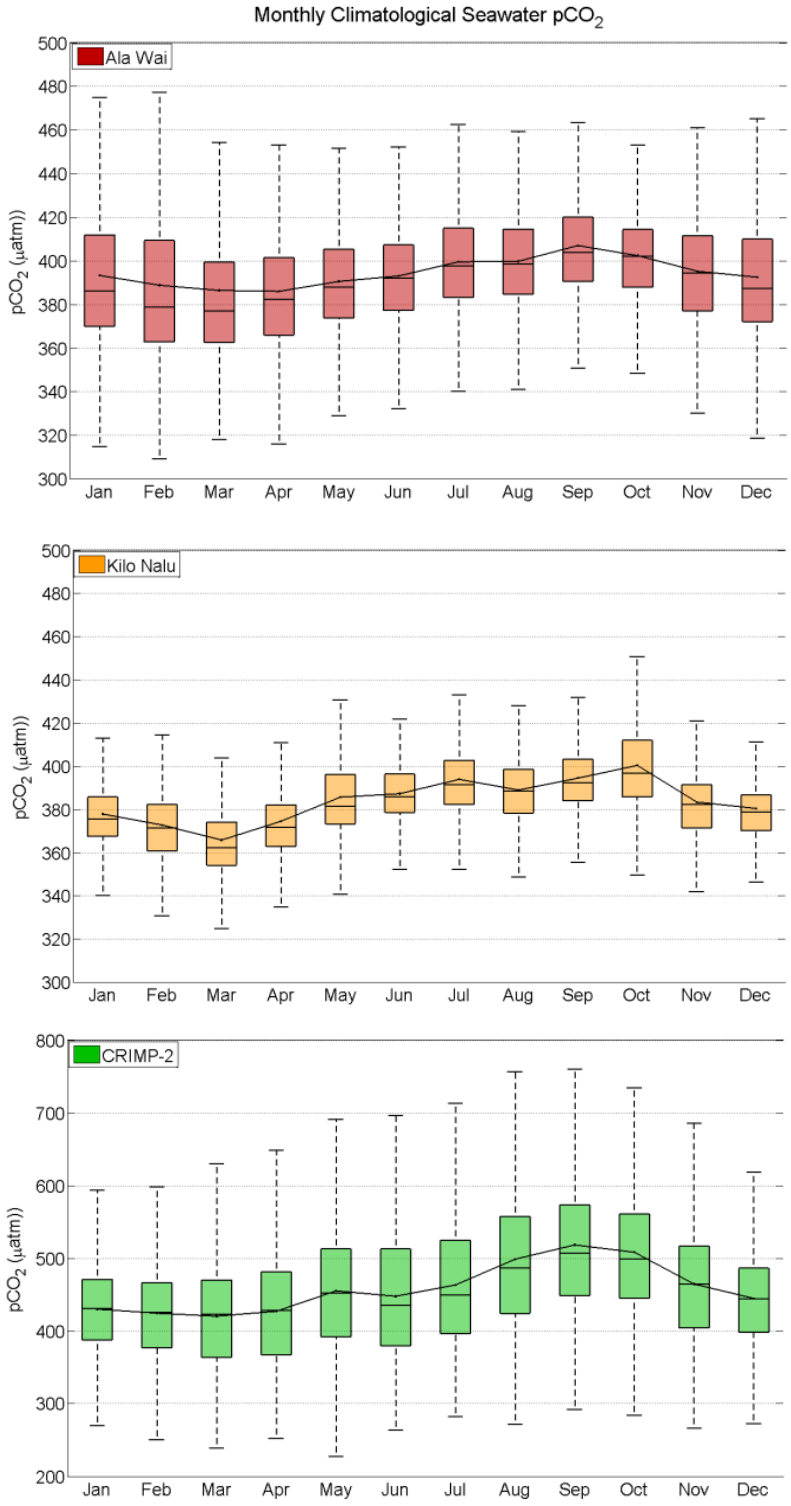

Figure A.4 Climatological monthly box plot of seawater pCO_2 (µatm) at Ala Wai (top panel), Kilo Nalu (middle panel), and CRIMP-2 (bottom panel)

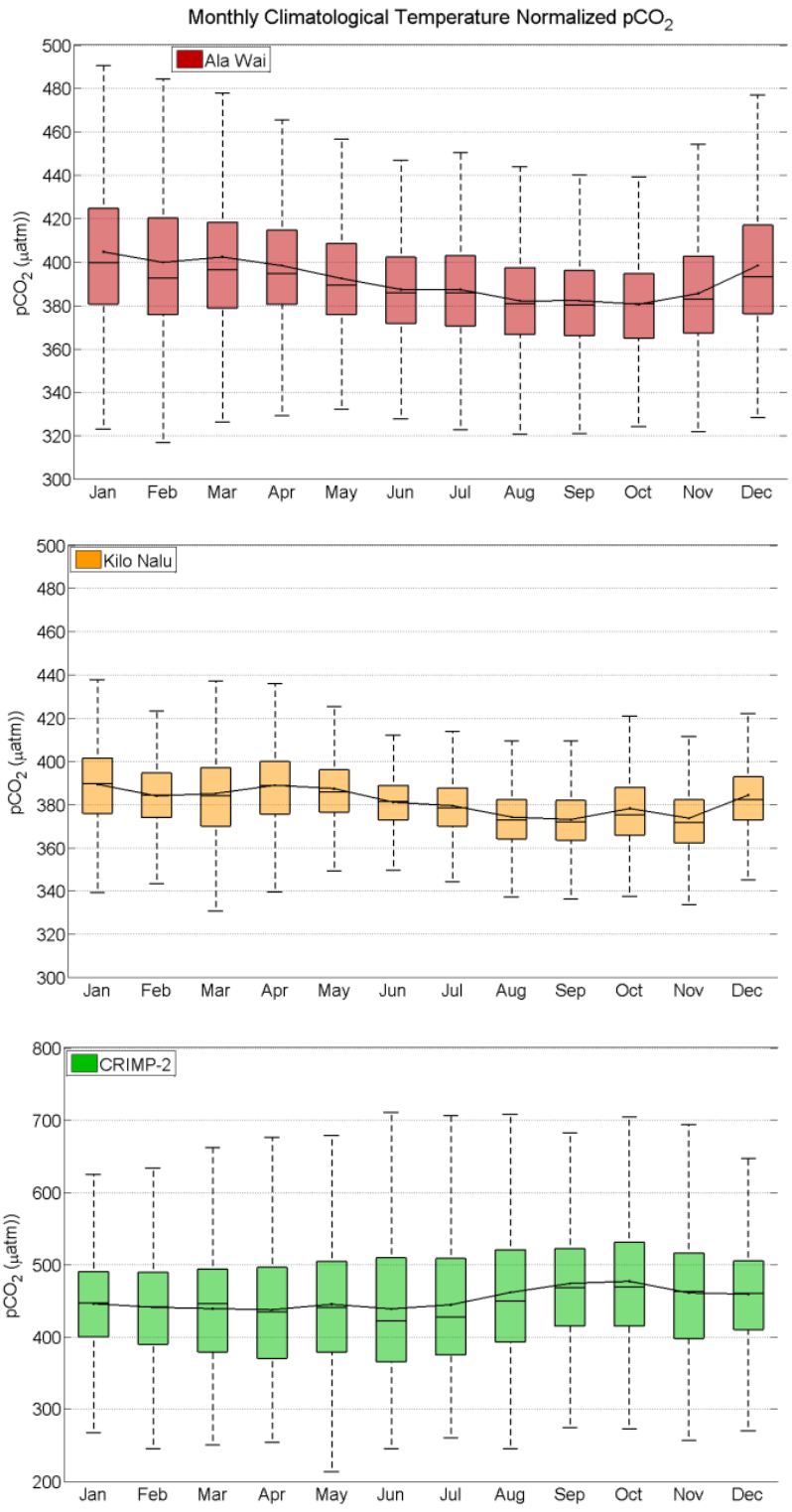

Figure A.5 Climatological monthly box plot of temperature normalized pCO_2 (µatm) at Ala Wai (top panel), Kilo Nalu (middle panel), and CRIMP-2 (bottom panel)

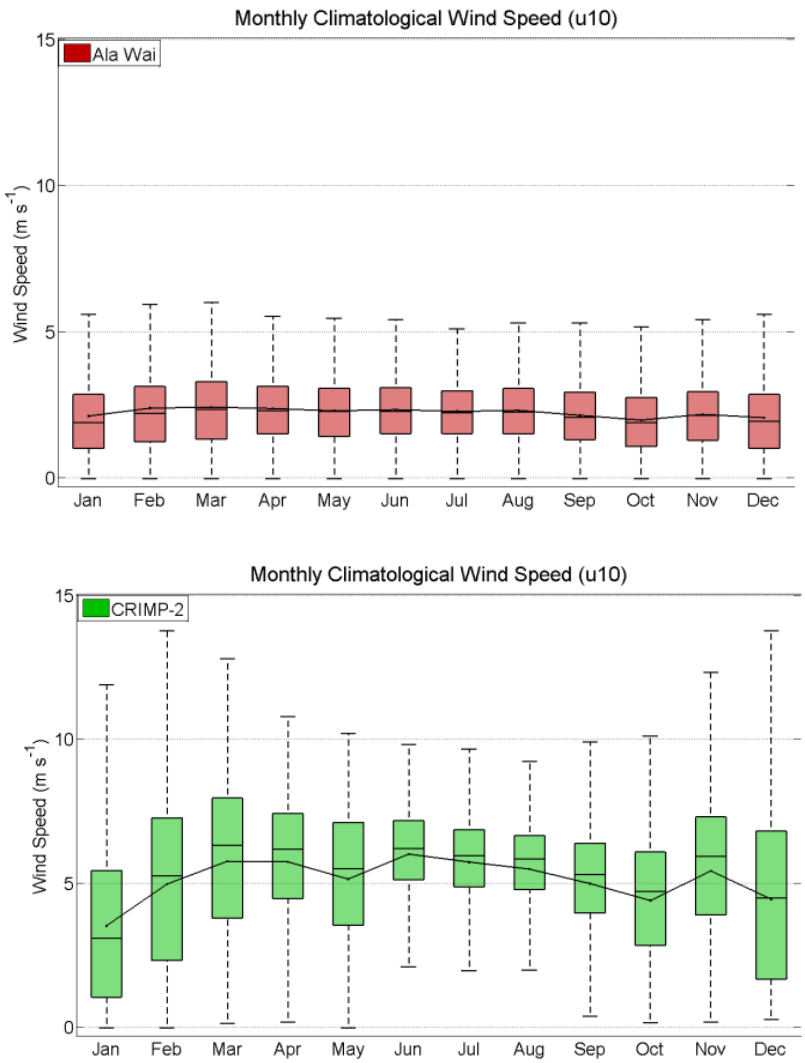

Figure A.6 Climatological monthly box plots of U10 wind speed (ms^{-1}) on the South Shore of Oahu (top panel) and in Southern Kaneohe Bay (bottom panel)

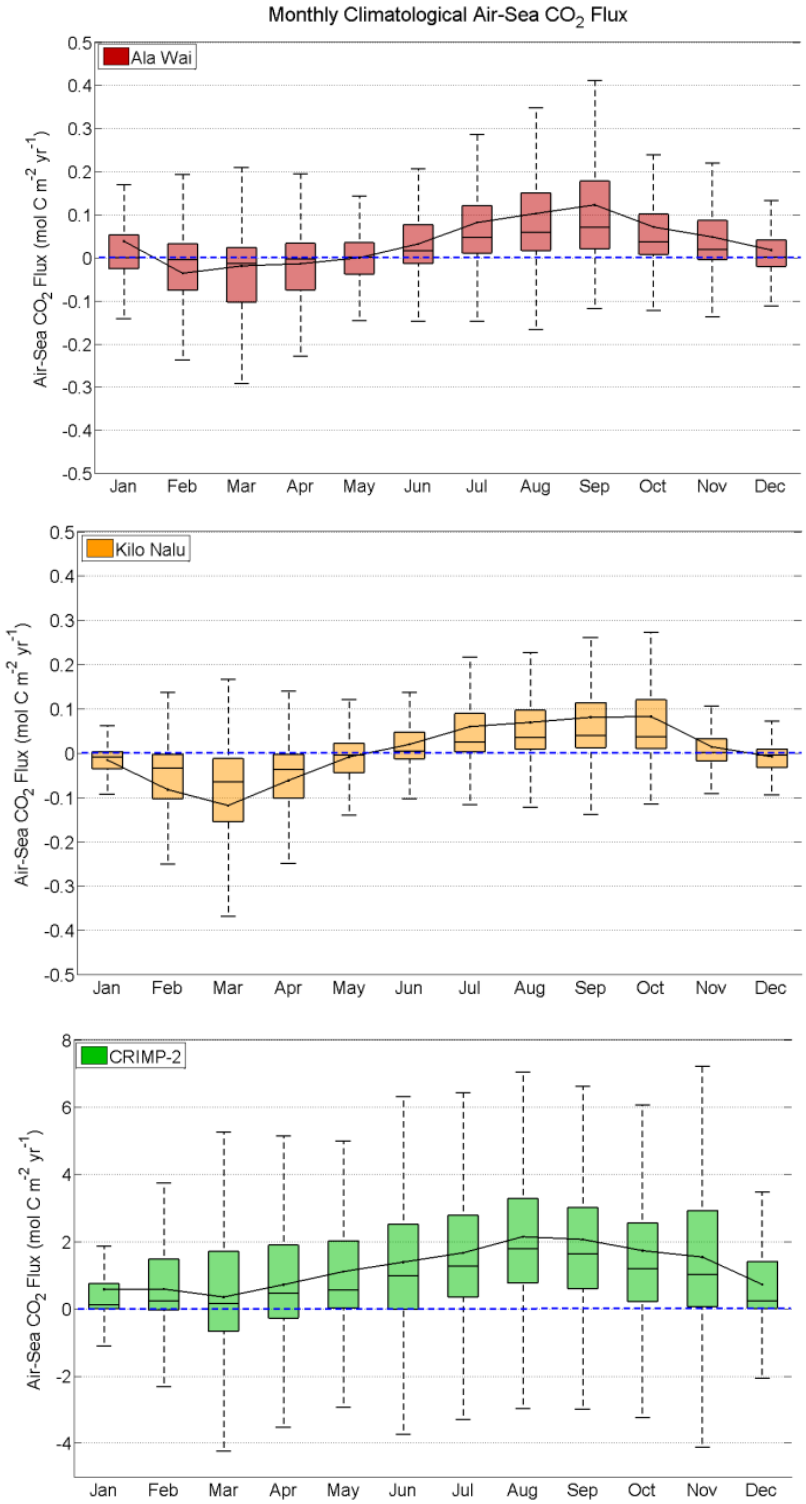

Figure A.7 Climatological monthly box plot of air-sea CO_2 fluxes (mol C m^{-2} yr^{-1}) at Ala Wai (top panel), Kilo Nalu (middle panel), and CRIMP-2 (bottom panel)

APPENDIX B. TIME SERIES FIGURES

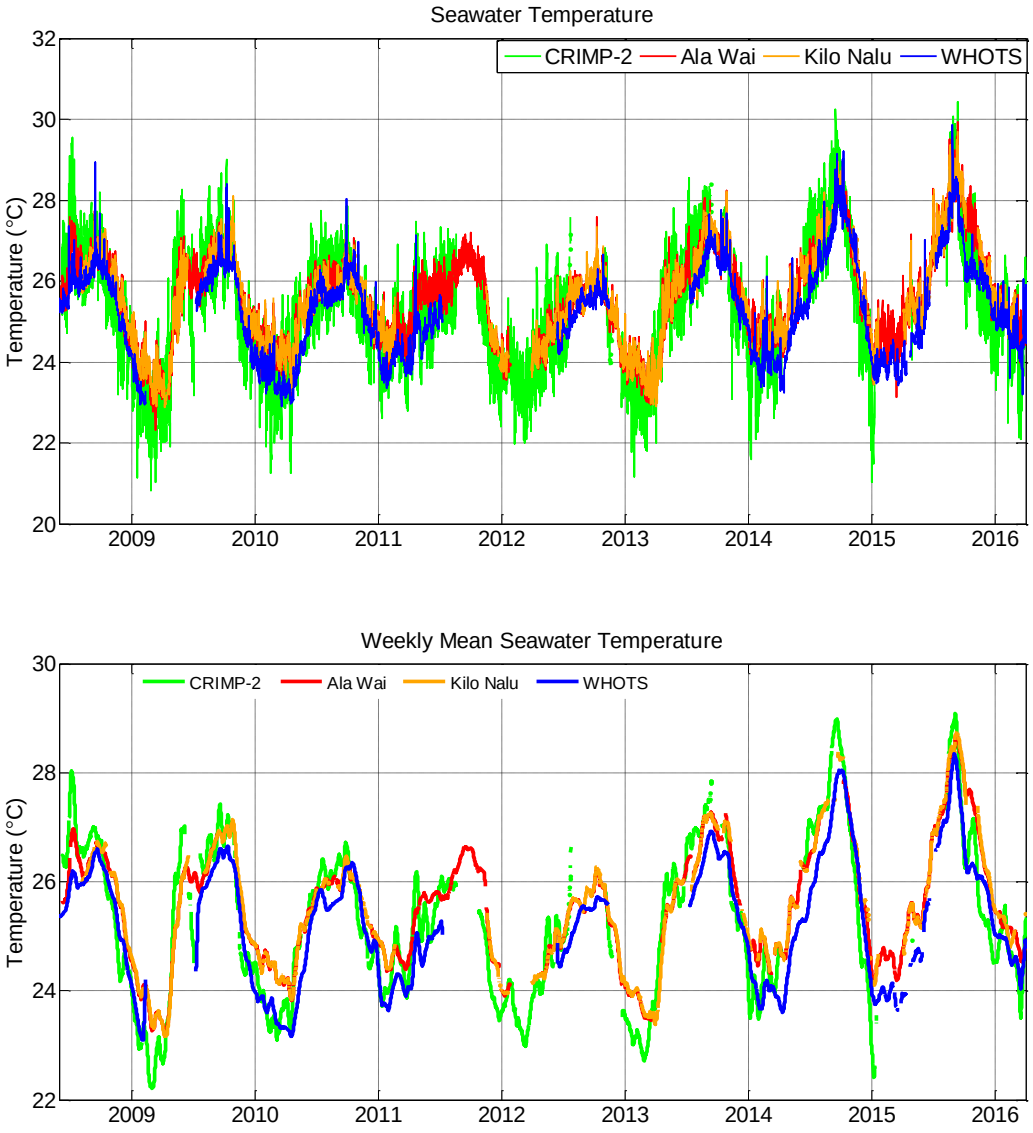

Figure B.1 Time-series of 3-hourly (top panel) and weekly mean (bottom panel) seawater temperature in units of °C at CRIMP-2, Ala Wai, Kilo Nalu, and WHOTS from June 2008 through March 2016.

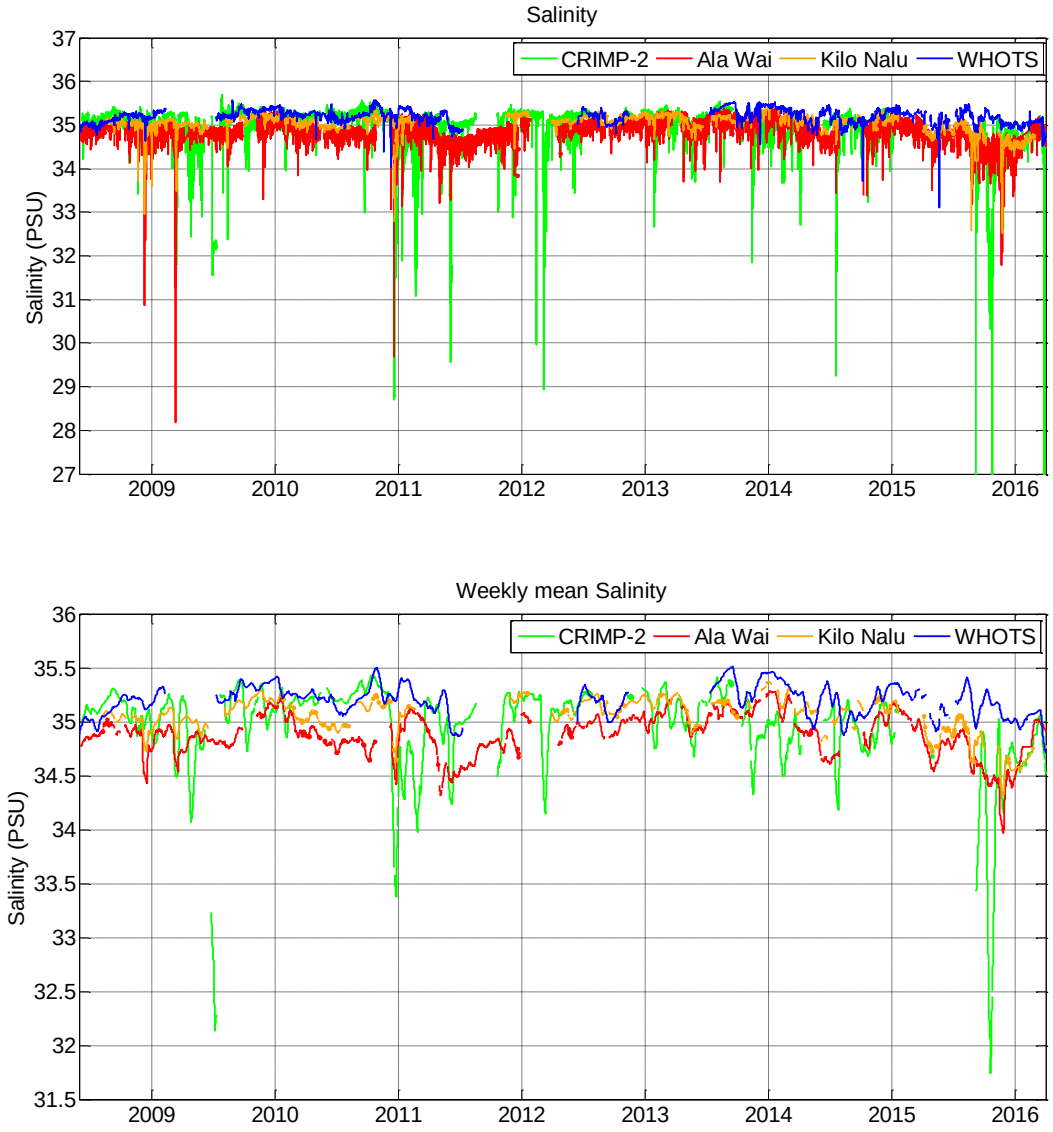

Figure B.2 Time-series of 3-hourly (top panel) and weekly mean (bottom panel) salinity in units of PSU at CRIMP-2, Ala Wai, Kilo Nalu, and WHOTS from June 2008 through March 2016

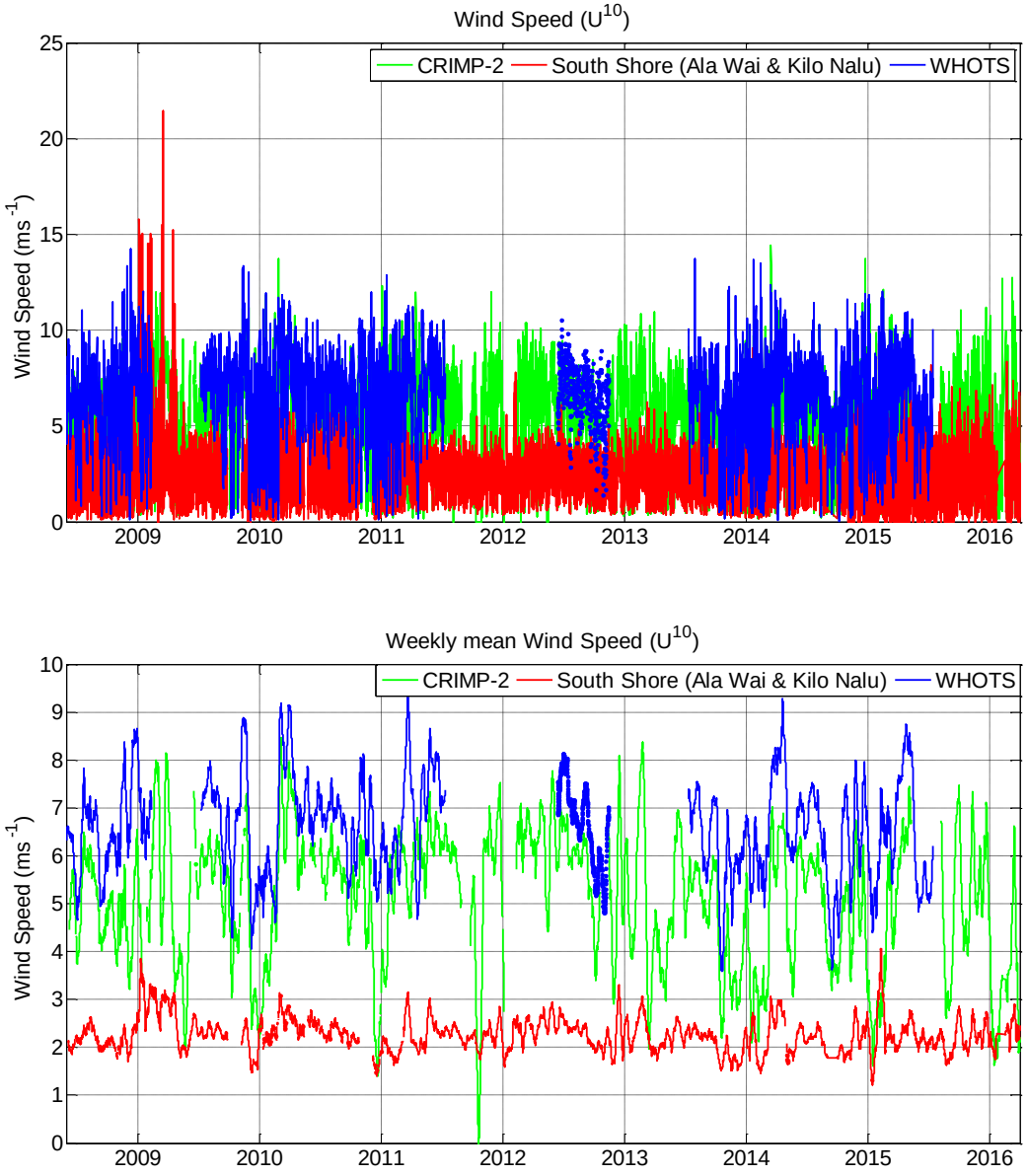

Figure B.3 Time-series of 3-hourly (top panel) and weekly mean (bottom panel) U10 wind speed in units of ms^{-1} at CRIMP-2, Ala Wai, Kilo Nalu, and WHOTS from June 2008 through March 2016

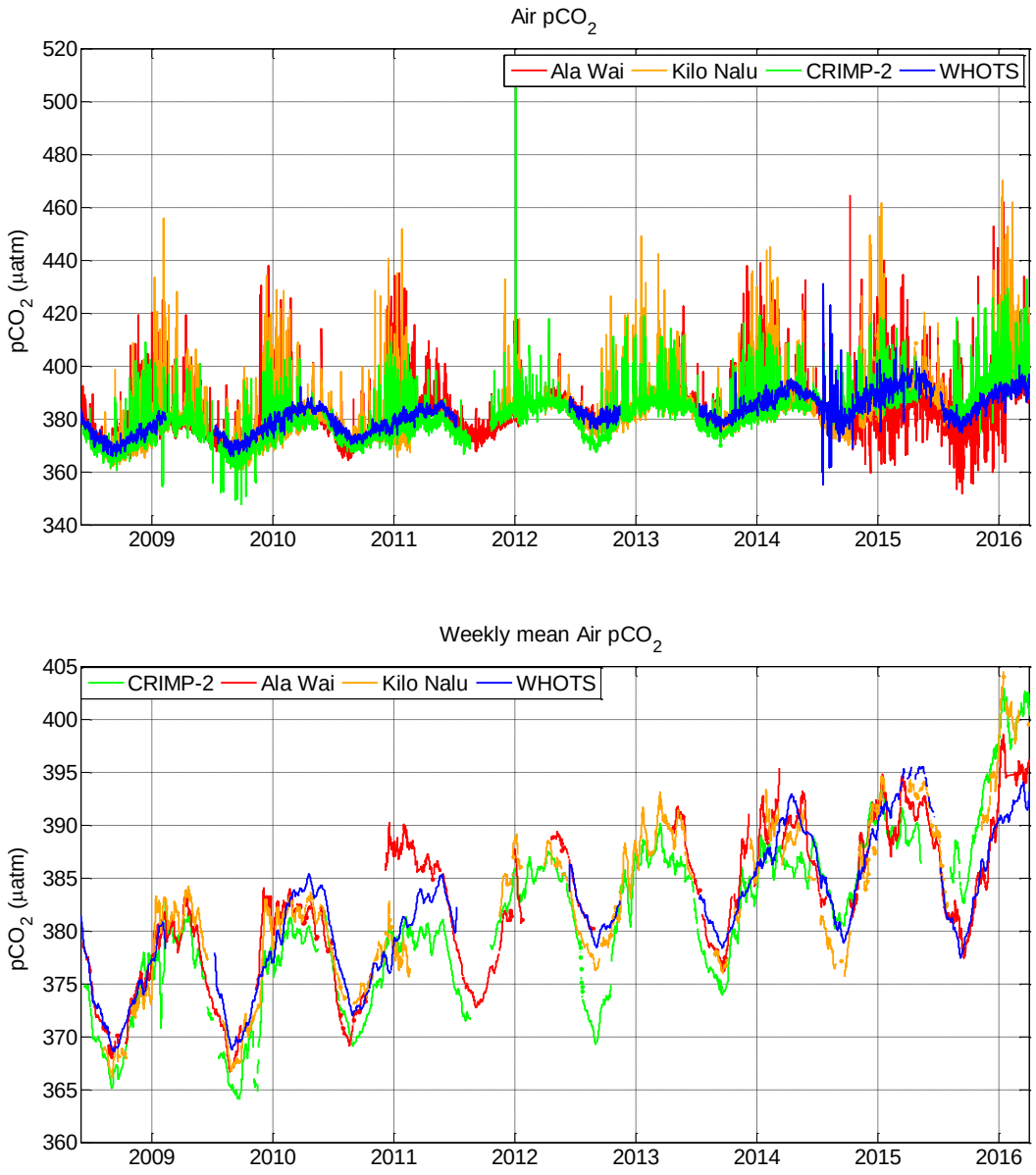

Figure B.4 Time-series of 3-hourly (top panel) and weekly mean (bottom panel) air pCO_2 in units of µatm at CRIMP-2, Ala Wai, Kilo Nalu, and WHOTS from June 2008 through March 2016.

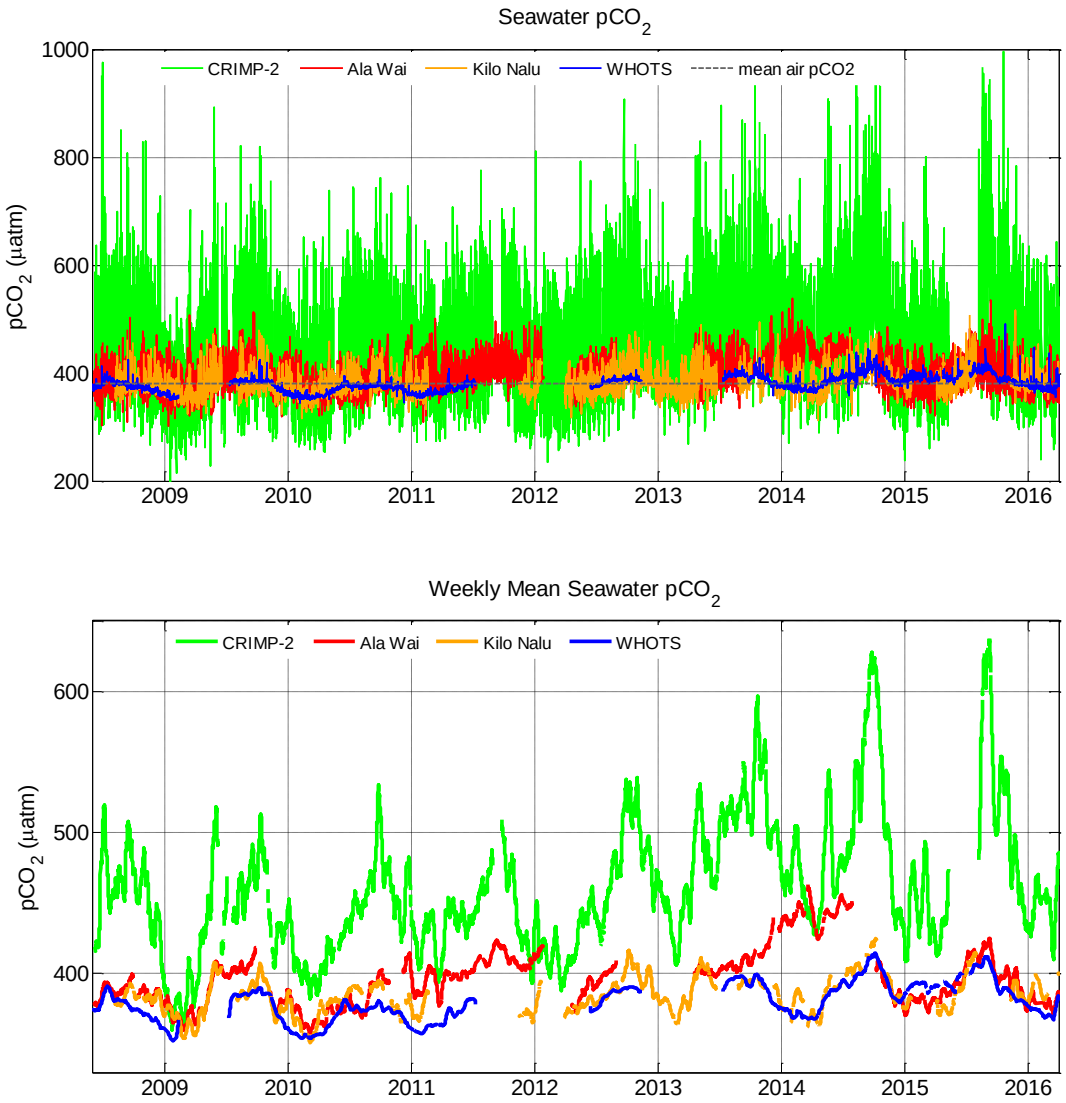

Figure B.5 Time-series of 3-hourly (top panel) and weekly mean (bottom panel) seawater pCO_2 in units of µatm at CRIMP-2, Ala Wai, Kilo Nalu, and WHOTS from June 2008 through March 2016.

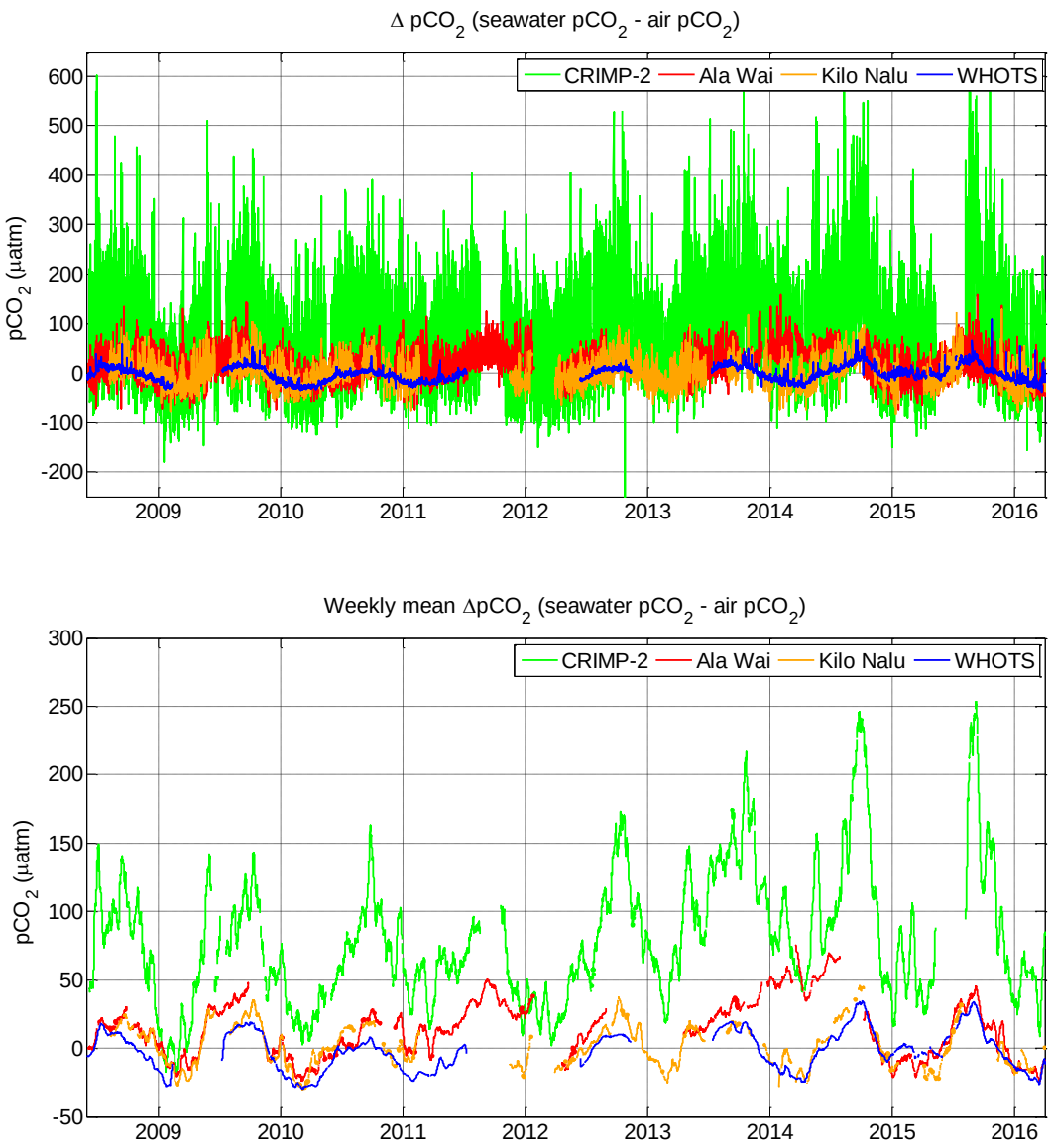

Figure B.6 Time-series of 3-hourly (top panel) and weekly mean (bottom panel) ΔpCO_2 (seawater pCO_2 – air pCO_2) in units of µatm at CRIMP-2, Ala Wai, Kilo Nalu, and WHOTS from June 2008 through March 2016.

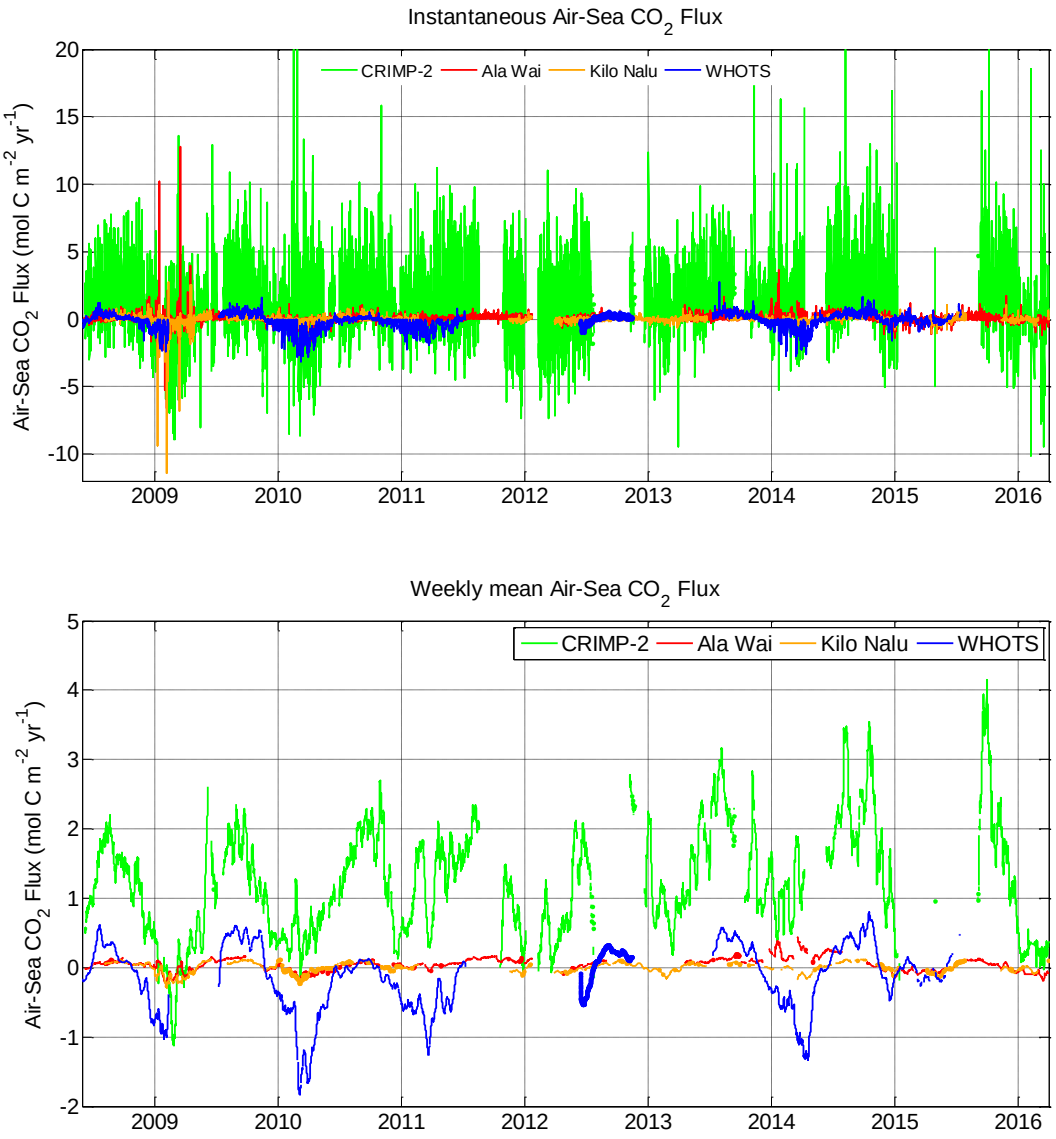

Figure B.7 Time-series of 3-hourly (top panel) and weekly mean (bottom panel) air-sea CO_2 fluxes in units of mol C m^{-2} yr^{-1} at CRIMP-2, Ala Wai, Kilo Nalu, and WHOTS from June 2008 through March 2016.

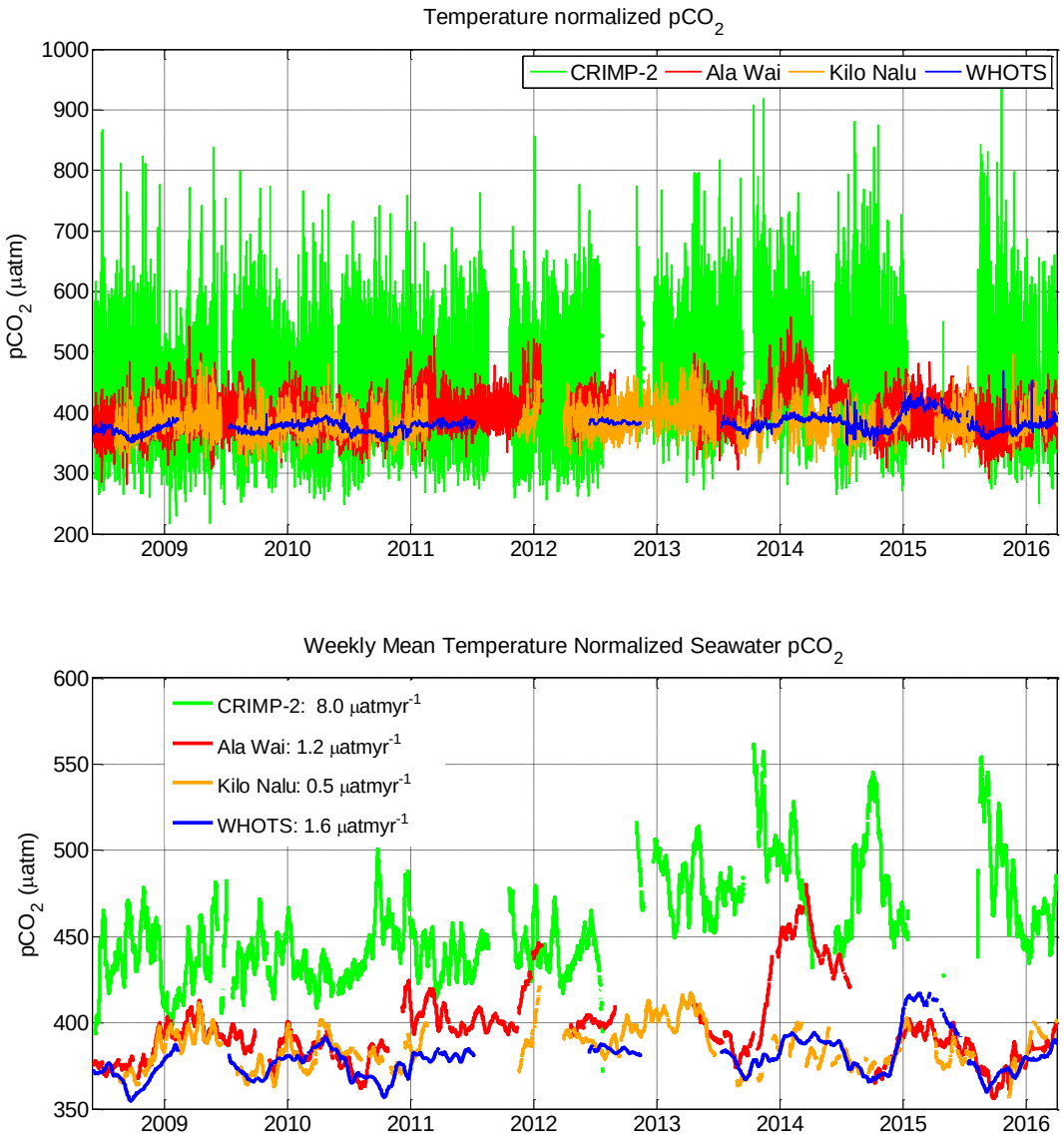

Figure B.8 Time-series of 3-hourly (top panel) and weekly mean (bottom panel) temperature normalized pCO_2 (Eq. 3.3) in units of µatm at CRIMP-2, Ala Wai, Kilo Nalu, and WHOTS from June 2008 through March 2016. Average rates of annual change of weekly mean values in units of µatm yr^{-1}were calculated from a linear fit through each time-series, and are displayed in the legend of the bottom panel.